Visualizing and Understanding the Role of cGMP in Breast Cancer

Dissertation

der Mathematisch-Naturwissenschaftlichen Fakultät

der Eberhard Karls Universität Tübingen

zur Erlangung des Grades eines

Doktors der Naturwissenschaften

(Dr. rer. nat.)

vorgelegt von

Mariagiovanna Barresi

aus Messina (Italien)

Tübingen

2023

Gedruckt mit Genehmigung der Mathematisch-Naturwissenschaftlichen Fakultät der Eberhard Karls Universität Tübingen.

Tag der mündlichen Qualifikation:	16.11.2023
Dekan:	Prof. Dr. Thilo Stehle
1. Berichterstatter:	Prof. Dr. Robert Feil
2. Berichterstatter:	PD Dr. Hannes Schmidt
3. Berichterstatter:	Prof. Dr. Peter Ruth

Zusammenfassung

Der zyklische Guanosinmonophosphat (cGMP)-Signalweg spielt eine entscheidende Rolle bei der Regulation verschiedener (patho)physiologischer Prozesse, einschließlich Herz-Kreislauf-Erkrankungen und Krebs. Die pharmakologische Modulation dieses Signalwegs wird bei der Behandlung von Erkrankungen wie erektiler Dysfunktion, Herzinsuffizienz und Lungenhochdruck erfolgreich eingesetzt. Zudem gibt es zahlreiche Hinweise, dass der cGMP-Signalweg als therapeutisches Ziel in der Krebstherapie adressiert werden könnte. Das Ziel dieser Arbeit war, ein tieferes Verständnis der Rolle des cGMP-Signalwegs bei der Entwicklung und Progression von Brustkrebs zu erlangen und das damit verbundene therapeutische Potenzial zu erforschen.

In der vorliegenden Arbeit wurde die Expression, Aktivität und funktionelle Relevanz des cGMP-Signalwegs in Brustkrebs- und Stromazellen untersucht. Hierzu wurde eine Kombination aus *in vitro*, *ex vivo* und *in vivo* Methoden eingesetzt. Ein zentrales Werkzeug war der Förster/Fluoreszenz-Resonanz-Energie-Transfer (FRET)-basierte cGMP-Biosensor cGi500, mit dem wir die cGMP-Konzentration in Echtzeit in lebenden Zellen und Geweben nach Stimulation der cGMP-erzeugenden Guanylylzyklasen (GC) verfolgen konnten. Insbesondere stimulierten wir die Stickstoffmonoxid (NO)-abhängige GC (NO-GC), GC-A und GC-B mit den entsprechenden Liganden NO, atriales natriuretisches Peptid (ANP) und C-Typ natriuretisches Peptid (CNP). Dieser innovative Ansatz ermöglichte es uns, die räumliche und zeitliche Entwicklung von cGMP-Signalen in verschiedenen Tumor- und Stromazellen innerhalb von Brusttumoren zu bestimmen. Mit Hilfe des cGMP-Biosensors sowie anderen biochemischen und immunhistochemischen Assays haben wir die Präsenz und Aktivität verschiedener cGMP-Signalwege in murinen und humanen Brustkrebsproben analysiert. Mit Hilfe des cGMP-Biosensors konnten wir auch die Wirkung von klinisch eingesetzten NO-GC Stimulatoren wie Riociguat und Vericiguat untersuchen und so wertvolle Einblicke gewinnen, in welchen Zellen diese Medikamente ihre Wirkung entfalten.

Die Analyse verschiedener Brustkrebszelllinien zeigte eine enorme Heterogenität hinsichtlich der Expression und Aktivität der cGMP-Signalwege. Interessanterweise zeigte sich, dass der CNP/cGMP- und der NO/cGMP-Signalweg insbesondere in Zellen des „Triple-Negativen“ Brustkrebs (TNBC, „triple negative breast cancer“) exprimiert war. Diese Ergebnisse konnten durch den Nachweis der NO-GC Expression in von TNBC-Patienten gewonnenen Organoiden und Biopsien untermauert werden. Riociguat verstärkte die NO-induzierte cGMP-Produktion in kultivierten Brustkrebszellen und schien apoptotische Ereignisse in den Organoiden zu verringern.

Unabhängig vom Brustkrebs-Subtyp wurde die NO-GC zusammen mit der cGMP-abhängigen Proteinkinase I (cGKI) in den Stromazellen des Tumormikromilieus (TME, „tumor microenvironment“) stark exprimiert. Aufgrund dieser Erkenntnis fokussierte sich die weitere Arbeit auf das Verständnis, wie die Modulation des cGMP-Signalwegs in Stromazellen möglicherweise das TME verändert und dadurch die Brustkrebsentwicklung beeinflusst.

Um die Rolle von cGMP speziell innerhalb des TME ohne potenzielle Effekte auf Tumorzellen zu untersuchen, haben wir ein präklinisches Mausmodell mit cGMP-unempfindlichen Krebszellen verwendet. Für dieses Modell wählten wir die murine E0771-Zelllinie, die weder Expression noch Aktivität von Komponenten des cGMP-Signalwegs zeigte. Die murinen E0771-Zellen wurden im dritten Brustfettkörper von weiblichen Mäusen implantiert, was die Untersuchung von Brustkrebs und des TME in einem immunkompetenten Modell ermöglichte. In diesem Modell konnten wir mittels des cGMP-Biosensors eine Aktivität der ANP/cGMP- und NO/cGMP-Signalwege im Tumorgefäßsystem nachweisen. Durch Stimulation von Tumorgewebeschnitten *ex vivo* mit einem NO-Donor wurde die cGMP-Konzentration in Tumorgefäß-assoziierten Perizyten stark erhöht. Dabei konnte das NO-induzierte cGMP-Signal potenziert werden, wenn NO in Kombination mit Vericiguat verabreicht wurde. Interessanterweise entwickelten Mäuse, die mit Vericiguat behandelt wurden, signifikant größere Brusttumore als Kontrolltiere, was vermutlich auf Veränderungen in der Tumorvaskularisierung zurückzuführen ist. Somit wurde in dieser Studie erstmals ein wachstumssteigernder Effekt von Vericiguat auf Brustkrebs gezeigt.

Zusammenfassend hat die vorliegende Arbeit eine heterogene Expression verschiedener cGMP-Signalwege in Brustkrebszellen sowie eine starke Aktivität des NO/cGMP Signalwegs in den Perizyten von Tumorgefäßen aufgezeigt. Unter den Brustkrebszellen scheint der cGMP-Signalweg in erster Linie in TNBC-Subtypen exprimiert zu sein, wobei die funktionelle Relevanz von cGMP in diesen Tumorzellen noch unklar ist. Eine wichtige Erkenntnis dieser Studie ist, dass NO-GC und cGKI bei Brustkrebspatientinnen unabhängig vom Tumor-Subtyp in Perizyten des TME exprimiert werden. Diese Ergebnisse wurden durch unser präklinisches Mausmodell untermauert, in dem ein funktionaler NO/cGMP-Signalweg in perivaskulären Zellen des TME identifiziert wurde. Eine Verabreichung des NO-GC Stimulators Vericiguat verstärkte die NO-induzierte cGMP-Produktion in Perizyten *ex vivo* als auch das Brusttumorwachstum *in vivo*. Die in dieser Studie im Mausmodell nachgewiesene signifikante Zunahme des Tumorwachstums durch Vericiguat sollte bei Brustkrebspatientinnen beachtet werden, die eine Vericiguat-Behandlung aufgrund von Herz-Kreislauf-Erkrankungen erhalten. Darüber hinaus unterstreichen die Ergebnisse dieser Arbeit das Potenzial der Modulation des cGMP-Signalwegs als Strategie zur Weiterentwicklung von Brustkrebstherapien.

Summary

The cyclic guanosine monophosphate (cGMP) signaling pathway plays a crucial role in the regulation of various (patho)physiological processes, including cardiovascular diseases and cancer. The pharmacological targeting of this pathway has proven successful in managing conditions such as erectile dysfunction, heart failure, and pulmonary hypertension. Increasing evidence suggests that cGMP-modulating drugs may also have potential for cancer treatment. The aim of this work was to gain further insights into the role of the cGMP signaling pathway in the development and progression of breast cancer and to explore its potential as a therapeutic target for this disease.

In the present study, expression, activity, and the functional relevance of the cGMP signaling pathway were investigated in breast tumors, both in cancer cells and in stromal cells. To achieve our goals, we employed a combination of *in vitro*, *ex vivo*, and *in vivo* methods. One central tool was the Förster/fluorescence resonance energy transfer (FRET)-based cGMP biosensor cGi500, which enabled us to monitor the cGMP concentration in real-time in live cells and tissues after stimulation of the cGMP-generating guanylyl cyclases (GC). Specifically, we stimulated the nitric oxide (NO)-dependent GC (NO-GC), GC-A, and GC-B with their ligands NO, atrial natriuretic peptide (ANP), and C-type natriuretic peptide (CNP), respectively. This innovative approach allowed us to determine the spatiotemporal profile of cGMP signals in various tumor and stromal cells within breast cancer tissue. Utilizing the cGMP biosensor as well as other biochemical and immunohistochemical assays, we analyzed the presence and activity of various cGMP pathways in murine and human breast cancer tissues. Using cGMP imaging, we were also able to examine clinically used NO-GC stimulators such as riociguat and vericiguat, thus, providing valuable insights in which cells these drugs exert their effects.

The analysis of different breast cancer cell lines revealed a tremendous heterogeneity in terms of cGMP pathway expression and activity. Interestingly, these experiments revealed the presence of the CNP/cGMP and NO/cGMP pathway particularly in cells belonging to the triple negative breast cancer (TNBC) subtypes. These results were corroborated by demonstrating expression of NO-GC also in TNBC patient-derived organoids and biopsies. Riociguat potentiated the NO-induced cGMP production in cultured breast cancer cells and might decrease apoptotic events in TNBC patient-derived organoids.

Regardless of breast cancer subtype, NO-GC was strongly expressed together with the cGMP-dependent protein kinase I (cGKI) in stromal cells of the tumor microenvironment (TME). These findings moved our interest toward understanding how modulation of the cGMP pathway in stromal cells could potentially modify the TME and, thereby, affect breast cancer development and progression.

Summary

To study cGMP signaling specifically in the TME without potential effects derived from tumor cells, we used a preclinical mouse model with cGMP-insensitive breast cancer cells. For this model, we chose the murine E0771 cell line, which showed no detectable expression or activity of cGMP pathway components. The murine E0771 cells were implanted into the 3rd mammary fat pad of female mice providing an immunocompetent model to study breast cancer and its TME. Using this model in combination with the cGMP biosensor, we found active ANP/cGMP and NO/cGMP pathways associated with the tumor vasculature. More specifically, upon *ex vivo* stimulation of tumor slices with an NO-donor, pericytes associated with the tumor vessels strongly increased their cGMP concentration The NO-induced cGMP signal was potentiated when vericiguat was co-applied. Interestingly, animals treated with vericiguat developed significantly larger breast tumors as compared to the non-treated control group, presumably due to changes in tumor vascularization. This study is the first to demonstrate a growth-enhancing effect of vericiguat on breast cancer.

Taken together, the present work has revealed heterogeneous expression of various cGMP signaling pathways in breast cancer cells and strong activity of the NO/cGMP pathway in pericytes of the tumor vasculature. Among breast cancer cells, the cGMP pathway appears to be primarily expressed in the TNBC subtype, although the functional relevance of cGMP in these tumor cells remains unclear. An important finding of this study is that NO-GC and cGKI are expressed in pericytes of the TME in breast cancer patients regardless of tumor subtype. These results were further supported by our preclinical mouse model, where a functional NO/cGMP pathway was identified in perivascular cells within the TME. The NO-GC stimulating drug vericiguat amplified NO-induced cGMP production in pericytes associated with tumor vessels *ex vivo* and promoted breast cancer growth *in vivo*. The significant increase in breast tumor growth caused by vericiguat in mice, as demonstrated in this study, should be considered for breast cancer patients undergoing vericiguat treatment for cardiovascular disease. In addition, the findings of the present study underscore the potential of modulating the cGMP pathway as a strategy to advance and refine breast cancer therapies.

Table of Contents

List of abbreviations

AF	alexa fluor
ANP	atrial/A-type natriuretic peptide
APS	ammonium persulfate
AUC	area under the curve
BME	basement membrane extract/Matrigel
BNP	brain/B-type natriuretic peptide
bp	base pairs
BSA	bovine serum albumin
CAF	cancer-associated fibroblast
CAG	cytomegalovirus early enhancer/chicken β-actin/β-globin
cAMP	cyclic adenosine monophosphate
CCD	charge-coupled device
CFP	enhanced cyan fluorescent protein
cGi500	cGMP indicator with an EC50 of 500 nM
cGK	cGMP-dependent protein kinase (see also PKG)
cGMP	cyclic guanosine monophosphate
CMOS	complementary metal-oxide-semiconductor
CMV	cytomegalovirus
CNG channel	cyclic nucleotide-gated ion channel
CNP	C-type natriuretic peptide
Cre	cyclization recombination
CXCL16	C-X-C motif chemokine 16
DEA/NO	diethylamine NONOate
DETA/NO	diethylenetriamine NONOate
DMEM	Dulbecco's modified eagle's medium
DMSO	dimethyl sulfoxide
DNA	deoxyribonucleic acid
DTT	Dithiothreitol
ECL	enhanced chemiluminescence
ECM	extracellular matrix
EDTA	ethylenediaminetetraacetic acid
EM-CCD	electron-multiplying charge-coupled device
eNOS	endothelial nitric oxide synthase
ER	estrogen receptor
FBS	fetal bovine serum
FDA	Food and Drug Administration
floxed	flanked by loxP sites
FPLC	fast protein liquid chromatography
FRET	Förster/fluorescence resonance energy transfer
GC	guanylyl cyclase
GTP	guanosine triphosphate
HEPES	4-(2-hydroxyethyl)-1-piperazineethanesulfonic acid
HER2	human epidermal growth factor receptor 2
HFD	high-fat diet
HFD + V	vericiguat-supplemented high-fat diet
hi	heat-inactivated
HRP	horseradish peroxidase
IB	imaging buffer
IF	immunofluorescence
iNOS	inducible nitric oxide synthase

L-NMMA	NG-monomethyl L-arginine
loxP	locus of X-over of P1
LSM	laser scanning microscope
MAPK	mitogen-activated protein kinase
MDSC	myeloid-derived suppressor cell
mT	membrane-targeted tandem dimer (td)Tomato
ND	normal diet
ND + V	vericiguat-supplemented normal diet
nNOS	neuronal nitric oxide synthase
NO	nitric oxide
NO-GC	NO-sensitive guanylyl cyclase (see also sGC)
NOS	nitric oxide synthase
NP	natriuretic peptide
NPR	natriuretic peptide receptor (see also GC)
PARP	poly(adenosine diphosphate-ribose) polymerase
PBS	phosphate-buffered saline
PCR	polymerase chain reaction
PD-1/PD-L1	programmed cell death protein 1 and its ligand
PDE	phosphodiesterase
PFA	paraformaldehyde
pGC	particulate guanylyl cyclase
PKG	protein kinase G (see also cGK)
PMSF	phenylmethyl-sulfonyl fluoride
PR	progesteron receptor
R ~ (cGMP)	CFP/YFP ratio (representing cGMP concentration)
rcf	relative centrifugal force
RPMI	Roswell Park memorial institute
SDS	sodium dodecyl sulfate
SEM	standard error of the mean
sGC	soluble guanylyl cyclase (see also NO-GC)
SMA	α-smooth muscle actin
TAE	Tris-acetate-EDTA buffer
TAM	tumor-associated macrophage
TBS	Tris-buffered saline
TCM	tumor conditioned medium
TEMED	tetramethylethylenediamine
tg	transgenic
TME	tumor microenvironment
TNBC	triple negative breast cancer
TPBC	triple positive breast cancer
UV	ultraviolet
VASP	vasodilator-stimulated phosphoprotein
VCM	vascular smooth muscle cell conditioned medium
VEGF	vascular endothelial growth factor
VPR	volume pressure recording
VSMC	vascular smooth muscle cell
WB	Western blot
wt	wildtype
YFP	enhanced yellow fluorescent protein

1. Introduction

1.1. The cGMP signaling pathway

The cyclic guanosine monophosphate (cGMP) signaling pathway is a highly conserved and essential signaling cascade in eukaryotes. In mammals, it regulates a multitude of physiological processes, including smooth muscle relaxation and neuronal communication (Hofmann, 2020). Recent studies suggested the potential of the cGMP pathway for the treatment of various diseases, including cancer (Stehle et al., 2023; Schlossmann & Schinner, 2012).

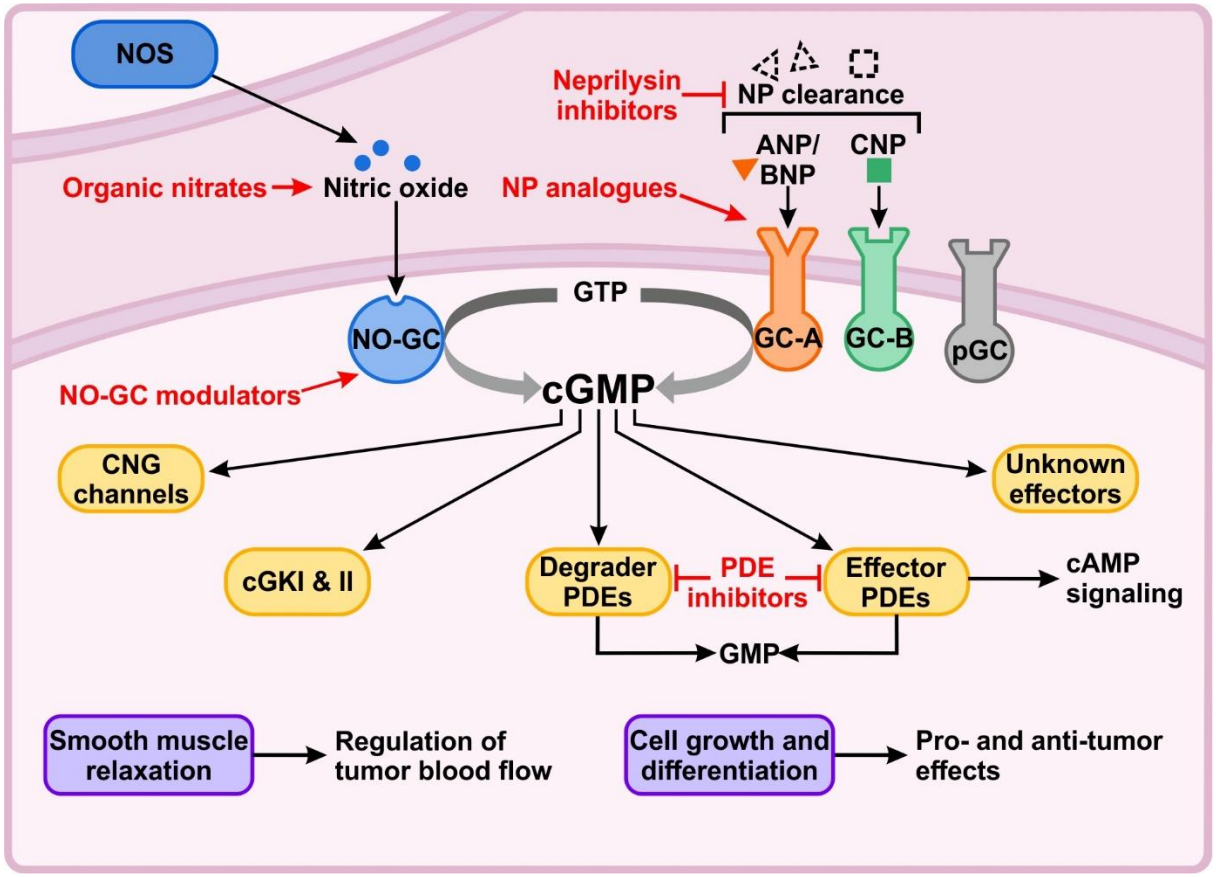

Figure 1. The cGMP signaling pathway. cGMP is generated from GTP by GCs. There are two classes of GCs: the soluble NO-GC (in blue), stimulated by nitric oxide synthesized by NOS (dark blue); and the pGC family (in gray as general), which among others includes GC-A (in orange) stimulated by ANP and BNP, GC-B (in green) stimulated by CNP. Among the downstream cGMP effectors (in yellow) are CNG channels, cGKs, and PDEs. The physiological effects of cGMP (in purple) include smooth muscle relaxation and the regulation of cell growth and differentiation, which can lead to altered blood flow and pro- or anti-tumor effects. Several drug classes have been developed to target the cGMP pathway (main examples indicated in red text) (adapted from Stehle et al. (2023)). NOS, nitric oxide synthase; NP, natriuretic peptide; ANP, atrial NP; BNP, brain NP, CNP, C-type NP; NO-GC, NO-sensitive guanylyl cyclase; GC-A and GC-B, guanylyl cyclase A and B; pGC, particulate guanylyl cyclase; GTP, guanosine triphosphate; cGMP, cyclic guanosine monophosphate; cGK, cGMP-dependent protein kinase; PDE, phosphodiesterase; cAMP, cyclic adenosine monophosphate.

1.1.1. The components of the cGMP pathway

The cGMP pathway is composed of cGMP generators, effectors, and degraders. The cGMP generators are guanylyl cyclases (GC) that catalyze the conversion of guanosine triphosphate (GTP) into cGMP (Potter, 2011b). There are two classes of GCs: the transmembrane particulate GCs (pGCs), which are commonly activated by extracellular ligands such as natriuretic peptides (NPs), and the soluble nitric oxide (NO)-dependent GCs (NO-GCs) (**Figure 1**). The pGCs are homodimeric glycoproteins. Each single-chain has an extracellular ligand binding domain, a transmembrane domain, an intracellular kinase-homology domain, and a catalytic GC domain (Potter, 2011b). The mammalian genome encodes seven pGCs (GC-A to GC-G), sharing the same structure but differing in their tissue specificity and ligands. GC-A is activated by the binding of atrial natriuretic peptide (ANP) or brain natriuretic peptide (BNP) (Potter, 2011b). The expression and activation of GC-A, with subsequent cGMP production, in vasculature, endothelium, heart and kidney has been shown to regulate various physiological processes, such as vasodilation, cardiac remodeling, diuresis, and natriuresis. These responses contribute to the regulation of blood pressure and fluid balance in the body (Pandey, 2014). GC-B, also known as the natriuretic peptide receptor B (NPR-B), is activated by the binding of C-type natriuretic peptide (CNP). GC-B is expressed in various tissues, including brain, kidneys, and reproductive organs. The activation of GC-B by CNP results in the production of cGMP, which regulates processes such as neuronal development, skeletal growth, and reproductive functions (Potter, 2011b). Furthermore, the CNP/GC-B system also plays a role in vascular regeneration following ischemic events by promoting angiogenesis (Yamahara et al., 2003). GC-C is activated by the binding of guanylin and uroguanylin peptides. It is primarily expressed in the intestinal epithelium, where it plays a role in regulating electrolyte and fluid transport, as well as modulating intestinal cell proliferation and differentiation (Takei, 2022). Differently to the other pGCs, GC-E and GC-F, expressed in the photoreceptor cells of the retina, are activated by calcium-dependent intracellular guanylyl cyclase-activating proteins (Kuhn, 2016). Lastly, GC-D and GC-G, considered pseudogenes in human, appear to sense external chemical messenger such as pheromones and they are mainly expressed in olfactory sensory neurons in the nose (Kuhn, 2016).

The NPs that stimulate GC-A and GC-B are synthesized as preprohormones and undergo processing to generate smaller mature forms that contain a well conserved 17-residue disulfide ring structure (Potter et al., 2006). ANP and BNP are primarily produced and stored in atrial granules, exerting endocrine effects on the heart (Goetze et al., 2020). In contrast, CNP is synthesized by various organs and is found in low concentration in the blood stream, suggesting it to have autocrine and paracrine actions (Moyes & Hobbs, 2019). These peptides are degraded by proteases like neprilysin and insulin-degrading enzyme, and by internalization

upon binding to the NP receptor-C (NPR-C) (Potter, 2011a). NPR-C, also known as the clearance receptor, is widely distributed in various tissues and plays a crucial role in controlling the duration and intensity of the NP signaling. Upon binding to NPs, NPR-C facilitates their internalization and subsequent degradation, effectively removing them from the circulation (Potter, 2011a). In addition to its role as a clearance receptor, NPR-C may also have cGMP-independent signaling capabilities by coupling to inhibitory G-proteins, thereby regulating the cyclic adenosine monophosphate (cAMP) signaling pathway (Anand-Srivastava, 2005).

NO-GC, also named soluble GC (sGC), is a heterodimeric enzyme composed of an α- and a β-subunit, and a prosthetic heme group bound to the β-subunit. Each subunit has two isoforms (α1/α2 and β1/β2). However, as the β2 subunit is a pseudogene in mammals, only two combinations are functional, the NO-GC1 (α1β1) and the NO-GC2 (α2β1), (Russwurm et al., 2013). The two enzymes differ in distribution among the organs and in their physiological relevance. While NO-GC1 is ubiquitously expressed and known to regulate different processes such as vascular tone and platelet aggregation, NO-GC2 is predominantly expressed in the brain, where it is thought to modulate synaptic transmission (Friebe et al., 2018). At the structural level, each subunit is composed of four domains: a N-terminal heme nitric oxide/oxygen binding domain, a Per/Arnt/Sim (PAS) domain, a coiled-coil domain, and a C-terminal catalytic domain (Kang et al., 2019). The enzyme contains one heme group per dimer, which is complexed by the histidine 105 residue of the β-subunit (Kang et al., 2019). This interaction between the β-subunit and the heme domain is crucial for the regulation of NO-GC activity. The binding of NO to the heme group induces conformational changes that activate the catalytic activity of NO-GC (Kang et al., 2019; Horst et al., 2019). However, the presence of a heme cofactor makes these enzymes sensitive to oxidative stress, which changes the heme's Fe(II) to Fe(III). The Fe(III)-heme weakly binds to the β-subunit, so it can be easily lost generating an apo-NO-GC that does not longer respond to NO. The disruption of the NO/NO-GC/cGMP signaling pathway by oxidative stress might contribute to the pathogenesis of various diseases (Sandner et al., 2021)

Under physiological conditions, NO production involves the enzymatic activity of nitric oxide synthases (NOS), which convert L-arginine into NO and L-citrulline (Farah et al., 2018). There are three isoforms of NOS according to their expression in different organs and cell types: neuronal NOS (nNOS or NOS1), inducible NOS (iNOS or NOS2), and endothelial NOS (eNOS or NOS3). Endothelial cells constitutively express eNOS, which is localized in various subcellular compartments such as the plasma membrane and caveolae. Stimulation of endothelial cells by shear stress hormonal factors, or other signals triggers the activation of different kinases which activate eNOS by phosphorylation of the residue Ser1177 and Thr495,

leading to the production of NO (Fleming & Busse, 2003). Endothelium-derived NO diffuses into vascular smooth muscle cells (VSMCs) and, through a cGMP-dependent mechanism, acts as a potent vasodilator, regulating blood vessel tone and maintaining vascular homeostasis (Farah et al., 2018). The nNOS is predominantly found in the central and peripheral nervous systems. Upon neuronal activation, calcium influx triggers the activation of nNOS, resulting in the production of NO. NO generated by nNOS serves as a diffusible neurotransmitter, modulating synaptic transmission, plasticity, and neuronal communication. Both eNOS and nNOS activities are tightly regulated by calcium-calmodulin (Förstermann & Sessa, 2012). On the other hand, iNOS is regulated by its expression, which is induced by pro-inflammatory cytokines, bacterial endotoxins, and other stimuli in immune cells. iNOS produces high amounts of NO, playing essential roles in immunological functions, including pathogen defense and immune response regulation. However, excessive NO production by iNOS can also contribute to tissue damage and inflammation in certain pathological conditions, such as septic shock and neurodegeneration (Förstermann & Sessa, 2012). Albeit the NO-GC/cGMP pathway serves as the primary mechanism for transmitting the effects of NO, non-classical processes such as S-nitrosylation of cysteine residues can also occur (Fernando et al., 2019).

The effectors of the cGMP signaling pathway include three classes of proteins: the cyclic nucleotide-gated (CNG) ion channels, the cGMP-dependent protein kinases (cGKs), and the phosphodiesterases (PDEs) (**Figure 1**). CNG channels are non-selective cation channels, allowing the influx of both sodium (Na^+) and calcium (Ca^{2+}) ions. The gating of these channels is regulated by the binding of cyclic nucleotides, specifically cAMP or cGMP (Biel & Michalakis, 2009). CNG channels typically form heterotetramers, consisting of α- and β-subunits. The different isoforms of CNG channels have varying sensitivities to cAMP and cGMP, which contribute to their specific physiological functions in different tissues. CNG channels are primarily expressed in sensory neurons of the visual and olfactory systems, playing a crucial role in sensation. Indeed, in the visual system, they are found in the outer segments of rod and cone photoreceptor cells, while in the olfactory system, they are present in olfactory receptor neurons located in the nasal epithelium (Biel & Michalakis, 2009). However, CNG channels can be found in other cell types, such as VSMCs, where they might be implicated in the regulation of vascular tone, blood pressure, and blood flow (Leung et al., 2010; Yao et al., 1999). It is important to note that the specific contributions of CNG channels to blood pressure and blood flow regulation are complex and may involve interactions with other signaling pathways and factors (Roberts & Dart, 2014).

Possibly, the most important class of cGMP effectors are the cGKs, also known as protein kinase G (PKG). cGKs, are homodimeric serine/threonine protein kinase, encoded by the genes *PRKG1* and *PRKG2* in humans. *PRKG1* encode for cGKI, which is present in 2 isoforms

cGKIα and cGKIβ differing only at the N-terminal, while *PRKG2* encodes for cGKII (R. Feil et al., 2003). In terms of molecular structure, both cGKI and cGKII contain conserved functional domains: a N-terminal region that mediates homodimerization, a regulatory domain, and a C-terminal catalytic domain. The regulatory domain contains two binding sites for cGMP, while the catalytic domain is responsible for the kinase activity of the protein. Binding of cGMP to the regulatory domain causes a conformational change that allows the catalytic domain to phosphorylate target proteins (Hofmann et al., 2006). The different cGKs differ in tissue expression, cGMP affinity, substrate specificity and subcellular localization. cGKI is a cytosolic protein expressed mainly in smooth muscle tissues, including those in the vasculature, lung, and gut, as well as in platelets and certain regions of the brain. The major role of cGKI is in the cardiovascular system, where it regulates vascular tone and blood flow. For instance, by mediating the NO-induced relaxation of vascular smooth muscle, the NO-GC/cGKI pathway promotes vasodilation (R. Feil et al., 2003). Moreover, cGKI plays a role in platelets aggregation and synaptic plasticity (Hofmann et al., 2006). The cGKII is a membrane-bound protein, predominantly found in the gastrointestinal epithelium, kidneys, bone, and certain brain regions, but not in cardiovascular system. cGKII is involved in the regulation of ion transport in the gut and kidneys and plays a role in bone growth (Hofmann et al., 2006).

The last class of known cGMP effectors are PDEs, a diverse family of enzymes that play a critical role in cellular signaling by hydrolyzing cGMP and cAMP into their non-cyclic forms (Bender & Beavo, 2006). There are at least 11 families of PDEs (PDE1 to PDE11), each with different specificities for cAMP and/or cGMP. PDE4, PDE7, and PDE8 primarily degrade cAMP, while PDE5, PDE6, and PDE9 are more specific for cGMP. Some PDEs, like PDE1, PDE2, PDE3, PDE10, and PDE11, can hydrolyze both cAMP and cGMP, although they may prefer one over the other (Francis et al., 2011). Some PDEs, together with their common degrading function (degrader PDEs), might also allow a crosstalk between the cGMP and the cAMP pathway (effectors PDEs) (**Figure 1**). For instance, cGMP can bind to an allosteric site on PDE2, stimulating cAMP hydrolysis. This establishes a negative feedback loop: an increase in cGMP concentration leads to a decrease in cAMP. In contrast, when the concentration of cGMP is high, it competes with cAMP at the catalytic site of PDE3. This competition sets up a positive feedback loop, resulting in increased cAMP concentration (R. Feil et al., 2022). PDEs consist of a conserved C-terminal catalytic domain and variable N-terminal regulatory domains. The catalytic domain is responsible for the hydrolysis of cAMP and cGMP, while the regulatory domains are involved in modulating the specificity of the enzyme and determining its localization within the cell (Kokkonen & Kass, 2017). PDEs are widely expressed throughout the body, with different isoforms having distinct tissue distributions. For instance, PDE1 is found in the brain, heart, and smooth muscle, PDE3 is present in cardiovascular and adipose

tissue, while PDE5 is present in VSMCs of the corpus cavernosum, blood vessels, and platelets. PDEs, regulating the intracellular levels of cAMP and cGMP, are involved in different physiological processes, such as cell proliferation, differentiation, apoptosis, inflammation, and muscle contraction (Francis et al., 2011).

1.1.2. Pharmacological relevance of the cGMP pathway

The cGMP signaling pathway is essential in several physiological processes, implicating its dysregulation in the pathogenesis of numerous diseases. Recognizing this, the cGMP pathway presented itself as a promising target for pharmacological intervention during the last decades. Here, the main classes of cGMP-modulating drugs (**Figure 1**) and their clinical relevance are discussed.

PDE5 inhibitors, including sildenafil (Viagra), tadalafil (Cialis), and vardenafil (Levitra), are possibly the most famous cGMP-elevating drugs. These drugs were approved by the Food and Drug Administration (FDA) between the late 1990s and early 2000s to treat erectile dysfunction (Tzoumas et al., 2020). Indeed, blocking PDE5 leads to increased blood flow in the vessels supplying the corpus cavernosum of the penis, aiding in maintaining erection (Sangiorgi et al., 2021). Furthermore, sildenafil was also approved for treatment of pulmonary arterial hypertension (Ghofrani et al., 2006). However, due to the broad expression of PDEs among tissues and the limited selectivity of the different inhibitors, side effects range from headaches, flushing, and dyspepsia to visual disturbances (Tzoumas et al., 2020).

Next, we have classes of drugs which act on the NP/pGC/cGMP pathway by inhibiting NP degradation or stimulating pGCs as agonists. Sacubitril/valsartan, known by the brand name Entresto, is a neprilysin/angiotensin receptor inhibitor approved in 2015 for treating chronic heart failure. By combining the inhibition of the neutral endopeptidase neprilysin with sacubitril and the inhibition of the angiotensin receptor with valsartan, this drug can both increase the NP levels (by inhibiting the enzyme that breaks down NPs) and block the harmful effects of angiotensin II on the heart (Solomon et al., 2020; McMurray et al., 2014). Due to the predominant role of cGMP signaling in VSMCs and the inhibition of the angiotensin system one of the most common side effects of sacubitril/valsartan is hypotension.

Similar to sacubitril, pGC agonist also induces increase in intracellular cGMP levels by activation of pGC. While the potential benefits of pGC agonists are significant, their use has been limited due to their poor *in vivo* stability and suboptimal pharmacokinetic properties. Indeed, pGC agonists are small peptides that are susceptible to enzymatic degradation by peptidases. Their pharmacokinetic challenges can also be attributed to factors such as rapid renal clearance and poor tissue penetration (Wang et al., 2022). However, there has been a notable achievement with vosoritide (VOXZOGO), a CNP analog that shows improved stability.

In 2021 vosoritide has been approved for the treatment of achondroplasia, the most common type of dwarfism (Duggan, 2021). The cause of achondroplasia is the increased activity of fibroblast growth factor receptor 3 signaling, causing inadequate chondrocyte proliferation and extracellular matrix (ECM) production. The GC-B/cGMP signaling activity, increased by vosoritide, effectively counteracts these negative effects, and significantly boosts the skeletal growth in patients with achondroplasia (Savarirayan et al., 2021). Furthermore, other clinical trials are currently investigating the potential of vosoritide to treat the compression of the cervicomedullary junctions in achondroplasia patients (NCT04554940) or other genetic conditions causing short stature, such as hypochondroplasia (NCT04219007) (Thrailkill et al., 2022).

The class of nitrates, like nitroglycerin, have been in use for over a century for treating angina pectoris (Murrell, 1879). Ensuring NO release by their conversion, nitrates lead to stimulation of the NO-GC/cGMP pathway and consequently relaxation of VSMCs in the blood vessels. This action facilitates the dilation of the blood vessels, improves the oxygen supply to the heart and lessens its workload. Although considered safe as treatment under a medical prescription, some adverse effects, such as drug dependence and incompatibility with other drugs, make the nitrates inadequate in certain situations.

Besides nitrates, other drugs targeting NO-GC are the NO-GC stimulators and activators (Sandner et al., 2021). Although both induce cGMP generation via NO-GC, their mechanism of action is different. NO-GC stimulators bind allosterically to the β-subunit of the enzyme stabilizing its activated form, while NO-GC activators replace the oxidized or missing heme cofactor and activate the enzyme otherwise incapable of producing cGMP (R. Liu et al., 2021) . Indeed, as mentioned in section **1.1.1**, oxidative stress present under several pathological conditions might lead to oxidation of the heme cofactor (oxidized NO-GC) and eventually its dissociation from the enzyme (heme-free apo-NO-GC). Both forms of NO-GC are insensitive to either endogenous NO or NO-GC stimulators, but sensitive to NO-GC activators (R. Liu et al., 2021).

In the past years, several NO-GC stimulators have been developed and are used as approved medication today. The NO-GC stimulator riociguat (Adempas) was approved in 2013 to treat pulmonary arterial hypertension and chronic thromboembolic pulmonary hypertension (Conole & Scott, 2013). Vericiguat (Verquvo), another NO-GC stimulator, was launched in 2021, serving patients with heart failure with reduced ejection fraction (Markham & Duggan, 2021). Both NO-GC stimulators are able to increase cGMP levels in the absence of NO, but more interestingly they are able to strongly potentiate the activity of NO-GC in the presence of low NO concentrations (Sandner et al., 2021). Among the NO-GC activators, one prominent drug is cinaciguat, initially investigated for the treatment of acute decompensated heart failure.

However, its development was discontinued after phase II clinical trials due to issues with hypotension (Liang & Liang, 2023), highlighting again a decrease in blood pressure as a potential side effect of drugs targeting the cGMP pathway. This should be taken into consideration in the balance between potential benefits and risks. Notwithstanding the observed side effects, the therapeutic potential of NO-GC agonists remains significant. They offer a promising avenue for the treatment of not only cardiovascular conditions, but also additional diseases such as fibrosis and metabolic syndrome (Sandner et al., 2021). Thus, these medications could reshape current therapeutic strategies, further broadening the scope of their use as medical treatment.

1.2. Real-time imaging of cGMP using the FRET-based biosensor cGi500

Traditionally, quantification of intracellular cGMP concentrations has been accomplished via antibody-based assays. In this process, tissues or cell samples are broken down and homogenized for examination. Although these immunoassays have been important in determining overall cGMP levels, recent advancements in biosensor technology have underscored the need of assessing cGMP at the (sub-)cellular level under close-to-native conditions. Interestingly, cells derived from the same tissue can display significant variability in their cGMP signaling properties, and the intracellular distribution of cGMP within an individual cell may also lack uniformity (R. Feil et al., 2022). Hence, genetically encoded cGMP biosensors have been developed to investigate and dissect the cell-to-cell heterogeneity. These innovative tools, combined with state-of-the-art microscopy techniques, allow for real-time monitoring of changes in cGMP concentration in living single cells and tissues.

A widely used class of biosensors are the Förster/fluorescence resonance energy transfer (FRET)-based ones. Many cGMP biosensors are based on the interaction between a FRET donor fluorophore and a FRET acceptor fluorophore, connected via the cGMP-binding domain derived from cGKs or PDEs (Sprenger & Nikolaev, 2013). The FRET process, which depends on the close proximity (~2 - 6 nm) and orientation of the fluorophores, is influenced by cGMP binding. In this study, we used the cGi500 biosensor, a cGMP indicator with an EC_{50} of 500 nM. This biosensor is composed of the cGMP-binding domain of the bovine cGKI nestled between the enhanced cyan fluorescent protein (CFP) and the enhanced yellow fluorescent protein (YFP) (**Figure 2A**) (Russwurm et al., 2007). In a low/absent cGMP condition (steady state), FRET takes place from CFP to YFP with high efficiency. As the cGMP concentration increases, the sensor undergoes conformational changes induced by cGMP binding, lowering FRET efficiency. As such, the ratio R~[cGMP] of CFP over YFP correlates with the cGMP concentration, thus providing a measurable output parameter (**Figure 2A**).

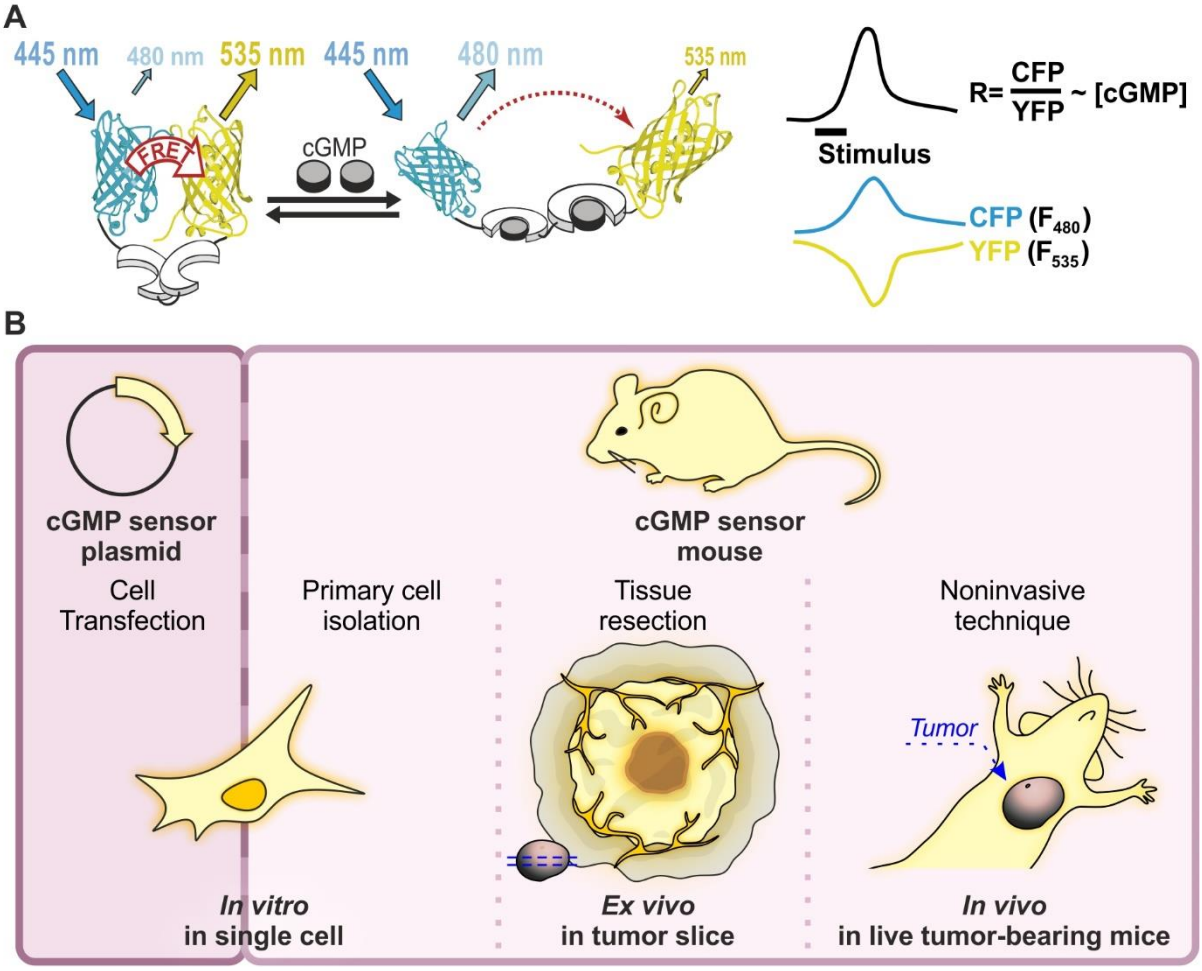

Figure 2. The FRET-based cGMP biosensor cGi500. A, Schematic representation of the cGi500 biosensor with CFP and YFP connected to the cGMP binding domain of cGKI. Absence of cGMP allows high FRET efficiency from CFP to YFP, while cGMP binding induces conformational changes reducing FRET efficiency. Ergo, the CFP/YFP ratio R is an indicator of the cGMP concentration (R~[cGMP]). **B**, Application of the cGMP sensor cGi500 plasmid and transgenic mouse line to measure cGMP changes *in vitro*, *ex vivo* and *in vivo* (adapted from Thunemann et al. (2013).

Although the plasmid encoding the cGi500 biosensor is a potent tool to perform real-time cGMP imaging *in vitro* upon cell transfection, it is not suitable to perform *ex vivo* and *in vivo* studies in live tissues and organs. To fill this lack, Thunemann et al. (2013) have engineered C57BL/6 transgenic mice that stably express cGi500 globally (cGi500(L1)) or enable its cell type-specific expression (mT/cGi500(L2)) (**Figure 2B**). In these mice, the cGMP sensor constructs are inserted into the *Rosa26* gene locus and expressed using the potent ubiquitous cytomegalovirus early enhancer/chicken β-actin/β-globin (CAG) promoter. The cell type-specificity of the mT/cGi500(L2) construct is made possible through the cyclization recombination (Cre)/locus of X-over P1 (loxP) system. Originating from a bacteria-infecting virus known as bacteriophage P1, the Cre/lox recombination system is made up of two primary elements: the Cre enzyme, a site-specific recombinase, and loxP sites, short and specific DNA

sequences that the Cre recognizes and interacts with (R. Feil, 2007). Depending on how these sites are oriented, the Cre enzyme can facilitate DNA excision, inversion, integration of DNA fragments or even chromosomal translocations. Such manipulation of genetic material permits to either activate or deactivate specific genes in somatic cells in a spatiotemporally-controlled manner, bringing an incredible level of control to genetic studies. In transgenic animal models, Cre-mediated DNA excision/deletion is broadly used, due to its highly efficient and almost irreversible feature The target DNA sequence typically flanked by loxP sites of the same orientation ("floxed") is excised by active Cre. While the application for gene knockout is straightforward, this technique can also be used to induce gene expression in a controlled manner. For instance, a floxed gene or stop cassette can be inserted between the promoter and the Cre-controlled gene. In the case of mT/cGi500(L2) mice, a floxed membrane-targeted tdTomato (mT) gene is placed between the CAG promoter and the cGi500 gene (**Figure 3**) (Thunemann et al., 2013).

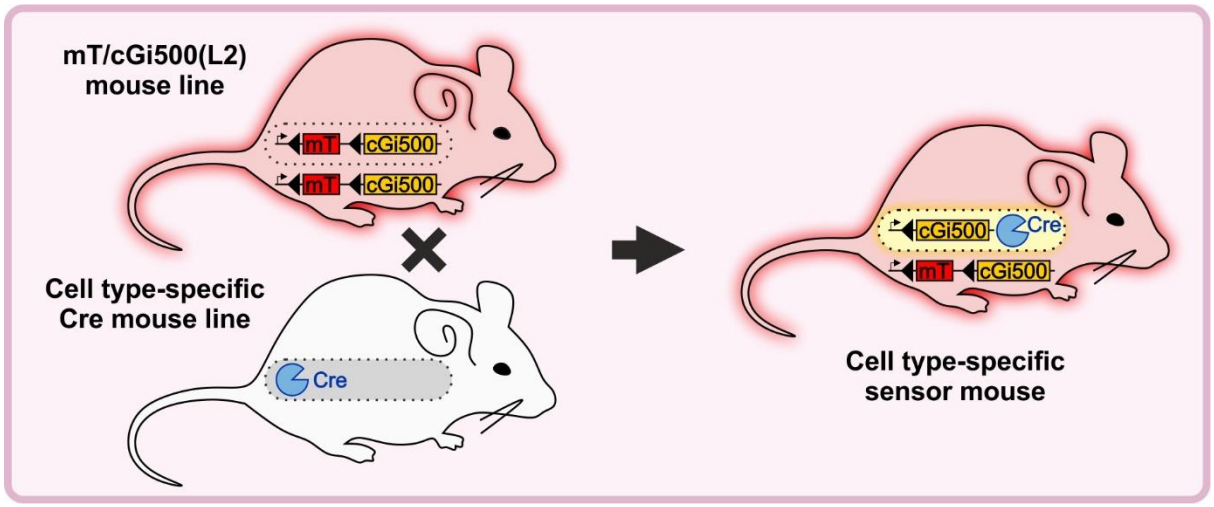

Figure 3. Cell type-specific cGMP sensor mice. In the Rosa26 locus of mT/cGi500(L2) mice, there is a transgene that includes the strong ubiquitous CAG promoter (small black arrows), a mT gene between two loxP sites (black arrowheads), and the cGi500 gene. In absence of Cre, mT is expressed in all cells (red filling). After crossbreeding the mT/cGi500(L2) mice with cell type-specific Cre-expressing mice (gray filling), recombination occurs only in the target cell population (Cre-expressing cells) of the offspring. In this specific cell population recombination triggers the removal of the mT gene and consequently cGi500 expression (yellow filling), while the untargeted cell/tissue will continue to express mT (red filling).

The Cre expression is usually under the control of a cell type-specific promoter to restrict recombination to the target cell population. Nowadays, the availability of transgenic Cre mouse lines is extensive, allowing not only cell specificity but also temporal control. For instance, Cre mouse lines driven by the α-smooth muscle actin (SMA, *Acta2*) or transgelin (SM22, *Tagln*) promoter result in recombination occurring specifically in smooth muscle cells and pericytes. To add temporal control to the Cre/lox system, ligand-activated Cre recombinases have been

developed. In the CreERT2 construct, Cre is fused to a modified estrogen receptor (ER) ligand-binding domain that binds 4-hydroxytamoxifen, a metabolite of the synthetic drug tamoxifen, instead of its endogenous ligand estrogen. Upon binding to 4-hydroxytamoxifen, the CreERT2 fusion protein moves into the nucleus and recombination occurs (S. Feil et al., 2009). Due to the irreversibility of DNA excision, recombinant cells will maintain the modification even when Cre is no longer active. Therefore, this system allows upon tamoxifen injection to genetically label and then track recombinant cell populations during developmental processes and disease progression(S. Feil et al., 2014).

1.3. Breast cancer

Breast cancer is a complex disease that involves abnormal growth of cells in the breast, forming a malignant tumor that can spread and metastasize to other parts of the body. It is the most common cancer in women worldwide (Nolan et al., 2023).

1.3.1. Breast cancer incidence and classification

Breast cancer remains one of the most prevalent types of cancer worldwide, with incidence rates varying across regions and demographics. According to the latest cancer statistics, it is projected that in 2023 in the United States nearly 300,000 women will be diagnosed with breast cancer and approximately 40,000 breast cancer-associated deaths will occur (Siegel et al., 2023).

Various factors contribute to the development of breast cancer, which can be categorized as modifiable and non-modifiable risk factors (Łukasiewicz et al., 2021). Modifiable risk factors include diet, physical activity, and alcohol consumption, whereas non-modifiable risk factors encompass sex, age, genetic predisposition, and family history. Incidence rates of breast cancer increase with age, and it is most frequently diagnosed in women aged over 50 years (Łukasiewicz et al., 2021). However, breast cancer can affect women of all ages, and when it occurs in younger women, it tends to be more aggressive (McGuire et al., 2015). Looking at the genetic predisposition, several genetic mutations have been associated with an increased risk of breast cancer. The most frequently mutated genes are *BRCA1* and *BRCA2*, which are tumor suppressor genes involved in the repair of double-strand DNA breaks and the maintenance of genomic stability. Mutations in these genes account for approximately 15% of familial breast cancer cases (Shiovitz & Korde, 2015).

Breast cancer is a heterogeneous disease, comprising several distinct subtypes that differ in marker expression, prognosis, and response to treatment (Nolan et al., 2023). The breast is primarily composed of adipose tissue, glandular tissue that produces milk, and connective

tissue that keeps everything in place. The glandular tissue is organized into lobules, which are the milk-producing glands, connected to a network of tiny tubes, or ducts, that carry the milk to the nipple (**Figure 4A**). Breast cancer can manifest as *in situ* carcinoma, starting in ducts or lobules and then progress as invasive ductal carcinoma or lobular carcinoma, spreading to the surrounding breast tissue and potentially to other parts of the body (**Figure 4B**). In the clinic, breast cancer is classified not only based on histological features but also on the immunohistochemical expression of specific markers (Nolan et al., 2023). The most common clinical subtypes include hormone receptor-positive breast cancer, human epidermal growth factor receptor 2-positive (HER2+) breast cancer, and triple negative breast cancer (TNBC). Hormone receptor-positive breast cancers, encompassing estrogen receptor-positive (ER+) and/or progesterone receptor-positive (PR+) tumors, are the most prevalent subtype, accounting for approximately 70% of all breast cancers. HER2+ breast cancers, characterized by the overexpression of the HER2/neu protein or amplification of the HER2 gene, represent approximately 15-20% of all breast cancers. TNBCs, lacking expression of ER, PR, and HER2, account for 10-15% of all breast cancers (Waks & Winer, 2019). However, the recent application of RNA-based molecular profiling revealed an even higher grade of breast cancer heterogeneity, influencing patient stratification and treatment selection (Nolan et al., 2023).

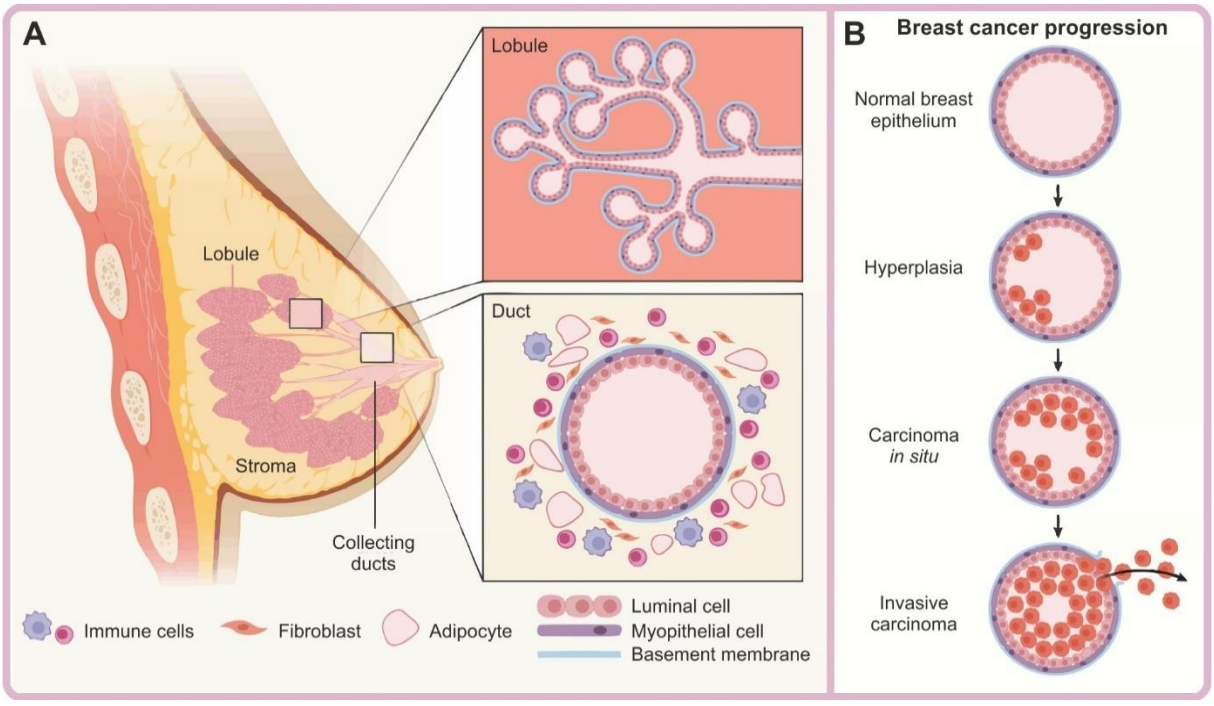

Figure 4. Breast structure and cancer progression. A, Representation of the human breast, pointing on the lobules and ducts, together with cross-sectional views. Breast ducts cross-section shows the duct cell composition and the surrounding cells (e.g. immune cells, fibroblasts, and adipocytes), which are involved in both physiological functions and cancer development in the breast. **B,** Schematic model of breast cancer development: abnormal cell proliferation in the epithelium of ducts or lobules can lead to pre-invasive conditions, called carcinoma *in situ*; upon tumor cell invasion of the surrounding stroma, breast tumor is classified as invasive carcinoma (adapted from Nolan et al. (2023)).

Moreover, these classifications only scratch the surface of breast cancer complexity. Indeed, a critical component of cancer biology that contributes to disease progression and therapeutic resistance is the tumor microenvironment (TME), which will be discussed in the following paragraph.

1.3.2. The tumor microenvironment in breast cancer

In recent years, the TME has been reported as a key player in cancer biology and disease progression. In the context of breast cancer, it has been shown that the TME plays a critical role in tumor development, growth, metastasis, and therapy response (Nolan et al., 2023).

In the TME, different cell types, such as cancer-associated fibroblasts (CAFs), immune cells, endothelial cells, and pericytes/smooth muscle cells can be found in close contact with cancer cells embedded in an altered ECM (**Figure 5A**) (Stehle et al., 2023). CAFs are particularly dominant in the breast TME. These cells produce ECM components and secrete numerous growth factors and cytokines that support tumor growth, angiogenesis, and an immunosuppressive environment (Sarkar et al., 2023). The immune cells within the TME, such as tumor-associated macrophages (TAMs), T lymphocytes, and myeloid-derived suppressor cells (MDSCs), can have dual roles in tumor progression. While these cells are typically involved in immune surveillance and the destruction of cancer cells, in the TME they can also be co-opted by tumor cells to promote tumorigenesis (Mantovani et al., 2008).

In recent years, the tumor vasculature has become a key element and target in the TME, due to its important role in cancer growth and metastasis. Tumor angiogenesis is regulated by a delicate balance between pro-angiogenic factors, such as vascular endothelial growth factor (VEGF) and basic fibroblast growth factor, and anti-angiogenic factors, such as thrombospondin-1 and endostatin (Folkman, 2002). In breast cancer, overexpression of pro-angiogenic factors like VEGF has been associated with increased vascular density, higher tumor grade, and poorer prognosis (Linderholm et al., 2009). Despite the formation of new blood vessels, the tumor vasculature is typically abnormal, with leaky vessels and poor blood flow. These characteristics can contribute to a hypoxic and acidic TME, which can drive tumor aggressiveness and resistance to therapies (Carmeliet & Jain, 2000). Furthermore, the tumor vasculature serves as a pathway for tumor cells to enter the circulation and disseminate to distant organs, leading to metastasis (Fares et al., 2020).

In the early 2000s, the concept of “vascular normalization” emerged as a novel strategy for cancer treatment (R. K. Jain, 2005, 2001). This approach aims to restore the structure and function of tumor blood vessels to resemble those in normal tissues (**Figure 5B**). Indeed, normalized vessels are more structured and less tortuous, with a functional endothelium and enhanced perivascular cell coverage. The goal of vascular normalization is twofold: first, to

improve the delivery and efficacy of chemotherapy and immunotherapy, and second, to reduce hypoxia and associated resistance to radiation therapy and some types of chemotherapy (Goel et al., 2011). Vascular normalization is typically induced by anti-angiogenic agents, targeting, for example, the VEGF pathway. Bevacizumab (Avastin), a monoclonal antibody that inhibits VEGF-A, has been developed and tested also to treat metastatic breast cancer (Garcia et al., 2020).

NO might be another vascular normalizing agent. It has been reported that a perivascular NO gradient is critical for vessel organization in preclinical models of melanoma and glioma (Kashiwagi et al., 2008; Kashiwagi et al., 2005). In these studies, perturbing the physiological NO gradient generated by eNOS in the endothelium, either acting on eNOS itself or by overexpression of iNOS in cancer cells, inhibited pericyte recruitment to the endothelium leading to an increased vessel permeability.

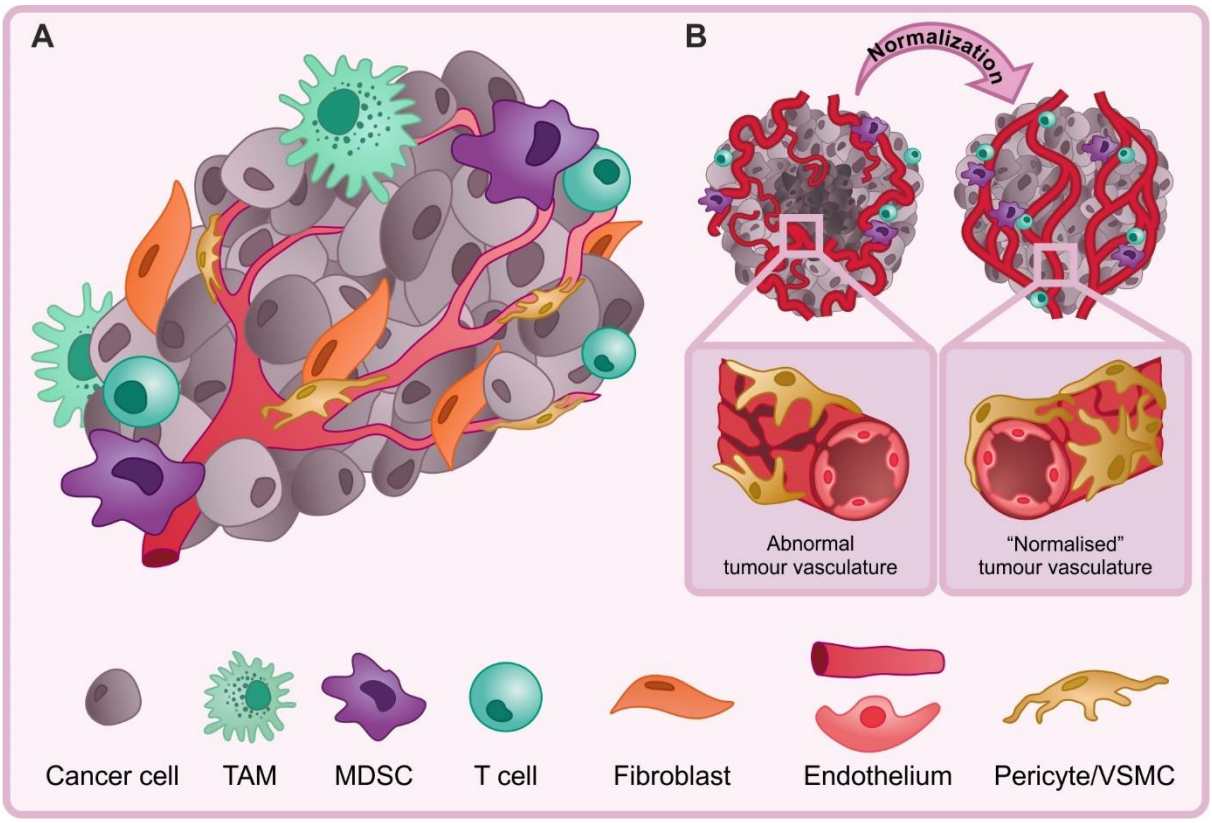

Figure 5. Tumor microenvironment and vascular normalization. A, Simplified representation of the complexity and diversity of cells being part of the breast tumor microenvironment. B, Representation of the tumor vasculature as characterized by an abnormal and dysfunctional phenotype (left panel) and after induced "vascular normalization" leading to restored and functional vessels, which might improve blood flow and drug delivery (right panel) (adapted from Stehle et al. (2023)). TAM, tumor-associated macrophages, MDSC, myeloid-derived suppressor cell; VSMC, vascular smooth muscle cell.

Both anti-VEGF and a restored perivascular NO gradient might promote maturation and normalization of tumor vessels. However, in breast cancer, the benefits of targeting the vasculature as monotherapy have been modest. Nowadays, both preclinical and clinical studies highlighted the beneficial role of combining vascular normalization agents with standard of care therapies, such as immune check point blockers or chemotherapy (Gomes-Santos et al., 2021; Boucher et al., 2021; Fukumura et al., 2018).

Overall, the TME in breast cancer is highly dynamic and complex, with extensive crosstalk between different cell types. This complexity has to be considered in order to define targets for therapeutic intervention.

1.3.3. Current therapies for breast cancer

Breast cancer treatment strategies have evolved significantly over the past few decades due to an increased understanding of the disease's molecular and cellular biology. Current therapies are typically multimodal and personalized based on various factors, including the patient's overall health, menopausal status, the tumor's histopathological characteristics, the disease stage, and the molecular subtype of the cancer (Łukasiewicz et al., 2021). The mainstay therapeutic modalities encompass surgery, radiation therapy, chemotherapy, hormonal therapy, targeted therapy, and immunotherapy (Waks & Winer, 2019).

Independent of the breast cancer molecular subtype, surgery remains a fundamental part of breast cancer treatment. Depending on the extent of the disease, this may involve lumpectomy (removal of the tumor and a small margin of healthy tissue), mastectomy (removal of the entire breast), and axillary lymph node dissection or sentinel lymph node biopsy to check for metastatic spread to the lymph nodes (Waks & Winer, 2019). Radiation therapy is typically used in conjunction with surgery and given before (neoadjuvant) or after (adjuvant) surgery. While the neoadjuvant therapy gives benefits in tumor boundaries reduction before surgery, radiation is especially helpful as adjuvant therapy in patients who undergo lumpectomy, to destroy any remaining cancer cells and reduce the risk of local recurrence (Ebctcg et al., 2014).

Similar to radiation, chemotherapy can also be used in the neoadjuvant setting to shrink tumors or in the adjuvant setting after surgery to eradicate microscopic disease and reduce the risk of recurrence. Neoadjuvant chemotherapy is the standard for HER2+ and TNBC in early breast cancer stages, while it is used for systemic disease control and symptom palliation in metastatic breast cancer (Harbeck et al., 2019).

Alongside these broad-spectrum therapies generally used in cancer treatment, advancements in research have allowed for the identification of specific targets associated with different subtypes of breast cancer (Nolan et al., 2023). This has led to the development of more

personalized, targeted therapeutic approaches that can be combined with the standard of care therapies. Endocrine therapy is an essential part of treatment for ER+PR+ breast cancers, given both as neoadjuvant and adjuvant therapy (Waks & Winer, 2019). The main types of hormonal therapies include selective ER modulators (e.g., tamoxifen), aromatase inhibitors (e.g., letrozole, anastrozole), and selective ER degraders (e.g., fulvestrant). These drugs work by blocking the estrogen signaling pathway, thereby inhibiting the growth of ER+PR+ breast cancer cells (Burstein, 2020). However, resistance to endocrine therapy is a common problem. Tumors can develop resistance through mutations in the ER, increased signaling through alternative growth pathways, or changes in the TME, among other mechanisms (Osborne & Schiff, 2011).

Targeted therapy has emerged as a critical component of breast cancer treatment, particularly for HER2+ breast cancer and some TNBCs. Trastuzumab (Herceptin) was the first monoclonal antibody targeting the extracellular domain of HER2 entering clinical trials. Different adjuvant trials demonstrated how one year of trastuzumab combined with standard adjuvant chemotherapy drastically improved disease-free survival and overall survival for patients with early stage HER2+ breast cancer (Piccart-Gebhart et al., 2005; Romond et al., 2005). Unfortunately, similarly to the endocrine therapy, compensatory signaling or masking of the HER2 receptor are mechanisms leading to therapy resistance (Pohlmann et al., 2009).

In contrast to the other breast cancer subtypes, no specific targets have been found for either early stage or metastatic TNBC. For this subtype, promising results have been achieved with immunotherapy. In 2018, the programmed cell death-ligand 1 (PD-L1) inhibitor atezolizumab (Tecentriq) in combination with the chemotherapeutic agent nab-paclitaxel became the first FDA-approved immunotherapy regimen for PD-L1-positive metastatic TNBC (Soare & Soare, 2019; Schmid et al., 2018). Additionally, in 2021, the FDA granted approval of a humanized antibody against the programmed cell death protein 1 (PD-1), pembrolizumab (Keytruda), in combination with chemotherapy as neoadjuvant treatment and as single adjuvant therapy for early stage TNBC (Schmid et al., 2022; Bagegni et al., 2022). Another option available for TNBC patients with germline *BRCA1* and *BRCA2* mutations are the poly(adenosine diphosphate-ribose) polymerase (PARP) inhibitors (e.g., olaparib and talazoparib). PARP inhibitors lead to cancer cell death by blocking the single-strand DNA repair in the homologous recombination deficiency condition caused by the mutated *BRCAs* (Nolan et al., 2023; Helleday, 2011). Although new treatment options are emerging for TNBC patients, the lack of a well-defined target and recurring drug resistance make treating this breast cancer subtype particularly challenging.

All the aforementioned therapies have improved breast cancer outcomes in recent years. However, due to the escalating issue of therapy resistance, coupled with the role of the TME

discussed in section **1.3.2**, it is essential to deepen our understanding about the molecular and cellular components of breast cancer and their interactions. This knowledge will aid in enhancing current therapies and designing new ones.

1.3.4. Breast cancer models: from cell lines to mouse models

Breast cancer research has substantially benefited from a variety of *in vitro* and *in vivo* models. Ranging from simple two-dimensional cell culture systems to complex animal models, these tools have been pivotal in understanding breast cancer biology and advancing therapeutic strategies.

Breast cancer cell lines are perhaps the simplest and most widely used tools in breast cancer research. Originally derived from human or murine breast tumors, they can be grown in culture indefinitely. These cell lines have provided invaluable insights into the genetic and molecular characteristics of breast cancer and have served as platforms for drug screening (Kitaeva et al., 2020). However, they often lack the complex cellular heterogeneity of actual tumors and do not adequately represent the TME, limiting their ability to fully recapitulate the behavior of tumors *in vivo* (Holliday & Speirs, 2011). Furthermore, long-term culture of these cell lines can lead to genetic drift, causing them to diverge from the original tumor (Ben-David et al., 2018).

Three-dimensional culture systems, such as organoids, offer a more complex model of breast cancer. Organoids can be grown from patient-derived tissues, mimicking the cell composition of the tissue of origin. This allows them to better represent the cellular heterogeneity and microenvironment of tumors, making them a useful tool for studying tumor biology and drug response (Mohan et al., 2021; Porter et al., 2020). Nevertheless, organoids still lack some important structures of the *in vivo* TME including the tumor vasculature.

Patient samples of primary tumor tissues and metastatic lesions provide a rich resource for studying the morphology and cell composition of the human diseases, since they maintain the genetic and cellular diversity of tumors (Kramer et al., 2022). However, their availability is often limited, and they offer just a snapshot of the disease, usually in advanced stages. Furthermore, the lack of a living system limits experimental manipulation and insights about interaction with the tumor cells (Kramer et al., 2022).

Animal models, specifically mouse models, have proven to be critical tools for studying the complex biology of breast cancer, offering insights into the molecular and cellular processes underlying tumorigenesis, metastasis, and treatment response (C. Liu et al., 2021; Zeng et al., 2020). Broadly, these mouse models can be classified as genetically engineered, xenograft and allograft models. Genetically engineered mouse models are typically established through the manipulation of specific genes believed to contribute to human breast cancer. One of the

first transgenic mouse lines was generated by using a mouse mammary tumor virus (MMTV)-c-myc fusion gene (Stewart et al., 1984), followed by a HER2-overexpression model (Muller et al., 1988). However, oncogene mutations can be deleterious during embryonic and mouse development. To overcome this obstacle, conditional knockout models were used, using systems such as Cre-loxP described in **1.2**. Indeed, Wap-Cre and MMTV-Cre lines have been used to develop mouse models carrying mutations in the *BRCA1* gene in the mammary gland (Xu et al., 1999). On the other hand, xenograft models involve the transplantation of human breast cancer cell lines or tissues into immunodeficient mice. These models permit to study the growth and behavior of human cancer cells *in vivo* (C. Liu et al., 2021). Moreover, implantation of patient-derived tissues facilitates the exploration of tumor heterogeneity and personalized therapies, as these tissues preserve the histological and genetic attributes of the original tumor. A limitation of these models is the lack of a functional immune system in the host mice. As a result, they cannot fully evaluate the immune system's role in tumor development and therapeutic response. (C. Liu et al., 2021).

Lastly, the allograft models involve the transplantation of murine cancer cells or tissues into syngeneic, i.e. genetically identical, hosts (Zeng et al., 2020). Although allograft models may not fully recapitulate the heterogeneity of human breast cancers, they can be suitable to investigate tumor-host interactions in the context of an intact immune system. Furthermore, transplantation can be orthotopic, taking place in the organ of origin of the studied cancer, which provides a more physiologically relevant TME (Zeng et al., 2020).

One of the most used murine cell line for the breast cancer allograft model is the E0771 cell line. These cells, derived from a medullary breast adenocarcinoma in C57BL/6 mice (Sugiura & Stock, 1952), are commonly considered belonging to the TNBC subtype (Le Naour et al., 2020). A key advantage of using the E0771 model is its immunocompetence, which allows researchers to study interactions between cancer cells and the stroma within an intact TME. These features, along with the C57BL/6 background which allows combination with cGMP sensor mice (see section **1.2**), make the E0771 mouse model a suitable tool for characterizing the expression and role of the cGMP pathway in breast cancer tumors, as performed in the current study.

1.4. cGMP in breast cancer

As mentioned above, the different breast cancer subtypes and the variety of cells in the TME significantly impact prognosis and treatment strategies. Additionally, this heterogeneity could also potentially involve the cGMP signaling pathway (Stehle et al., 2023).

Studies revealed variations in the expression of cGMP pathway components corresponding to the severity of breast cancer. For instance, the mRNA levels of cGKI and cGKII were significantly diminished in human breast tumors compared to normal tissue (Karami-Tehrani et al., 2012). Additionally, more aggressive HER2+ and TNBC subtypes demonstrated higher PDE5 expression than ER+/PR+ breast cancer. The high PDE5 expression was also associated with shorter patient survival (Catalano et al., 2016). Together, these results suggested that the reduction of cGMP signaling may correlate with increased breast cancer aggressiveness. However, other studies have linked iNOS overexpression, which might activate the NO/cGMP pathway, with reduce survival rates for patients with ER-negative breast cancer (Basudhar et al., 2017; Glynn et al., 2010). These discrepancies might be attributed to the heterogeneity of breast cancer; indeed no correlation was found between iNOS expression and ER+ breast cancer. Moreover, as already mentioned in **1.1.1**, the NO produced by iNOS can induce cGMP-independent effects (Fernando et al., 2019).

The correlation between high PDE5 expression, leading to a decreased intracellular cGMP concentration, and reduced survival in breast cancer patients, made PDE5 inhibitors potential anti-breast cancer drugs (Di Iorio et al., 2021). At the molecular level, the PDE5 overexpression seems to be involved in increasing cell proliferation, mobility, and invasion. Silencing of PDE5 in MDA-MB-468 (TNBC) cells induced a decrease in cell mobility and proliferation. At the same time, MCF-7 and T47D (both ER+PR+) cells overexpressing PDE5 showed a more aggressive behavior in comparison to their parental lines, and this detrimental behavior could be attenuated by treatment with the PDE5 inhibitor sildenafil (Catalano et al., 2016). Additionally, Tinsley et al. (2009) showed that the non-steroidal anti-inflammatory drug sulindac sulfide induces apoptosis in different breast cancer cells. Sulindac should mainly inhibit cyclooxygenases; however it has been reported that it might also inhibit PDE5 and PDE10 (Piazza et al., 2020; Lee et al., 2016). In MDA-MB-231 (TNBC) cells, as well as of ZR75-1 (ER+PR+) and SK-BR-3 (HER+) human breast cancer cells, sulindac decreased cell growth and increased activation of apoptotic effectors, such as caspase-3 and caspase-7 (Tinsley et al., 2009). Similarly, in both MDA-MB-468 and MCF-7 cells, apoptosis induction was also observed after treatment with the PDE9 inhibitor BAY73-6691 (Saravani et al., 2012). Of note, MCF-7 cells were more sensitive to BAY73-6691 than MDA-MB-468 cells, suggesting different sensitivity between the ER+PR+ and the TNBC subtypes to PDE9 inhibition. Altogether, these

studies showed that, at least *in vitro*, PDE5, PDE9 and PDE10 inhibitors can induce apoptosis in breast cancer cells.

Furthermore, studies have explored co-treatments with the PDE5 inhibitor sildenafil and chemotherapy agents to augment the chemotherapy's effectiveness and potentially mitigate its side effects. *In vitro* combination of sildenafil with the chemotherapeutic agent cisplatin significantly decreased cell viability of MCF-7, MDA-MB-468 and MDA-MB-231 cells compared to chemotherapy alone (Hassanvand et al., 2020; Di et al., 2010). Similarly, inhibiting effects on tumor cell growth and viability were also obtained upon co-treatment of MDA-MB-231 cells with sildenafil and the chemotherapeutics paclitaxel, camptothecin and doxorubicin *in vitro* (Di et al., 2010). *In vivo* studies showed that sildenafil significantly reduced tumor cell count and growth in the Ehrlich ascites carcinoma model (Morsi et al., 2023; El-Naa et al., 2016). Sildenafil, either alone or in combination with cisplatin was shown to boost cellular immune responses by increasing the plasma levels of granzyme B and interferon-gamma, and by enhancing the presence of splenic T cytotoxic and T helper cells (Morsi et al., 2023). Furthermore, cotreatment with sildenafil and cisplatin lowered the expression of angiogenin and VEGF, and decreased the overall tumor volume (El-Naa et al., 2016). Additionally, the co-administration of sildenafil and doxorubicin, as opposed to doxorubicin alone, enhanced the intra-tumoral concentration of doxorubicin and slowed the growth of 4T1 (TNBC) mammary tumors (Greish et al., 2018; Di et al., 2010). Interestingly, sildenafil alone slightly reduced tumor growth *in vivo*, but did not affect 4T1 cell growth *in vitro* (Greish et al., 2018). Taken together, these findings indicate that sildenafil might enhance the efficacy of anti-breast cancer drugs in rodent models, possibly by improving the anti-tumor immunity and tumor vasculature.

Interestingly, the PDE5 inhibitor vardenafil, when combined with a polyphenol found in green tea, has been shown to induce cancer cell death, by activation of the eNOS/NO/cGMP pathway (Kumazoe et al., 2013). *In vivo* administration of green tea polyphenol diminished the growth of MDA-MB-231 xenografts, and this anti-tumor effect was amplified by co-treatment with vardenafil. Still, it is important to note that in the absence of other therapies, vardenafil administration alone seemed to slightly increase breast cancer growth.

Apart from PDEs, other components of the cGMP signaling pathway have also been investigated as prospective targets for breast cancer treatment. An intriguing study found that NOS inhibitors reduced tumor growth and prolonged survival in TNBC xenograft mice (Granados-Principal et al., 2015). A phase I/II clinical trial (NCT02834403) assessed the efficacy of co-treatment with the pan-NOS inhibitor NG-monomethyl L-arginine (L-NMMA) and the chemotherapy drug docetaxel for chemoresistant TNBC patients, with a 46% overall positive response rate (Chung et al., 2021). The advantageous effects of NOS inhibition were linked to a more immunosupportive TME. As described in **1.3.2**, the restoration of the

perivascular NO gradient might improve blood flow and tumor tissue oxygenation in a model for glioma, enhancing the response to radiation therapy (Kashiwagi et al., 2008). Thus, it's plausible that a similar mechanism could contribute to the improved anti-tumor immunity observed in TNBC patients receiving L-NMMA/docetaxel treatment (Chung et al., 2021).

While most studies seem to suggest that an increase of cGMP inhibits breast cancer growth, some studies have identified a growth-promoting effect of cGMP in breast cancer cells. A study by Schwappacher et al. (2013), reported that activation of the NO/cGMP/cGKI pathway increased the mobility and invasiveness of MDA-MB-231 cells via cGKI-dependent phosphorylation of the actin/myosin-associated protein caldesmon. Similarly, Lv et al. (2020) identified a connection between increased *de novo* nucleotide synthesis and breast cancer metastasis. This pathway led to generation of GTP, the substrate of GCs (as described in **1.1.1**). Elevated GTP concentrations, resulting from an altered guanylate metabolism, may promote tumorigenesis through enhancement of cGMP signaling (R. Feil, 2017). Indeed, the study of Lv et al. (2020) on TNBC 4TO7 cells revealed that increased *de novo* nucleotide synthesis activated the cGMP/cGKI pathway, stimulated the mitogen-activated protein kinase (MAPK), and fostered greater stemness and sphere formation capacity *in vitro*. Furthermore, the highly aggressive 4TO7Lung cells, derived from 4TO7 lung metastases, exhibited higher cGMP levels than their parent 4TO7 cells (Lv et al., 2020). This pro-growth effect of cGMP was attributed to the activation of the MAPK pathway, a signaling crosstalk also noted in melanoma (Dhayade et al., 2016). Further investigations would be valuable to determine whether a common mechanism ties cGMP and MAPK signaling in various cancer cell types.

In conclusion, previous studies indicate that compounds that enhance cGMP signaling can exert both anti-cancer and pro-cancer effects, depending on the specific breast cancer subtype, tumor stage, and whether the agents target cancer or stromal cells (Stehle et al., 2023). The complexity and diversity of cGMP's role in cancer biology emphasizes the need for continued research in this area.

2. Aim of the study

The cGMP pathway plays a vital role in various biological processes such as vasorelaxation, cell growth and differentiation. Within this pathway, specific proteins offer promising targets for therapeutic intervention in numerous diseases. As a result, a wide range of drugs that modulate cGMP has been developed.

While previous research has indicated the involvement of cGMP in breast cancer, our understanding of the underlying cellular and molecular mechanisms remains limited. Hence, the aim of this study was to gain a comprehensive understanding of the cGMP signaling pathway in both cancer and stromal cells of breast tumors. FRET-based cGMP biosensors allow real-time imaging of cGMP within intact cells and tissues. Using these biosensors we studied the spatiotemporal changes and roles of cGMP in breast cancer in live cells and tumor tissues. The current study investigated the cGMP pathway in several breast cancer models, ranging from cell lines and patient-derived samples to a preclinical *in vivo* mouse model.

The goal of this study was to gain a better understanding of the role of cGMP in breast cancer progression and therapy. Firstly, the research aimed at identifying the tumor and/or stromal cells generating cGMP and determining which GC ligands induce cGMP generation in a particular cell population. Then, it aimed to elucidate the pathophysiological significance of cGMP in breast cancer, investigating how stimulation of the cGMP signaling pathway specifically in cancer cells or stromal cell populations might influence tumor growth both *in vitro* and *in vivo,* with a focus on the TME. These analyses were expected to suggest novel therapeutic strategies for breast cancer by targeting the cGMP signaling pathway.

3. Materials and methods

The following part outlines reagents, buffers, and techniques used in the current study. It provides detailed information on the background and context of each technique, the materials required, and precise instructions for practical application as stated in the protocols used in the Feil working group and already described in other doctoral theses (Stehle, 2022; Lehners, 2022; Dobrowinski, 2019). The solutions were prepared using H_2O from the Milli-Q Biocel Water Purification System, and pH was adjusted using 10 M aqueous NaOH and HCl solutions unless otherwise stated. Autoclaving was performed using a DX-200 autoclave (Systec) at 121°C for 20 minutes to sterilize the solutions, pipette tips, tubes, and glass coverslips. Centrifugation was carried out using either an Eppendorf 5417C/R centrifuge (1.5 mL and 2 mL tubes) or an Eppendorf 5804R centrifuge (15 mL and 50 mL tubes).

3.1. General materials

3.1.1. Chemicals

Table 1. Chemicals used in the current study.

Chemical	Brand	Chemical	Brand
Acetic acid	Sigma-Aldrich	KH_2PO_4	Merck
β-escin	Sigma-Aldrich	2-Mercaptoethanol	Roth
6-Aminohexanoic acid	Roth	Methanol	Sigma-Aldrich
APS	Roth	$MgCl_2 \cdot 6H_2O$	Roth
Bromophenol blue	Roth	Milk powder	Roth
$CaCl_2$, anhydrous	Roth	Na_2HPO_4	Roth
Citric acid	Roth	NaCl	Roth
CuSO4, anhydrous	RanReac AplliChem	NaOH pellets	Roth
DTT	Roth	PFA	Roth
DMSO	Roth	PMSF	Roth
EDTA	Roth	SDS	Roth
Ethanol	Sigma-Aldrich	D-Sucrose	Roth
D-Glucose	Fisher	TEMED	Roth
Glycerol	Roth	Toluene	Sigma-Aldrich
Glycine	Sigma-Aldrich	Tris (Trizma base)	Sigma-Aldrich
HCl, 37% fuming	Roth	Triton X-100	Roth
HEPES	Roth	Trypan Blue, 0.4%	GIBCO
Isopropanol	Sigma-Aldrich	Tween-20	Roth
KCl	Sigma-Aldrich	Xylene cyanol	Roth

Footnotes: APS, ammonium persulfate; DMSO, dimethyl sulfoxide; DTT, Dithiothreitol; EDTA, ethylenediaminetetraacetic acid; HEPES, 4-(2-hydroxyethyl)-1-piperazineethanesulfonic acid; PFA, paraformaldehyde; PMSF, phenylmethyl-sulfonyl fluoride; SDS, sodium dodecyl sulfate; TEMED, tetramethylethylenediamine.

3.1.2. cGMP pathway-modulating compounds and drugs

Table 2. List of compounds and drugs used in the current study.

Name	Brand	Stock	Solvent
cGMP	BIOLOG	100 µM	H_2O
8Br-cGMP	BIOLOG	100 mM	H_2O
DEA/NO	Enzo	100 mM	Alkaline solution
DETA/NO	Enzo	100 mM	Alkaline solution
ANP	Tocris	100 µM	H_2O
CNP	Tocris	100 µM	H_2O
Riociguat	Sigma-Aldrich	10 mM	DMSO
Vericiguat	Sigma-Aldrich	10 mM	DMSO

Footnotes: 8Br-cGMP, 8-Bromo-cGMP; DEA/NO, diethylamine NONOate; DETA/NO, diethylenetriamine NONOate; Alkaline solution: 10 mM NaOH in H_2O.

3.1.3. Buffers and solutions

- Dulbecco's modified eagle's medium (**DMEM**): DMEM high-glucose (4.5 g/L D-Glucose) + GlutaMAX™ (containing the dipeptide L-alanyl-L-glutamine) + pyruvate (110 mg/L Na-pyruvate) (GIBCO). Unless stated otherwise, medium was supplemented with 10% fetal bovine serum (FBS; GIBCO; heat-inactivated (hi) for 30 minutes at 57°C) and 100 U/mL penicillin and 100 µg/mL streptomycin (10x stock from GIBCO). Stored at 4°C.
- Roswell Park memorial institute (RPMI) 1640 medium:
  - **RPMI-4**: RPMI 1640 + L-glutamine (300 mg/L) +HEPES (6 g/L) (GIBCO). Unless stated otherwise, medium was supplemented with 10% hiFBS (GIBCO) and 100 U/mL penicillin and 100 µg/mL streptomycin (10x stock, GIBCO). Stored at 4°C.
  - **RPMI-E**: RPMI 1640 + GlutaMAX™ (containing the dipeptide L-alanyl-L-glutamine) (GIBCO). Unless stated otherwise, medium was supplemented with 10% hiFBS (GIBCO), 10 mM sterile-filtered HEPES and 100 U/mL penicillin and 100 µg/mL streptomycin (10x stock, GIBCO). Stored at 4°C.
- Trypsin/EDTA: 0.05% trypsin, 0.5 mM EDTA (10x stock, GIBCO) in PBS. Stored at 4°C.
- Imaging Buffer (IB): 140 mM NaCl, 5 mM KCl, 1.2 mM $MgCl_2$, 2 mM $CaCl_2$ and 5 mM HEPES in H_2O. Adjusted to pH 7.4, autoclaved and stored at room temperature (RT). Before use,10 mM D-Glucose (sterile-filtered 2.5 M stock) was added.
- Phosphate-buffered saline (PBS): 135 mM NaCl, 3 mM KCl, 8 mM Na_2HPO_4 and 2 mM KH_2PO_4 in H_2O. Adjusted to pH 7.4, autoclaved and stored at RT.
- Tamoxifen injection solution: 10 mg/mL tamoxifen (Sigma-Aldrich), 2% ethanol in sunflower oil (THOMY). Tamoxifen was pre-dissolved in ethanol, followed by addition of sunflower oil to final volume. Dissolved under sonication. Stored at -20°C for up to 1 month.
- Tris-buffered saline (TBS): 150 mM NaCl and 10 mM Tris in H_2O. Adjusted to pH 8.0 and stored at RT.
- TBS-T: 0.1% Tween-20 in TBS. Stored at RT.

3.1.4. Antibodies

Table 3. List of primary and fluorescent dye-conjugated antibodies used in the current study.

Antibody	Source	Company & Reference	Dilution	
			WB	**IF**
αSMA Cy3-linked	Mouse	Sigma #C6198	n/a	1:100
Caspase 3	Rabbit	Cell Signaling #9662	1:1000	n/a
CD31	Rat	BD Pharmingen #BD550274	n/a	1:50
cGKI	Rabbit	workgroup Feil (3)	1:5000	1:800
Clathrin HC	Mouse	BD Transduction #610500	1:2000	n/a
eNOS	Rabbit	Santa Cruz #sc-654	1:500	1:100
GAPDH	Rabbit	Cell Signaling #2118	1:1000	n/a
GC-B	Guinea pig	workgroup Schimdt (1)	1:5000	n/a
GFP	Chicken	Abcam #13970	n/a	1:2000
iNOS	Rabbit	Cell Signaling #13120	1:1000	n/a
NG2	Rabbit	Millipore #AB5320	n/a	1:100
nNOS	Rabbit	Thermo Fisher #61-7000	1:1000	n/a
NO-GC β1 1A	Rabbit	workgroup Friebe (4)	n/a	1:1000
NO-GC β1 2A	Rabbit	workgroup Friebe (4)	1:10000	n/a
PARP	Mouse	BD Biosciences #556494	1:1000	n/a
PDE5	Rabbit	workgroup Jaffe (2)	1:20000	n/a
pSer239-VASP	Rabbit	Cell Signaling #3114	1:1000	n/a

Footnotes: Antibody dilutions were prepared in 5% BSA (PanReac AppliChem ITW Reagents), 0.05% NaN_3 in TBS-T for WB and in 1% normal goat serum (Millipore), 0.1% Triton X-100 in PBS for IF; (1) Ter-Avetisyan et al. (2014); (2) Egbert et al. (2016); (3) Valtcheva et al. (2009); (4) Friebe et al. (2007); WB, western blot; IF, immunofluorescence; n/a, not applicable.

Table 4. List of secondary antibodies used in the current study.

Antibody	Source	Company & Reference	Dilution	
			WB	**IF**
HRP-linked anti-rabbit	Goat	Cell Signaling #70749	1:10000	n/a
HRP-linked anti-guinea pig	Donkey	Dianova #706-035-148	1:10000	n/a
HRP-linked anti-mouse	Mouse	Santa Cruz #516102	1:10000	n/a
AF488-linked anti-rat IgG	Goat	Jackson ImmunoResearch #112-545-167	n/a	1:1000
AF488-linked anti-chicken IgY	Goat	Invitrogen #A11039	n/a	1:1000
AF647-linked anti-rabbit IgG	Donkey	Jackson ImmunoResearch #711-605-152	n/a	1:1000

Footnotes: Antibody dilutions were prepared in 1% milk powder in TBS-T for WB and in 1% normal goat serum (Millipore), 0.1% Triton X-100 in PBS for IF; WB, western blot; IF, immunofluorescence; HRP, horseradish peroxidase; AF, alexa fluor; IgG, immunoglobulin G; n/a, not applicable.

3.1.5. Software

In the current study, analysis of images was performed with Fiji (Rueden et al., 2017; Schindelin et al., 2012), while for data analysis both Excel 365 (Microsoft) and Origin2021b (OriginLab) were used. Figures and illustrations were created with BioRender.com (2023) and CorelDRAW 2017 (Alludo).

3.2. Breast cancer cell culture

Breast cancer cell lines have been extensively used in *in vitro* and *in vivo* studies, as they offer a nearly limitless source of uniform, self-replicating material that can be easily grown in standard media using straightforward methods. Much of our current understanding of breast carcinomas comes from research conducted with these cell lines, classified according to the presence/absence of important markers such as ER, PR and HER2. In this study, the cGMP signaling pathway was analyzed at the molecular level in various cultured murine and human breast cancer cell lines.

The collection of murine and human breast cancer cell lines represented different breast cancer subtypes (**Table 5**). The human breast cancer cell lines MCF-7, T47D, MDA-MB-231, MDA-MB-157 (kindly provided by the Prof. H. Brauch, Institute of Clinical Pharmacology and Head of Breast Cancer Susceptibility and Pharmacogenomics, Stuttgart) and SK-BR-3, MDA-MB-468, BT549, Hs578T (kindly provided by Dr. A. Koch and Prof. S. Brucker, Gynecological Hospital, Tübingen) were cultured in DMEM. The murine 4T1 cell line was obtained from the American Type Culture Collection (ATCC) and cultured in RMPI-4 medium. Lastly, the murine E0771 cell line was purchased from CH_3BioSystems and cultured in RPMI-E medium. E0771 cells were also used for *ex vivo* and *in vivo* experiments upon implantation into the 3rd mammary fat pad of female mice (see **3.8**).

Table 5. List of breast cancer cell lines analyzed in the present study.

Name	Origin	Breast cancer sub-type
MCF-7	human	ER+ PR+
T47D	human	ER+ PR+
SK-BR-3	human	HER2 overexpression
MDA-MB-231	human	TNBC
MDA-MB-468	human	TNBC
MDA-MB-157	human	TNBC
BT-549	human	TNBC
Hs578T	human	TNBC
4T1	murine	TNBC
E0771	murine	TNBC

Footnotes: ER+ PR+, estrogen and progesterone receptor positive; HER2, human epidermal growth factor receptor 2; TNBC, triple negative breast cancer.

All cell lines were cultured in a humidified CO_2 incubator (Heracell 150i, Fisher) at 37°C and 6% CO_2. To maintain their growth, cells were either fed with fresh medium (confluence ≤ 60%) or passaged, according to the protocol below. Before use, solutions were warmed to 37°C in a $CuSO_4$-supplemented WNB14 water bath (Memmert). The experiments were performed in

a Herasafe KS18 clean bench (Thermo). The cells were monitored by visual inspection with a halogen lamp Axiovert 40C microscope (ZEISS).

- ❖ Buffers and chemicals: PBS, DMEM, RPMI-4 or RPMI-E, Trypsin/EDTA, and DMSO.

I. Cells were gently washed 1x with PBS and incubated with trypsin/EDTA for 5 minutes at 37°C and 6% CO_2 to detach them.

II. The respective pre-warmed medium was added to stop the trypsin reaction (4x cell suspension volume), the cells were resuspended and centrifuged at 200 rcf for 5 minutes at RT.

III. The supernatant was discarded, and the cell pellet was resuspended in 3 mL medium per 25 cm² growth area. To determine the cell concentration, 2 µL cell suspension was diluted 1:20 in PBS and trypan blue (0.04% final concentration) was added to stain dead cells. The alive cells were counted with a Neubauer improved chamber (MARIENFELD).

IV. The cells were then seeded at the desired density with splitting ratios of 1/2 to 1/15, depending on the cell line (see **Figure S1** for additional information).

V. To freeze cells, the cell pellet was resuspended in 10% DMSO medium (1 mL per 25 cm^2 culture area) and 1 mL aliquots were prepared in cell culture cryogenic tubes (Sarstedt).

VI. Cell aliquots were frozen in a cryo 1°C freezing container (NALGENE) at -80°C. After one week, an aliquot was tested for quality control. If the cells grew normally, the rest of frozen aliquots was transferred into liquid nitrogen for long-term storage.

VII. As necessary, frozen stocks were quickly thawed in the water bath at 37°C. Cells were quickly resuspended and transferred into 9 mL pre-warmed medium to dilute DMSO.

VIII. The cell suspension was then centrifuged at 200 rcf for 5 minutes at room temperature (RT). After centrifugation, the cells were resuspended in fresh medium and plated onto a T25 flask, unless specified otherwise.

3.3. Human-derived samples

Human tissue is essential for cancer research, offering insights into the molecular and genetic traits of cancer cells. Compared to cell lines, tissue samples and organoids yield a more accurate representation of human diseases, enhancing our understanding of cancer biology, susceptibility measurement, and risk factor identification.

3.3.1. Organoids

In cancer research, tumor organoids are 3D structures made from a patient's cancer cells. They maintain the genetic and physical traits of the original tumor. In the present study, patient-derived TNBC organoids were established and cultured by our collaborator C. Öder, MSc (in the working group of Dr. A. Koch and Prof. S. Brucker, Gynecological Hospital, Tübingen). In order to understand the role of the cGMP signaling pathway, $1.5 \cdot 10^5$ organoid cells were seeded in Matrigel (Culturex reduced growth factor basement membrane extract

(BME) type 2, Bio-techne) per 24-well and stimulated with cGMP pathway-modulating compounds and drugs for one week before being collected to perform protein analysis (as described in **3.10**).

3.3.2. Human sections

Human tissue sections are essential tools in cancer research as they enable the study of tumor characteristics, including tissue structure and presence of biomarkers. Breast cancer tissue sections from patient biopsies with different subtypes of breast cancer (triple positive breast cancer (TPBC), ER+PR+, HER2+ and TNBC), were kindly provided by Dr. A. Koch and Prof. S. Brucker from the Gynecological Hospital in Tübingen. Human biopsies were fixed in 4% formaldehyde, followed by dehydration and paraffin embedding. To analyze the presence and localization of the cGMP pathway components, 2.5 µm paraffin-embedded sections were stained (see **3.11.2**) after deparaffination. Deparaffination was performed as follow:

- Buffers and chemicals: toluene, ethanol, H_2O, PBS

I. The paraffin-embedded sections were allowed to equilibrate to RT from storage at 4°C for approximately 30 minutes.
II. Deparaffination occurred though incubation with 100% toluene under a fume hood for 2x 2 minutes at RT.
III. Sections were rehydrated by placing them in a series of decreasing concentrations of ethanol (2x 1.5 minutes in 100% ethanol, 1.5 minutes in 90% ethanol, 1.5 minutes in 80% ethanol, 1.5 minutes in 70% ethanol, 1.5 minutes in 60% ethanol).
IV. Finally, incubation of the sections in PBS for 5 minutes removed any remaining traces of ethanol and it was possible to proceed with the staining as described in **3.11.2** step III.

3.4. Impact of conditioned media

Tumors are characterized by a complex interplay between cancer and stroma cells, which is essential for tumor growth and progression. However, to unravel the specific cell-to-cell interactions involved, simplified systems such as co-cultures of different cell types or stimulations of a single cell type with tumor-conditioned medium (TCM) are required. In this study, the influence of TCM derived from the murine 4T1 cell line on primary VSMCs, possible components of the tumor vasculature, was investigated. Furthermore, it was investigated whether pre-stimulation of the cGMP signaling pathway in the cancer cells might influence the TCM composition.

3.4.1. Isolation of primary VSMCs

The vasculature in tumors is often abnormal, with irregular and leaky blood vessels that contribute to the growth and spread of cancer cells. One of the cell types that can be found in vessels are VSMCs, which are responsible for vessel contraction and relaxation.

- ❖ Buffers and chemicals:
  - ♦ Ca^{2+}-free medium: 85 mM Na L-glutamate, 60 mM NaCl, 10 mM HEPES, 5.6 mM KCl, 1 mM $MgCl_2$, adjusted pH to 7.4 with HCl, autoclave, stored at 4°C.
  - ♦ Lysis buffer A: 0.7 mg/mL papain (P4762, Sigma-Aldrich), 1 mg/mL DTT, 1 mg/mL BSA (A6588, PanReac AppliChem ITW Reagents) in Ca^{2+}-free medium, prepared freshly.
  - ♦ Lysis buffer B: 1 mg/mL hyaluronidase (H3506, Sigma-Aldrich), 1 mg/mL collagenase (C7926, Sigma-Aldrich), 1 mg/mL BSA (A6588, PanReac AppliChem ITW Reagents) in Ca^{2+}-free medium, prepared freshly.
  - ♦ PBS, DMEM and Trypan blue.

I. Mice were sacrificed with CO_2 and death was verified by the loss of the inter-toe reflex.

II. After disinfection of the chest with ethanol, the abdominal cavity was opened, esophagus and trachea were cut, lungs and liver were removed. The aorta was collected by grabbing the heart and cutting along the spine caudal until below the kidneys. Then, the aorta was stored in cold PBS.

III. Under a stereo microscope, the heart and all surrounding tissue were removed until the aorta was fully clean. The aorta was then cut into several pieces (1-2 mm in length).

IV. Aortic pieces were incubated in lysis buffer A (0.25 mL/aorta) for 1 hour at 37°C in the water bath while shaking.

V. Then aortic pieces were centrifuged at 200 rcf for 3 minutes at RT, supernatant discarded and incubated in lysis buffer B (0.25 mL/aorta) for 12 minutes at 37°C in the water bath.

VI. The tissue digestion was stopped by adding full medium and centrifuged at 200 rcf for 8 minutes at RT.

VII. Cells were resuspended in full medium (0.5 mL/aorta). Cell concentration was determined by counting with a Neubauer improved chamber (MARIENFELD), adding trypan blue (0.04% final concentration) to stain dead cells. Note that per aorta usually $2 \cdot 10^5$ VSMCs were isolated.

VIII. The cell suspension was diluted to $3 \cdot 10^5$ cells/mL using DMEM. Subsequently, 1.7 mL ($5 \cdot 10^5$ cells) were added to a 10 cm Petri dish, while 70 µL ($2.1 \cdot 10^4$ cells) were seeded in each well of the scratch assay plate (Culture-Insert 2 well in µ-Dish, Ibidi). VSMCs were cultured until 70-80% confluence (~4 day) or 90-100% confluence (~7 days) at 37°C and 6% CO_2 before proceeding with the desired experiment (see **3.4.2** and **3.5.**)

3.4.2. Conditioned media

The TCM contains soluble factors, such as cytokines, growth factors, and ECM proteins, which are secreted by the tumor cells. These factors may affect the behavior of other cells, such as promoting angiogenesis or enhancing tumor cell migration and invasion. The protocol below describes how the TCM from 4T1 was prepared. Furthermore, to ensure that the observed effects were specific to the TCM, the VSMC conditioned medium (VCM) was included as an additional control condition. A timeline of the experimental workflow is showed in **Figure 6**.

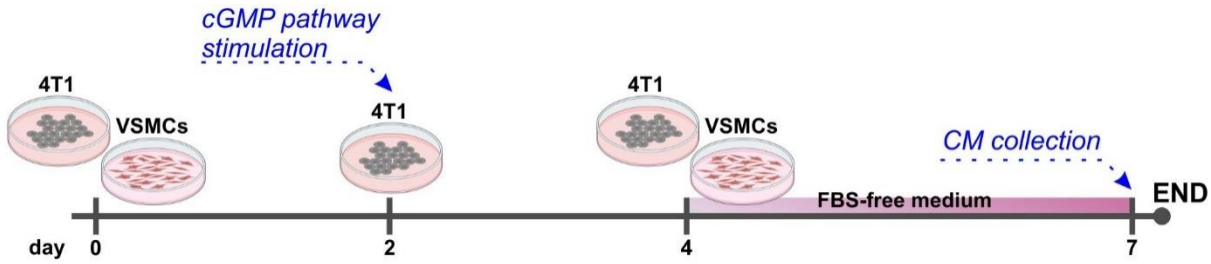

Figure 6. Timeline for the preparation of the conditioned media (CM). 4T1 cells and VSMCs were seeded in 10 cm Petri dishes (day 0). 48 hours after seeding, 4T1 were stimulated with cGMP pathway-modulating compounds/drugs in full medium (day 2). Then, 48 hours after 4T1 cell stimulation and 98 hours after cell seeding, both 4T1 cells and VSMCs were incubated in FBS-free medium (day 4). Collection of conditioned media occurred three day later (day 7), and it was used for further experiments.

- ❖ Buffers and chemicals: PBS, DMEM, RPMI-4, Trypsin/EDTA, trypan-blue.

I. 4T1 and the VSMC cell suspensions were prepared as described in **3.2** and **3.4.1**.

II. $2 \cdot 10^5$ 4T1 cells and $5 \cdot 10^5$ VSMCs were seeded per 10 cm Petri dish and cultured at 37°C and 6% CO_2.

III. When the 4T1 cells reached 70-80% confluency (after 48 hours), they were washed 1x with PBS and incubated with RPMI-4 medium containing the desired cGMP pathway-modulating compound or drug for stimulation.

IV. 96 hours after cell seeding and 48 hours after 4T1 cell stimulation, both cell cultures were washed 2x with PBS and incubated with FBS-free RPMI-4 at 37°C and 6% CO_2 for an additional 72 hours before collecting the conditioned media.

V. The medium from each Petri dish was collected and centrifuged at 15000 rcf for 10 minutes. Then, the supernatant was sterile filtered (0.20 µm pore size CHROMAFIL Xtra PES, MACHEREY-NAGEL) and stored at 4°C.

VI. The different obtained conditioned media were applied to stimulate VSMCs in scratch assay plates (Culture-Insert 2 well in µ-Dish, Ibidi) as described in **3.5**.

3.5. Scratch assay

The scratch assay is a widely used technique to investigate cell migration *in vitro*. It involves creating a scratch or a gap in a layer of cells, and then observing the cells as they migrate and fill in the gap over time. This technique can be used to study the effects of various factors, such as growth factors or drugs, on cell migration.

- ❖ Buffers and chemicals: PBS, DMEM, RPMI-4, Trypsin/EDTA, trypan blue

I. Breast cancer or VSMC cell suspension was prepared as described in **3.2** or **3.4.1**.

II. The cell suspension was diluted to $3 \cdot 10^5$ cell/mL with the respective medium.

III. Carefully 70 µL of the cell suspension ($2.1 \cdot 10^4$ cells) were aliquoted to each well of the scratch assay plate (Culture-Insert 2 well in µ-Dish, Ibidi) as shown in **Figure 7A** and **B**, taking care not to shake the plate as this could have resulted in uneven cell distribution.

IV. When the cells reached 100% confluency (24 hours for the breast cancer cells and 7 days for the VSMCs) the insert was gently removed by using sterile tweezers (**Figure 7C**).

V. 2x PBS washes removed non-adherent cells or cell debris. Cells were then stimulated with the desired cGMP pathway-modulating compound/drug in 1% FBS DMEM (breast cancer cells) or with FBS-free conditioned medium (VSMCs) (**Figure 7D**).

VI. Images of the scratch (**Figure 7E**) were acquired at the timepoint 0 with an EOS 750D camera (CANON). The cells were cultured at 37°C and 6% CO_2. After 24 and/or 48 hours the scratch area was imaged again.

VII. The scratch area was determined with the plugin *"Wound_healing_size_tool_updated.ijm"* of Fiji (Rueden et al., 2017; Schindelin et al., 2012), adjusting the settings according to the picture brightness.

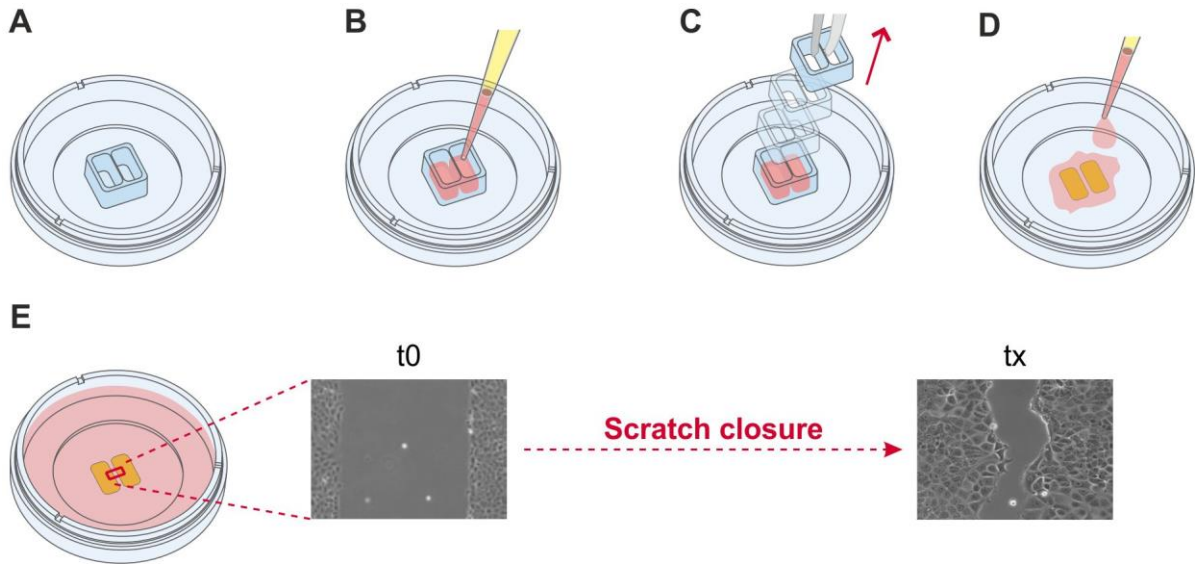

Figure 7. Experimental workflow for scratch assay. A, Culture-Insert 2 well scratch plate from Ibidi; **B**, Seeding of cells; **C**, Removing of the silicon culture-insert; **D**, Filling of the well with medium; **E**, Visualization and documentation of the cell-free gap over time. Figure adapted from Ibidi (2023).

3.6. Real-time growth assay

To assess cell proliferation, growth dynamics, and the impact of cGMP signaling pathway stimulation on breast cancer cells, an impedance-based growth assay was employed. The xCELLigence RTCA DP system (Roche Diagnostics GmbH) enables the real-time monitoring of cell growth using gold microelectrodes fused to the bottom of microtiter well plates (E-Plates) (Agilent, 2023). The electrodes, covering 70-80% of the surface area, measure the electron flow through the bulk solution within each well. Upon attachment to the microelectrodes, the cells obstruct the electron flow between the negative and positive terminals. This electronic readout is shown as a unitless relative value known as cell index (CI). The calculation of CI involves subtracting the background resistance (R_{t0}) measured in presence of only medium in the wells from the resistance at a specific time point (R_{tn}). The magnitude of impedance can be correlated to various cellular processes, such as cell adhesion and proliferation (Limame et al., 2012).

- ❖ Buffers and chemicals: PBS, DMEM, RPMI-4 or RPMI-E, Trypsin/EDTA.

I. Breast cancer cell suspension was prepared as described in **3.2**.
II. Cell suspension was diluted to $5 \cdot 10^4$ cell/mL with the respective medium. If required, the desired cGMP pathway-modulating compounds/drugs were added directly to the cell suspension before seeding.
III. The experimental design was set and scheduled in the RTCA software (step 1: 1 sweep for 1 minute, step 2: 700 sweeps with 15 minutes intervals).
IV. After filling each well of the E-Plate with 100 µL pre-warmed medium, the plate was inserted in the RTCA device for the acquisition of the background resistance (step 1).
V. The E-Plate was carefully removed and 100 µL of the cell suspension were added per well ($5 \cdot 10^3$ cells/well), ensuring an even distribution across the well.
VI. The E-Plate was placed back in the RTCA device and incubated at 37°C and 6% CO_2.
VII. Before starting with step 2, cells were allowed to settle down for 30 min.

3.7. Transgenic and wildtype mice

Animal models serve as a powerful tool, offering the opportunity to observe the vital interconnections between various cell types *in vivo*. This method, complementing the insights gained from *in vitro* studies, broadens our understanding of biological processes and their complexities. In this study, wildtype mice and transgenic mice expressing a FRET-based cGMP biosensor were utilized. The transgenic sensor mice facilitated the identification and characterization of cell types with functional cGMP signaling within the breast cancer TME, while wildtype animals were suitable to test the impact of cGMP-elevating drugs on breast cancer progression.

3.7.1. Animal ethics

All animal experiments performed in this study complied with the ethical guidelines of the EU (Directive 2010/63/EU) and the regulations of the German Animal Welfare Act and the local authority (Regierungspräsidium Tübingen).

3.7.2. Mouse lines

The mice were kept under standard conditions, with a 12-hour light / 12-hour dark cycle, at a temperature of 22°C and humidity of 50-60%. They had *ad libitum* access to tap water and standard rodent chow (Altromin). Experimental animals were housed in type III cages, with 3-5 mice per cage, and each cage was furnished with a wooden tunnel, a plastic house, standard wood bedding and paper. The transgenic mice used in the study had been backcrossed for at least 10 generations on a C57BL/6NCrl (Bl6; Charles River) genetic background. At 3 weeks of age, mice were weaned, ear-tagged, and genotyped as described in section **3.7.3**. All experiments were conducted with mice aged 8-16 weeks old with genotypes specified in **Table 6** and **Table 7**.

Table 6. List of the wildtype and transgenic mice used in this study.

Short name	Systematic name	Description	Ref.
Bl6	C57BL/6NCrl	Wildtype mice, background of all the following mouse lines	(1)
cGi500(L1)	Bl6;129-Gt(ROSA)26Sor$^{tm1.1(ACTB-cGi500)Feil}$	Global expression of cGi500 under the control of the CAG promoter. The cGi500 is targeted to the Rosa26 locus.	(2)
mT/cGi500(L2)	Bl6;129-Gt(ROSA)26Sor$^{tm1(ACTB-tdTomato,-cGi500)Feil}$	Cre-inducible cGi500 expression under the control of the CAG promoter. The Cre/loxP system controls the switch from mTomato to cGi500. The construct is targeted to the Rosa26 locus.	(2)
SMA-CreERT2	Bl6-Tg(Acta2-cre/ERT2)^{51Pcn}	Tamoxifen-inducible CreERT2 expression under control of the *Acta* (αSMA) promoter. The transgene is integrated randomly.	(3)
SM22-Cre	Bl6-Tg(Tagln-cre)^{1Her}	Constitutive Cre expression under the control of the *Tagln* (SM22) promoter. The transgene is integrated randomly.	(4)

Footnotes: Ref., first reference; (1) RRID:IMSR_CRL:027; (2) Thunemann et al. (2013); (3) Wendling et al. (2009); (4) Holtwick et al. (2002).

Detailed information about cGi500 and the cGMP sensor mouse lines cGi500(L1) and mT/cGi500(L2) were provided in section **1.2**. Briefly, cGi500(L1) mice express the cGMP indicator cGi500 globally, while mT/cGi500(L2) mice allow one to control cGMP sensor expression using the Cre/loxP system. To obtain experimental animals with cell type-specific expression of cGi500 in the mT/cGi500(L2) line, mice were intercrossed with different Cre

mouse lines. **Table 7** summarizes the experimental animal lines used in the current study, including information about the breeding plan, final genotype, and specific characteristics that were relevant for our research.

Table 7. Characteristics of the experimental animals used in the current study.

Short name	Breeding plan	Final genotype	Characteristics
Bl6	C57BL/6NCrl x C57BL/6NCrl	C57BL/6NCrl	Wildtype mice.
Global cGi500	C57BL/6NCrl x cGi500(L1)$^{L1/L1}$	cGi500(L1)$^{+/L1}$	Constitutive expression of the cGi500 biosensor in all cells/tissues.
SMA-cGi500	SMA-CreERT2$^{tg/+}$ x mT/cGi500(L2)$^{L2/L2}$	SMA-CreERT2$^{tg/+}$ mT/cGi500(L2)$^{+/L2}$	Inducible expression of the cGi500 biosensor in pericytes/smooth muscle cells
SM22-cGi500	SM22-Cre$^{tg/+}$ x mT/cGi500(L2)$^{L2/L2}$	SM22-Cre$^{tg/+}$ mT/cGi500(L2)$^{+/L2}$	Constitutive expression of the cGi500 biosensor in pericytes/smooth muscle cells

Footnotes: tg, random integration of transgene in the genome; L1, targeted knockin after Cre recombination (1 loxP remained); L2, targeted knockin before Cre recombination (2 loxP); +, wildtype allele.

3.7.3. Genotyping

It is important to accurately determine the genotype of experimental animals when using transgenic mice as a model. Incorrect genotype assignment can lead to misinterpretation of data. Animal genotypes were assessed at the age of 3 weeks and verified again after the experiment ended, if applicable. Genotyping was performed using polymerase chain reaction (PCR). For all the mouse lines, designed primers allowed to distinguish between wildtype and transgenic DNA/alleles either with differences in the sizes or absence of amplified DNA fragments (see **Table 8**).

Table 8. Genotyping PCR primers.

Transgene	Primer name	Sequence (5' → 3')	PCR product size
cGi500(L1) and mT/ cGi500(L2)	BB01 (F)	CTC TGC TGC CTC CTG GCT TCT	wt: 322 bp tg: 249 bp
	BB02 (wt R)	CGA GGC GGA TCA CAA GCA ATA	
	BB03 (ki R)	TCA ATG GGC GGG GGT CGT T	
Cre and CreERT2	Cre800 (F)	GCT GCC ACG ACC AAG TGA CAG CAA TG	wt: none tg: 402 bp
	Cre1200 (R)	GTA GTT ATT CGG ATC ATC AGC TAC AC	

Footnotes: Primers (Sigma-Aldrich) were stored as 25 µM stocks in HPLC-grade H_2O. F, forward primer; R, reverse primer; wt, wildtype; tg, transgenic; bp, base pairs.

❖ Buffers and chemicals:

- ♦ Ear biopsy lysis buffer: 1 mg/mL proteinase K (Genaxxon) in 1x "complete II KCl" reaction buffer (10x stock solution, BIORON).
- ♦ Master mix: 10 mM Tris (pH 8.3), 50 mM KCl, 1.5 mM $MgCl_2$, 0.2 mM of each deoxynucleotide (NEB), 0.3 µM of each primer (see Table 4) and 0.04 U/µL DFS-Taq DNA polymerase (BIORON).
- ♦ 6x DNA loading dye: 30% glycerol, 0.05% bromophenol blue and 0.05% xylene cyanol in TAE. Concentrations correspond to the 6x stock solution used in this protocol. Stored at 4°C.
- ♦ Tris-acetate-EDTA (TAE) buffer: 40 mM Tris, 20 mM acetic acid and 1 mM EDTA in H_2O. Stored at RT.
- ♦ 2% agarose gel: 0.003% Midori Green Advance (NIPPON Genetics) and 2% LE Agarose (Biozym) in TAE.
- ♦ 1 kb Plus DNA Ladder (Invitrogen) and HPLC-grade H_2O (Fisher).

I. Ear biopsies were incubated with 50 µL ear biopsy lysis buffer overnight at 56°C.

II. Tissue lysates were shortly mixed, centrifuged at 18000 rcf for 5 minutes and the supernatant (DNA) was transferred into fresh tubes.

III. Inactivation of proteinase K occurred for 15 minutes at 95°C in a peqSTAR 2X (PEQLAB) thermal cycler. DNA samples were stored at -20°C or PCR was directly performed.

IV. Per tube 2 µL DNA sample was added and filled up to 25 µL with the master mix.

V. The specific transgene PCR program (**Table 9**) was run in a Biometra TAdvanced (Biometra) thermal cycler. After PCR program, 5 µL 6x DNA loading dye were added.

VI. 10 µL of DNA sample or 1 kb Plus DNA Ladder containing DNA loading dye were loaded per pocket of a 2% agarose gel. Bands were allowed to separate for ~30 minutes at 100 V (PowerPac 300, Bio-Rad).

VII. Images of PCR products were acquired using UV light at a ChemiDoc Imaging System (Bio-Rad) with *"Gel Green"* setting.

Table 9. Genotyping PCR programs.

Step	Temperature		Time	Cycle nr.
	cGi500(L1) and mTcGi500 (L2)	***Cre and CreERT2***		
Initial denaturation	95°C	95°C	5 min	1
Denaturation	95°C	95°C	10 sec	35
Annealing	61°C	58°C	30 sec	
Elongation	72°C	72°C	30 sec	
Final elongation	72°C	72°C	5 min	1
Hold condition	8°C	8°C	∞	1

3.7.4. Tamoxifen injection

The SMA-Cre mouse lines used in the current study expressed the tamoxifen-inducible CreERT2 construct. Experimental animals expressing CreERT2 were treated with 1 mg/d tamoxifen (tamoxifen solution in **3.1.3**) by intraperitoneal injection starting at the age of 6 to 8 weeks. Specifically, CreERT2 experimental animals received 2 cycles of tamoxifen injection for 5 consecutive days, with a 9 days break in between, starting 6 weeks before the E0771 cells implantation as described in **3.8.1** (**Figure 8**).

Figure 8. Timeline of tamoxifen injection applied in the current study. Intraperitoneal tamoxifen injection occurred in 2 cycles of 5 consecutive injections, followed by 3 weeks break before tumor cell implantation. Tam, tamoxifen.

3.8. E0771 breast cancer mouse model

Currently, we have a wide range of animal models that can be used to study different human diseases, including breast cancer. These models provide an opportunity to investigate the progression and development of such diseases in a near-to-native environment. Furthermore, the role of specific genes, proteins, and pathways can be analyzed and understood by combining these models with specific transgenic mice.

3.8.1. Tumor cell implantation

For this study, the syngeneic E0771 breast cancer mouse model was utilized. This experimental model involves an orthotopic injection of the murine E0771 breast cancer cells in immunocompetent Bl6 mice aged between 8 to 16 weeks. This approach offered several advantages, including the ability to mimic the breast cancer TME in a close-to-native manner, and the development of an immunocompetent mammary neoplastic model. Furthermore, the cGMP signaling pathway is not present in the E0771 cell line (as shown in section **4.1.1**), allowing us to specifically focus on the analysis of the cGMP pathway in the tumor stroma components. This last point was also facilitated by the common Bl6 genetic background of the E0771 cells and the cGMP sensor mice, allowing syngeneic transplantation for cGMP imaging in cells of the tumor stroma.

- ❖ Buffers and chemicals: PBS, Trypsin/EDTA, RPMI 1640-E, trypan blue and isoflurane (Cp-pharma).

I. The E0771 cells were kept in culture as described in **3.2**. According to the experimental set up of this study, a 70-80% confluent 175 cm^2 flask is suitable for 15 injections.

II. After centrifugation (section **3.2** point II), the medium was discarded, and the cell pellet was washed 2x with PBS and resuspended in 500 µL PBS per 175 cm^2 growth surface.

III. To determine the cell concentration, 2 µL of the cell suspension were diluted 1:20 in PBS, and trypan blue (0.04% final concentration) was added to stain dead cells. The alive cells were counted with a Neubauer improved chamber (MARIENFELD).

IV. The cell suspension was diluted to $16.7 \cdot 10^6$ cells/mL with PBS and the required amount of 0.5-1 mL aliquots (according to the number of mice to inject) was prepared. The aliquots were kept on ice before the injection.

V. The mouse was anesthetized with 5% isoflurane in O_2 with the chamber of the anesthesia unit "RESEARCH" (Eickemeyer). Once anesthesia occurred, isoflurane concentration was set to 1.5-1%.

VI. The mouse was then transferred on a heating pad and placed in supine position, still administrating isoflurane by inhalation. Anesthesia status was tested with the toe pinch reflex before proceeding with the next steps.

VII. The area below the left armpit, around the 3rd mammary fat pad, was carefully shaved with the hair trimmer (Basein). Special care was taken to avoid damaging the nipple or the skin.

VIII. Once the 3rd left nipple was identified, 30 µL of cell suspension ($5 \cdot 10^5$ E0771 cells) were injected into the 3rd mammary fat pad using an Omnican 50 syringe (B. Braun; each indicator on the syringe corresponds to 10 µL).

IX. After the injection of the tumor cells, the animal was returned to its cage. It was closely monitored until it woke up from anesthesia, which typically occurred within a few minutes.

3.8.2. Monitoring of tumor growth

Following the E0771 cell implantation into the 3rd mammary fat pad, daily monitoring was conducted to assess tumor size (and ulceration, if applicable), as well as animal weight and overall condition (i.e., coat care, breathing, movement, and social interaction). Tumor's length (l) and width (w) were measured in mm with a digital precision caliper (0-150 mm). The recorded values were then used to calculate the tumor volume in mm^3 according to the formula $V = w^2 \cdot l/2$. Animals that met the termination criteria prematurely (i.e., tumor with l or w ≥ 13 mm, tumor ulceration, weight loss ≥ 20% during the experiment, or strange behavior) were immediately euthanized and excluded from the experiment.

3.8.3. Pharmacological treatment per os

To investigate the impact of cGMP signaling pathway stimulation on breast cancer, the NO-GC stimulator vericiguat was administered to wildtype mice. To minimize the stress on the animals, pharmacological treatment was given *per os* through their diet. The experimental animals were randomly assigned to control group or treated group. The body weight of mice did not differ

between the groups. Two days prior to tumor cell injection, the animals' diet was switched to either placebo or vericiguat (150 mg/kg) supplemented diet until the end of the experiment (when at least one of the experimental animals had a tumor with l or w ≥ 13 mm, ~21 days after cell injection) (**Figure 9A**). Vericiguat was added to high-fat diet (HFD) for the 1st cohort of animals (**Figure 9B**) and to normal diet (ND) for the 2nd cohort (**Figure 9C**). The vericiguat supplemented diets were prepared by mixing 150 mg of vericiguat per kg of diet (HFD or ND) by Ssniff. In the 1st cohort, a group of animals were fed with ND as further control group (**Figure 9B**). Detailed information of the different diets used in the present study can be found in **Table** S1.

Mice were euthanized, and the experiment ended when at least one of the tumors reached the volume of 1000 mm^3 (l and/or w = 13 mm). Tumors, organs (i.e., spleen, liver) and blood plasma were collected for further analysis. In particular, blood plasma was examined by our collaborator Dr. Ute Hofmann at the Dr. Margarete Fischer-Bosch Institute of Clinical Pharmacology in Stuttgart to determine the circulating drug concentration.

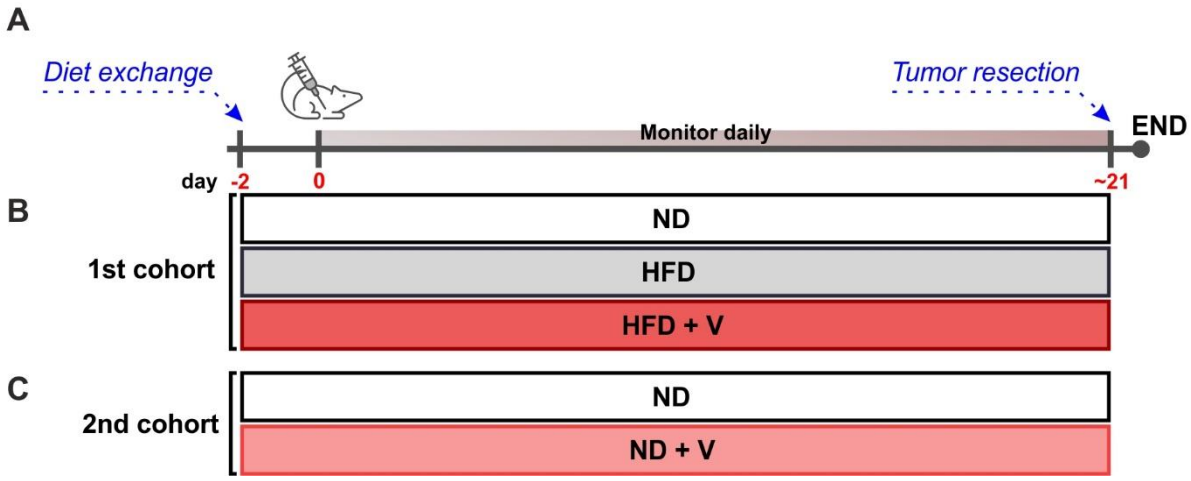

Figure 9. Timeline of the pharmacological modulation *per os*. A, Experimental timeline showing the main time points: diet exchange (day -2), E0771 cell implantation (day 0) and tumor resection (circa day 21) marked in red. **B**, In the 1st cohort, animal groups received normal diet (ND), high-fat diet (HFD) or vericiguat-supplemented HFD (HFD + V). **C**, In the 2nd cohort, animal groups received normal diet (ND) or vericiguat-supplemented ND (ND + V).

3.8.4. Blood pressure measurement

Due to the well-known role of the cGMP signaling pathway in vasodilation, blood pressure was measured with the noninvasive blood pressure system CODA Monitor (Kent Scientific corporation). This tail-cuff system is a specialized tool for measuring the blood pressure of individual mice or rats by a volume pressure recording (VPR) sensor technology, which has been validated and widely used for measuring tail blood pressure (Feng et al., 2008). The CODA monitor, through the occlusion cuff and VPR-cuff, measures six different parameters,

namely systolic, diastolic and mean blood pressure, heart rate, tail blood volume, and blood flow. The devices used in this study enabled simultaneous recording of these parameters in four animals.

During this experiment, E0771 breast cancer cells were not injected. However, the timeline mimicked the time of the experiment described in **3.8.3**. The experimental animals were randomly assigned to control group or treated group. The body weight of mice did not differ between the two groups. Mice were trained to enter in the CODA rodent tubular holder 7 days before the supposed tumor cell injection and 5 days before the diet exchange. In order to compare the effect of vericiguat treatment on blood pressure, three recording sessions occurred before and seven after the diet exchange (**Figure 10**). To limit the variability in the recorded blood pressure values due to their oscillation during the day, all measurements were performed in the morning starting at 10 am.

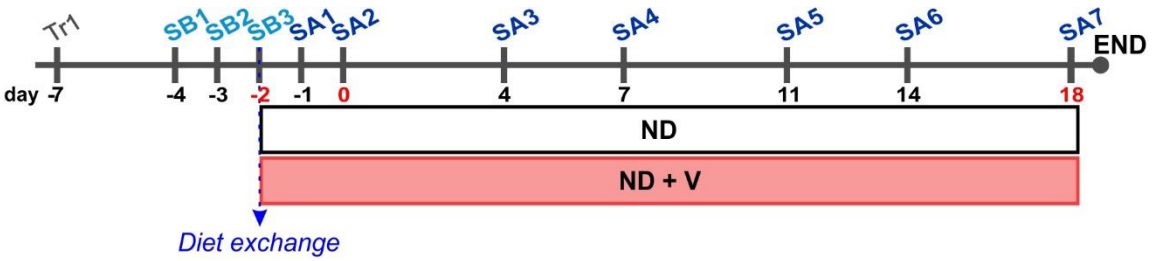

Figure 10. Timeline of the blood pressure measurement. Bl6 mice were acclimated to the system three days prior to beginning blood pressure recording. Blood pressure was recorded in three sessions before the diet was changed to either a normal diet (ND) or a vericiguat-supplemented normal diet (ND + V), and then in seven sessions after the diet change. The sessions before the diet change are marked in light blue (SB), and the sessions after the diet change are marked in dark blue (SA). The day of diet exchange (-2), the supposed tumor cell injection timepoint (0), and the last day of recording (18) before tumor resection or end of the experiment are marked in red. Note that these mice did not receive tumor cells.

I. The warming platform was set to level 5 and the four tubular holders were prewarmed on it.

II. In the CODA software, the user and the mouse identification number were inserted into the database. Then, a new experiment was created assigning user and animals.

III. At the beginning, a new session was initiated, and the settings were configured to have 5 acclimation cycles and 15 cycles per set.

IV. Four mice were gently placed in the tubular holders, with one mouse per holder. It was ensured that the mouse's nose protruded through the hole in the nose cone and its tail extended through the rear hatch. Each holder was then securely fastened, and the tails were covered with a fleece blanket for added comfort.

V. An infrared thermometer was utilized to measure the temperature at the base of the tail of each mouse, which was ensured to be above 35°C.

VI. The cuffs were carefully positioned on the tail of each mouse, starting with the occlusion cuff placed near the base and then sliding the VPR-cuff further up the tail, ensuring there was a small gap between the two. The tubes of the cuffs were fixed to the respective tubular holder. The four tails and cuffs were then covered with the fleece blanket for added comfort.

VII. Mice were allowed to settle down and their blood pressure to stabilize for 2 minutes. Following this, the measurement process started.

VIII. After each session, the mice were returned to their cage. The holders and warming platform were cleaned thoroughly with soap and water.

IX. Before exporting the data, the recorded blood pressure values of each cycle were checked, and any incorrect cycles were excluded from the data set.

3.8.5. Primary tumor resection

To investigate the role of the cGMP signaling pathway in breast cancer lung metastasis, the primary tumor of the E0771 breast cancer mouse model had to be surgically removed upon reaching a volume of 1000 mm^3. Then, the mouse was allowed to survive for further 4 weeks, the time estimated for lung metastases to form. To ensure animal welfare and to prevent infection, surgical procedures were carried out in aseptic conditions using sterile instruments and supplies. Autoclaved instruments (e.g., scissors, forceps, and clamps) could be reused after sterilization, while scalpel blades, suture needles, gauzes were single-use. Personnel wore sterile gloves, masks, and gowns to prevent contamination of the surgical field.

- Buffers and chemicals:
  - Carprofen solution: 1 mg/mL carprofen in NaCl 0.9% (Braun).
  - 3-component narcotic: 500 mg/L midazolam, 50 mg/L medetomidine, 5 mg/L fentanyl in 0.9% NaCl.
  - Antidote solution: 250 mg/L atipamezole, 50 mg/L flumazenil in 0.9% NaCl.
  - NaCl 0.9%, PBS, PFA or IB.

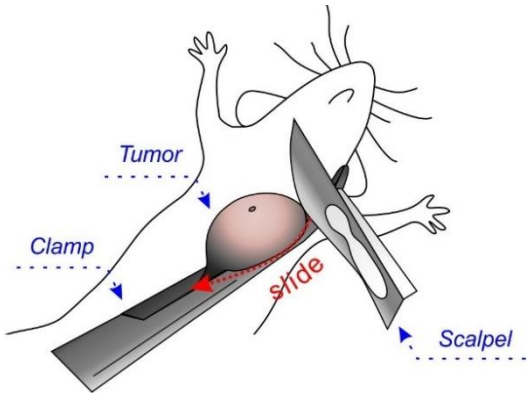

Figure 11. Representation of primary tumor resection in a female mouse. The primary tumor is held from the bottom with a surgical clamp. The scalpel slides over the clamp resecting the tumor with a clean cut.

I. The animal was anesthetized with intraperitoneal injection of the 3-component narcotic (10 µL/g body weight). After injection, the mouse was returned to its cage to wait for the anesthesia to take effect (~20 min).

II. After testing the anesthesia status with the toe pinch reflex, the mouse was placed in supine position on a heating mat and ophthalmic cream (Bepanthen) was applied on its eyes.

III. The tumor area and surroundings were shaved with the hair trimmer (Basein) and sterilized with 70% ethanol.

IV. The primary tumor was resected with a scalpel while holding it from the bottom with a clamp (**Figure 11**). The tumor was washed with PBS, the skin was removed, and it was then placed in a Falcon tube with either ice-cold IB for FRET/cGMP imaging (see **3.9.2** and **3.9.3**) or 4% PFA in PBS for immunofluorescence staining (**3.11**).

V. The wound and surrounding tissue were inspected for any residual tumor tissue or swollen lymph nodes that needed removal. As well, peritoneum integrity was checked to ensure it was still intact.

VI. The wound was sutured using resorbable stitches, making sure no folds were created.

VII. Mice received 100 µL carprofen solution (5 mg/kg animal) to relieve pain, followed by administration of the antidote solution (10 µL/g animal body weight) to terminate anesthesia. Both solutions were given via subcutaneous injection.

VIII. The mouse was returned to its home cage and closely monitored until it was fully awake.

After tumor resection, the mice were monitored twice a day for the first 72 hours and then daily, checking the wound status and the body weight. Furthermore, in the first 72 hours after surgery, 100 µL carprofen solution (5 mg/kg animal) was administrated subcutaneously every 24 hours. Mice were euthanized 4 weeks after the primary tumor resection and the lung collected to analyze breast cancer metastases. Animals that prematurely reached the termination criteria (infected wound, weight loss ≥ 20% during the experiment or strange behavior) were immediately euthanized.

3.9. FRET-based cGMP measurements

The FRET-based biosensor cGi500 (Russwurm et al., 2007) is an elegant tool to visualize changes in cGMP concentration in an alive system after a specific stimulation with cGMP pathway-modulating compounds and/or drugs over time. The structure and mechanism of action of the cGi500 biosensor are explained in **1.2**. In this study, the use of the cGi500 biosensor in cultured breast cancer cells and transgenic mice revealed which components of the cGMP pathway were active in the cancer and stromal cells of breast tumors.

3.9.1. Cell transfection

The process of transfection involves the introduction of genes into cells via expression vectors using various methods such as lipofection. The cGi500 expression vector pCMV-cGi500 (Feil working group) was used to transiently express the biosensor in the breast cancer cell lines mentioned in **3.2**. In this eukaryotic expression plasmid, the expression of the cGi500 biosensor is driven by the strong ubiquitous cytomegalovirus (CMV) promoter (pCMV-cGi500 plasmid map in **Figure S2**). Upon transfection, it was possible to perform real-time imaging of cGMP concentration changes in response to various cGMP pathway-modulating compounds or drugs stimuli in the different breast cancer lines (see **3.9.3**).

- ❖ Buffers and chemicals: PBS, DMEM, RPMI-4 or RPMI-E, Trypsin/EDTA, trypan blue and GenaxxoFect Transfection Kit (containing GenaxxoFect and dilution buffer; GENAXXON)

I. The cell suspension was prepared for the different cell lines as described in **3.2**.

II. $3 \cdot 10^4$ cells were seeded on 12 mm coverslips in each well of a 24-well-plate and cultured at 37°C and 6% CO_2.

III. When the cells reached 50-60% confluency (24 hours after seeding), the two transfection solutions, A (0.3 µg pCMV-cGi500 in 40 µL dilution buffer) and B (2 µL GenaxxoFect in 40 µL dilution buffer) were prepared, vortexed and then mixed together. The resulting mixture (A+B) was vortexed again and incubated for 30 minutes at RT.

IV. The cells were rinsed 1x with PBS and 350 µL fresh full medium was added. Then, 80 µL of the combined transfection solution (A+B) was added dropwise per well. Gently swirling of the plate allowed an even distribution of the solution. The cells were incubated at 37°C and 6% CO_2.

V. After 18 hours, the transfection solution was removed and replaced with fresh medium. Cells were allowed to grow for additional 1-2 days until they reached ~80% of density.

VI. 18-30 hours prior to cGMP imaging experiment, the cells were serum-starved by incubation with FBS-free medium to synchronize the cell cycle.

3.9.2. Preparation of tumor slices

To analyze cells in a close-to-native situation, it is important to shift the focus from *in vitro* cell culture to *in vivo* experiments. The cGi500 biosensor mice enabled real-time cGMP imaging in freshly isolated tissues, which maintain the actual cell composition and cell-to-cell interaction. This tool allowed us to determine which components of the pathway were present in a given tissue or cell type. In this study, primary E0771 breast cancer tumors were harvested from cGMP sensor mice and prepared as follows to perform cGMP imaging.

- ❖ Buffers and chemicals: 70% ethanol, PBS, IB and superglue (Pattex).

I. We proceeded either as described in **3.8.5** or euthanized the tumor-bearing mouse with CO_2 followed by cervical dislocation. The area surrounding the tumor was shaved with the hair trimmer (Basein).

II. Tumor was resected with a scalpel while holding it from the bottom with a clamp (see section **3.8.5** and **Figure 11**) and placed in a Petri dish with PBS.

III. The skin was removed using a scalpel. Then, the tumor was placed and stored in ice-cold IB. The cGMP imaging was performed within the 8 hours following the resection.

IV. The tumor was attached with its mammary fat pad side onto the tape-covered support plate of a VT1200 vibratome (Leica) with superglue. The superglue was allowed to solidify for 10-15 minutes, before transferring the support into the vibratome chamber filled with ice-cold IB.

V. Slices were prepared with a thickness of 500 µm at a speed of 0.3 mm/s and an amplitude of 1.0 mm. Then, tumor slices were transferred into the superfusion chamber (see **3.9.3**) and the rest of the tumor was stored in ice-cold IB. Fresh slices had to be prepared before performing cGMP imaging.

3.9.3. Imaging of cancer cell lines and tumor slices

FRET-based cGMP imaging was conducted as previously described by Thunemann et al. (2013), with slightly different set ups for cell and tissue samples, respectively. For the cell culture, the setup included an Axiovert 200 (ZEISS) epifluorescence microscope equipped with a computer-controlled xenon short-arc lamp and electronic shutter (Oligochrome, TILL Photonics), a HAL 100 light source for brightfield illumination (ZEISS), a long-distance condenser 0.35 with DIC/Senarmount slider, a 1.0/1.6x Optovar lens, and a fluorescence-grade air objective (EC Plan-NEOFLUAR 10x/0.3, ZEISS). YFP fluorescence was detected using a 497/16 nm excitation filter, 516 nm dichroic mirror, and 535/22 nm emission filter, while for FRET-based cGMP imaging, CFP was excited at 445/20 nm. Simultaneous acquisition of CFP and YFP fluorescence occurred though the use of a Dual-View beam splitter (Photometrics) with 480/50 nm and 535/40 nm emission filters for detection of CFP and YFP fluorescence, respectively. For signal acquisition, an electron-multiplying charge-coupled device (EM-CCD) camera (Retiga R1, QImaging) was used at a frame rate of 0.2 Hz and 300 ms exposure time.

To examine tissue samples, a set up was used comprising an upright Examiner.Z1 (ZEISS), a Yokogawa CSU-X1 spinning disk confocal scanner (YOKOGAWA), three diode lasers (445 nm, 488 nm, and 561 nm), and a water immersion objective (W Plan-APOCHROMAT 20x/1.0 DIC (UV) VIS-IR, ZEISS). A CCD camera (SPOT Pursuit, SPOT Imaging) detected mCherry and mT fluorescence using the quad band laser clean-up filter ZET/405/488/561/635M (CHROMA) after excitation with the 561 nm laser, and YFP fluorescence of cGi500 using a 525/50 nm emission filter after excitation with the 488 nm laser. FRET-based cGMP imaging was conducted by exciting CFP with the 445 nm laser and using a Dual-View beam splitter

(Photometrics) with a 505 nm dichroic mirror and 470/24 nm and 535/30 nm emission filters for simultaneous CFP and YFP acquisition. Signals were recorded using an EM-CCD camera (QuantEM 512SC, Photometrics) at 0.2 Hz frame rate and 300 ms exposure time. Both systems were controlled by the VisiView software (Visitron) to acquire images online.

During the experiments, cells and tumor slices were continuously superfused with IB at RT with or without drugs of interest, and the flow rate was maintained at 1 mL/min. The custom-built superfusion system consisted of a fast protein liquid chromatography (FPLC) pump (Pharmacia P-500, GE Healthcare), FPLC injection valves (Pharmacia V-7, GE Healthcare), a magnetic platform (Warner Instruments), a superfusion chamber (RC-26, Warner Instruments), and sample loops of different sizes. Tissue slices were pinned down with a mesh-assisted Slice Hold-Down (SHD-26H/10, Warner Instruments), and the same drug volumes were applied for the same time span to ensure comparable drug exposure between imaging sessions. Excess buffer was constantly removed by a vacuum pump (Laboport N86, KNF Neuberger). FRET/cGMP imaging was performed as follows:

I. The superfusion system was equilibrated with IB buffer using the solvent exchange mode of the FPLC pump (10 minutes at 5 mL/min).
II. The cGi500-expressing samples were prepared via transfection (see **3.9.1**) or tumor slices from cGMP sensor mice (see **3.9.2**). Then, they were placed into the superfusion chamber filled with IB to prevent sample drying.
III. The chamber was placed under the microscope and connected to the in (injection) and out (aspiration) inlets. Superfusion was started and inlets adjusted to ensure a constant and even buffer level and flow.
IV. Through the YFP filter, a suitable field of view was identified.
V. Camera (binning, gain), light source (intensity) and image acquisition (exposure time, frame rate) settings were adjusted, avoiding pixel saturation.
VI. Several regions of interest were selected in the field of view to monitor the recording over time during the measurement.
VII. At the beginning of each measurement, the baseline of CFP and YFP intensities was recorded for at least 2 min.
VIII. Compounds and drugs of interest were diluted in IB shortly before application via the sample loop. The system's dead volumes caused a delay in drug delivery, which was considered during data analysis.
IX. The following application occurred when the CFP/YFP ratio was back to baseline, the sample loops were rinsed 2x with IB and if necessary, focus drift correction was done.
X. At the end of the measurement, additional pictures (e.g., brightfield pictures, yellow and red fluorescence with higher resolution, z-stacks) were acquired, avoiding intense photobleaching before the start of the FRET/cGMP measurement.

XI. The superfusion system was switched off, the sample removed, the superfusion chamber disassembled and the objective wiped with water. Lastly, the superfusion system was flushed with 20% ethanol in solvent exchange mode.

3.9.4. cGMP-imaging analysis and quantification

Analysis of the images acquired in **3.9.3** allowed us to visualize and quantify changes in the cGMP concentration after different stimuli in both transfected breast cancer cells and E0771 breast cancer tumor slices. The images were first processed with Fiji (Rueden et al., 2017; Schindelin et al., 2012) to obtain the values of CFP and YFP intensities over time and then further analyzed with Excel 365 (Microsoft) and Origin2021b (OriginLab).

I. If sample movement occurred during the measurement, image stacks were aligned in x/y dimension using the plugin “MultiStackReg v1.45” of Fiji (Rueden et al., 2017; Schindelin et al., 2012).

II. Only for transfected cells: CFP and YFP intensities were corrected for background fluorescence, whose intensity was calculated in a region of the coverslip without cells.

III. The CFP/YFP ratio, which correlates with the cGMP concentration (R~[cGMP] in all the shown graphs), was calculated.

IV. R~[cGMP], CFP and YFP intensity were normalized to the baseline recorded at the beginning of each experiment.

V. Smoothed R~[cGMP] traces were obtained using the Savitzky-Golay filtering method, paying attention to not change the signal shape.

VI. If baseline drift occurred during the measurement (e.g., due to photobleaching or focus drift), an additional baseline correction was performed with the “Subtract Baseline” tool of Origin2021b.

VII. The area under the curve (AUC) was calculated for each signal using the “Peak Analyzer” tool of Origin2021b.

3.10. Protein analysis

Analysis of (phospho-)proteins in cell and tissue lysates is a highly quantitative and sensitive tool for detecting differences in protein expression and phosphorylation status between experimental groups. In this study, SDS-polyacrylamide gel electrophoresis (SDS-PAGE) followed by Western Blot analysis was used to examine proteins extracted from breast cancer cell lines, organoids, and murine organs. This method allowed us to characterize the expression of the cGMP signaling pathway proteins and cGMP-dependent protein phosphorylation in different breast cancer cell lines. Furthermore, changes in protein expression in patient-derived organoids after stimulation of the cGMP signaling pathway were investigated.

3.10.1. Protein extraction from cells, organoids, and tissues

For all samples (cell lines, patient-derived organoids), proteins were extracted with an SDS-containing lysis buffer supplemented with PMSF and phosphatase inhibitor to inhibit cellular proteases and phosphatases, which might degrade the protein or the phosphorylation of interest. The different lysis protocol for cells, organoids and tissues are described below.

- Buffer and chemicals:
  - 10x PhosSTOP stock: 1 tablet PhosSTOP EASYpack (Roche) in 1 mL H_2O.
  - Cell lysis buffer: 21 mM Tris pH 8.3, 0.67% SDS, 0.2 mM PMSF and 1X PhosSTOP in H_2O.
  - Tissue lysis buffer: 50 mM Tris pH 8.0, 100 mM NaCl, 5 mM EDTA, 2% SDS, 2.5 mM PMSF and 1X PhosSTOP in H_2O.
  - PBS, DMEM, RPMI-4 or RPMI-E.

3.10.1.1. Protocol for cell lysis

I. Cells were cultured until 60-80% confluency as described in **3.2**. Then, cells were serum-starved by incubation with FBS-free medium for 3 hours to synchronize the cell cycle.

II. For cGKI-induced VASP phosphorylation: after serum starvation, cells were stimulated with the desired cGMP pathway-modulating compound/drug in FBS-free medium for 10 min.

III. Samples were washed 2x with ice-cold PBS and then 0.5 mL of lysis buffer were added per 10 cm dish. The cells were detached with a cell scraper (BIOLOGIX).

IV. The viscous protein-containing lysate was transferred into a 1.5 mL tube and immediately denatured for 5 minutes at 95°C in a Thermomixer compact (Eppendorf).

V. Samples were then centrifugated at 18000 rcf for 10 minutes at 4°C. The protein-containing supernatant was transferred into a new tube.

VI. Protein samples were stored at -20°C or immediately processed to determine their concentration and proceed with the SDS-PAGE/Western blot analysis.

3.10.1.2. Protocol for organoid lysis

I. TNBC patient-derived organoids were cultured and stimulated as described in **3.3.1**.

II. After 7 days of stimulation, the medium was removed, and the organoids were resuspended in 1 mL ice-cold PBS to allow Matrigel (Bio-techne) to liquify. Then, this mixture of organoids and Matrigel was transferred in a 15 mL tube and filled up to 7 mL with PBS.

III. Samples were centrifugated at 200 rcf for 5 minutes at 4°C. and the Matrigel-containing supernatant was discarded. The organoid pellet was resuspended in 0.5 mL ice-cold PBS and transferred in 1.5 mL tubes to be centrifugated at 200 rcf for 5 minutes at 4°C.

IV. The supernatant was discarded and 50 µL of cell lysis buffer were added per 1.5 mL tube. Each sample was resuspended vigorously.

V. The protein-containing samples were denatured for 5 minutes at 95°C in a Thermomixer compact (Eppendorf).

VI. Samples were then centrifuged at 18000 rcf for 10 minutes at 4°C and the protein-containing supernatant was transferred into a new tube.

VII. Protein samples were stored at -20°C or immediately processed to determine their concentration and proceed with the SDS-PAGE/Western blot analysis.

3.10.1.3. Protocol for tissues lysis

I. Organs (such as kidneys and brain) were collected from mice euthanized as described in **3.4.1**. The weight of the tissues was determined with an analytical balance (QUINTIX35-1S; SARTORIUS). Then, the tissue samples were shock-frozen in liquid nitrogen. Samples were stored at -80°C, unless they were not immediately processed.

II. The tissue samples were transferred into FastPrep 2 mL Lysing Matrix Tubes, containing ~2 mm Garnet Lysing Matrix A and one 6.35 mm ceramic sphere (all from MP Biomedicals).

III. 7.5 µL of tissue lysis buffer were added per mg of tissue sample (max 1 mL per tube).

IV. Tissues were mechanically disrupted with two cycles of 30 seconds at 6.5 m/s in the FastPrep-24 (MP Biomedicals). After each cycle, samples were centrifugated at 18000 rcf for 2 minutes at 4°C.

V. The protein-containing samples were denatured for 5 minutes at 95°C in a Thermomixer compact (Eppendorf).

VI. Samples were then centrifuged at 18000 rcf for 10 minutes at 4°C and the protein-containing supernatant was transferred into a new tube, avoiding to transfer the upper layer full of fat and the lower layer full of precipitate and sand.

VII. Protein samples were stored at -20°C or immediately processed to determine their concentration and proceed with the SDS-PAGE/Western blot analysis.

3.10.2. Protein quantification

The Lowry method (Lowry et al., 1951) for protein quantification is a protein assay that is very sensitive and not affected by moderate concentrations of SDS. In the present study, the Peterson's modified version of the Lowry (Peterson, 1977) method was used. All samples were analyzed in duplicate or more.

- Buffer and chemicals:
  - Bovine serum albumin (BSA, Sigma-Aldrich) standards: 12.5 to 400 µg/mL BSA serial dilution in H_2O. Stored at -20°C.
  - Total Protein Kit - Micro Lowry - Peterson's Modification (Sigma-Aldrich; contains BSA standard, Lowry reagent, and Folin-Ciocâlteu phenol reagent).

I. The appropriate amount of lysate (5 µL for cell lysates, 2 µL for organoid lysates, 1 µL for organs) was added in 1.5 mL tube and filled up to 100 µL with H_2O. The same amount of lysis buffer was used as the blank control.

II. The BSA standards were used to create a standard curve for determining the protein concentration of each sample. Therefore, 100 µL of BSA standards or H_2O as blank control were aliquoted in 1.5 mL tubes.

III. 100 µL of Lowry reagent were added in each tube, and thoroughly mixed, before 20 minutes incubation at RT.

IV. 50 µL of Folin-Ciocâlteu phenol reagent were then added per tube. Each sample was then thoroughly mixed and incubated for 30 minutes at RT in the dark.

V. For each sample 100 µL were transferred in duplicates to a 96-well flat-bottom plate.

VI. The OD_{620} was measured with a multi-well plate reader (Multiskan EX, Thermo). The protein concentration was determined based on the BSA standard upon subtraction of the respective blank control.

3.10.3. SDS-PAGE and Western Blot analysis

The denatured proteins in this study were analyzed using the SDS-PAGE molecular weight-based separation method (Laemmli, 1970). Subsequently, specific proteins were immunostained using Western Blot (Towbin et al., 1979). This method combined the specificity of the protein's migration behavior with specific antibodies and the high sensitivity of enhanced chemiluminescence (ECL) detection, enabling to detect even small differences in protein levels between samples.

The SDS-PAGE and Western Blot protocols utilized in this study are described below.

- Buffer and chemicals:
  - 4x Tris/SDS pH 8.8: 1.5 M Tris, 0.4% SDS in H_2O. Adjust pH to 8.8, stored at 4°C.
  - 4x Tris/SDS pH 6.8: 0.5 M Tris, 0.4% SDS in H_2O. Adjust pH to 6.8, stored at 4°C.
  - 5x SDS loading dye: 320 mM Tris pH 6.8, 40% glycerol, 15% SDS, 25% 2-mercaptoethanol and 1 mg/mL bromophenol blue. Stored at -20°C.
  - SDS running buffer: 25 mM Tris, 192 mM glycine and 0.1% SDS in H_2O. Stored at RT.
  - Anode buffer I: 300 mM Tris and 20% methanol in H_2O. Stored at RT.
  - Anode buffer II: 25 mM Tris and 20% methanol in H_2O. Stored at RT.
  - Cathode buffer: 40 mM 6-aminohexanoic acid, 25 mM Tris and 20% methanol in H_2O. Adjust pH to 7.6, stored at RT.
  - WB blocking solution: 5% milk powder in TBS-T. Stored at 4°C.
  - ECL substrate: Solution A and solution B of WesternBright Sirius ECL substrate (Biozym) mixed in an equivalent manner.

- Rotiphorese Gel 30 (37.5:1) (Roth).
- TEMED, APS (20% in H_2O).
- Protein ladder (PageRuler Prestained Protein Ladder; Thermo).
- Whatman blotting paper (A. Hartenstein).
- PVDF membrane (Roche).
- H_2O, isopropanol, TBS-T, and antibodies (in **3.1.4** the complete list of primary antibodies (AbI) and secondary antibodies (AbII) used in the current study).

I. The 10% SDS gels were prepared using a Mini-PROTEAN Tetra Cell system (Bio-Rad; 1.5 mm glass plates; 15 pockets/gel), as following:
   - Stacking gel (4%): 0.65 mL Rotiphorese, 1.25 mL Tris/SDS pH 6.8, 3.05 mL H_2O, 10 µL TEMED, and 25 µL APS.
   - Separating gel (10%): 3.30 mL Rotiphorese, 2.5 mL Tris/SDS pH 8.8, 4.10 mL H_2O, 10 µL of TEMED, and 50 µL APS.

   Making sure that the gels were completely polymerized before combs were removed.

II. The protein samples, if necessary, were thawed and diluted to the desired concentration (usually 1-5 µg/µL final concentration) with H_2O and 5x SDS loading dye.

III. The diluted protein samples were denatured for 5 minutes at 95°C in a Thermomixer compact (Eppendorf).

IV. The denatured samples were loaded (usually 10-50 µg total protein) into the 10% SDS gel, adding 5 µL of protein ladder as a size reference.

V. The proteins were allowed to separate in SDS running buffer by applying 100 V for 15 minutes and 120 V for an additional 1 hour (Standard Power Pack P25, Biometra).

VI. To ensure the protein transfer from the SDS gel to the PVDF membrane the sandwich was built and placed in the chamber of a discontinuous Trans-Blot SD Semi-Dry Transfer Cell system (Bio-Rad). The current of 60 mA was applied per blotting sandwich for 85 minutes (Standard Power Pack P25, Biometra).

VII. The PVDF membrane was incubated for 1 hour at RT in WB blocking solution, and then washed 2x with TBS-T. If necessary, the membrane was cut.

VIII. The PVDF membrane was incubated with the AbI (complete list of antibodies used in the current study in **3.1.4**) overnight at 4°C.

IX. 3x washes with TBS-T for 10 minutes were performed before incubation of the PVDF membrane with the HRP-conjugated AbII in 1% milk/TBS-T for 2 h at RT. Then, again 3x washes with TBS-T for 10 minutes were performed.

X. To visualize the different stained proteins, the ECL substrate was added to the PVDF membrane (0.1 mL of solution/cm^2 of membrane) and the chemiluminescence was detected with a ChemiDoc Imaging System (Bio-Rad).

XI. Pictures were also acquired with the "Colorimetric" setting of the ChemiDoc to assign protein sizes to each band using the protein ladder.

3.11. Immunofluorescence on human and murine breast cancer sections

In contrast to the analysis of tissue lysates, staining of tissue sections allows the examination of protein expression at the single-cell level within its native context. Studying protein expression in cells and tissues can be used to investigate a wide range of biological processes, including cell signaling, protein-protein interactions, and disease pathology. In the current study, it was used to visualize the distribution and localization of the cGMP pathway components in sections of human and murine breast tumors.

3.11.1. Fixation and preparation of frozen murine tumor sections

To study protein expression in tissues at the single-cell level, it was necessary to prepare and fix murine tissue, which underwent cutting in 10 µm sections. The process of fixation and preparation involved several steps, which are described below.

- ❖ Buffer and chemicals: PBS, PFA, sucrose, O.C.T compound Tissue-Tek (Sakura)

I. Murine E0771 breast tumors were resected as described in **3.8.5** or **3.9.2** and immediately transferred in falcon tubes containing 4% PFA in PBS.
II. The tissues were fixed for 3 to 4 hours at 4°C. Then, tumors were washed 3x with PBS for 15 minutes and incubated in 30% sucrose in PBS overnight at 4°C.
III. Each tumor was then placed in a mold on dry ice and frozen in O.C.T compound Tissue-Tek.
IV. When Tissue-Tek was completely solidified, tumors were stored at -20°C or cut in 10 µm-thick frozen tissue sections using the HM 505 E cryostat (MICROM) on SuperFrost Plus object slides (Thermo).
V. The tissue sections obtained were allowed to properly adhere onto the object slides for approximately 30 minutes at RT before storing them at -20°C.

3.11.2. Immunofluorescence staining of paraffin or frozen tissue sections

The availability of several fluorescent dyes combined to different antibodies makes immunofluorescence (IF) a suitable tool to detect multiple proteins in a sample. In this work, 4′,6-diamidino-2-phenylindole (DAPI, Invitrogen), a nuclear stain, was combined with green (Alexa Fluor (AF) 488), red (Cy3) or far red (AF647) fluorescence to analyze the colocalization of cell type-specific marker proteins with components of the cGMP signaling pathway. Spectral overlap between fluorescent dyes and reporter proteins was minimized by avoiding multiple green (cGi500 and AF488) or red fluorophores (mTomato and Cy3), increasing the accuracy of their colocalization analysis. The acquired images were then processed with Fiji (Rueden et al., 2017; Schindelin et al., 2012).

- ❖ Buffer and chemicals:
  - ♦ IF washing solution: 0.1% Triton X-100 in PBS. Stored at RT.

- IF blocking solution**:** 1% normal goat serum (Millipore) in IF washing solution. Stored at 4°C.
- PBS, H_2O, antibodies (in **3.1.4** the complete list of primary antibodies (AbI) and secondary antibodies (AbII) used in the current study), DAPI (Invitrogen) and Immu-Mount (Thermo Fisher Scientific).

I. Paraffin sections were processed as described in **3.3.2** before continuing with step III, while frozen sections were allowed to equilibrate from storage at -20°C to RT (typically 20-25°C) for approximately 30 minutes.

II. To remove the O.C.T compound Tissue-Tek, frozen sections were washed 1x with PBS for 10 min.

III. A hydrophobic barrier was drawn around the sections with a Super Pap Pen Liquid Blocker (BIOZOL).

IV. Unspecific antibody binding sites were blocked with IF blocking solution for 1 hour at RT. If necessary, after removal of the IF blocking solution, the hydrophobic barrier was drawn again.

V. Incubation with the AbI occurred overnight at 4°C in a humidified chamber to prevent drying-out. For co-staining, all the AbI were mixed together, avoiding using antibodies with the same species of origin.

VI. Sections were washed 1x with PBS and 3x with IF washing solution for 5 minutes at RT.

VII. Incubation with AbII and DAPI (1 µg/mL final concentration) occurred for 2 hours in the dark at RT. From here, samples were kept in the dark. Fluorescent dye-conjugated primary antibodies (e.g., SMA-Cy3) were also added in this step together with the AbII.

VIII. Sections were washed 3x with IF washing solution for 10 minutes at RT.

IX. The object slide with tissue sections were then quickly immersed in H_2O. Then, all liquid was tried to be removed before proceeding with the next step.

X. An appropriate amount of Immu-Mount was added dropwise per object slide and the coverslip of suitable size was placed, avoiding trapping air bubbles.

XI. Immu-Mount was allowed to solidify, and images were acquired either using the confocal laser scanning microscope (LSM) 710 or the confocal THUNDER Imager Live Cell and 3D Assay microscope (Leica) setup. Specifics of the two systems are given below.

In the LSM 710 setup, the microscope platform was an inverted Axio Observer.Z1 stand (ZEISS). The system included multiple lasers for excitation of different fluorophores: a diode laser (405 nm) for DAPI, a multiline Argon laser (458 nm, 488 nm, and 514 nm) for AF488, a diode-pumped solid-state laser (561 nm) for Cy3, and a He/Ne laser (633 nm) for AF647. Part of the system was also a Plan-APOCHROMAT 20x/0.8 air objective lens (ZEISS) for capturing high-resolution and high-contrast images. The ZEN Black software from ZEISS was used to control the microscope and acquire images.

In contrast, the confocal fluorescence THUNDER setup, located at the Werner Siemens Imaging Center in Tübingen, was equipped with a DMi8 fully motorized inverted microscope

and a K5 scientific complementary metal-oxide-semiconductor (sCMOS) camera (both from Leica). The system included a light-emitting diode (LED3, Leica) light source and multiple filters: LED 405 (ex 375/435 nm; em 450/490 nm) for DAPI, FITC (ex 460/500 nm; em 512/542 nm) for AF488, TXR (ex 540/580 nm; em 592/668 nm) for Cy3, and Y5 (ex 590/650 nm; em 662/738 nm) for AF647. Furthermore, the HC PL FLUOTAR 10x/0.32 and HC PL APO 20x/0.80 air objective lens (Leica) allowed for high-resolution images. The Leica Application Suite X (LasX) software was used to control the microscope and acquire images.

3.12. Statistical analysis

In this study, statistical analysis was performed using Origin2021b (OriginLab). For normally distributed data, Student's t-test (equal variances) was used to determine statistical differences between groups. For multifactorial comparisons, one-way ANOVA and *post-hoc* Bonferroni t-test were utilized. Paired t-test and repeated measures ANOVA were applied to analyze data involving paired samples. However, for non-normally distributed data, Mann-Whitney U or Kruskal-Wallis ANOVA tests were used for single or multiple comparisons, respectively. Wilcoxon signed-rank test or Friedman ANOVA with *post-hoc* Dunn’s test were used for paired non-normally distributed data sets. A P-value of less than 0.05 was considered statistically significant. The significance levels were denoted by asterisks (*), where *$P < 0.05$, **$P \leq 0.01$, and ***$P \leq 0.001$.

4. Results

4.1. The cGMP signaling pathway in breast cancer cell lines

4.1.1. Characterization of the cGMP pathway in several breast cancer cell lines

The conflicting findings from previous research discussed in **1.4** indicate that additional efforts are needed to enhance our understanding of the underlying mechanisms of cGMP signaling in breast cancer and to ultimately exploit this pathway as a therapeutic target. Thus, in this study, the cGMP signaling pathway was characterized in breast cancer cells and other cell types within the TME. Firstly, protein expression of the cGMP pathway components was examined across various human and murine breast cancer cell lines. Furthermore, to evaluate the ability of the GCs to synthesize cGMP, multiple breast cancer cell lines were transfected with pCMV-cGi500, and imaging analysis was performed. YFP fluorescence was employed to identify cells expressing the cGMP biosensor, while FRET/cGMP imaging was utilized to monitor changes of the intracellular cGMP concentration in response to physiological GC ligands such as NO, ANP, and CNP.

The tumor cell lines that were analyzed represented a diverse range of genotypes and phenotypes, originating from both mouse and human subjects, and varied in terms of the presence of markers defining different breast cancer subtypes (see **3.2**, **Table 5** and **Figure S1**). The different breast cancer cell lines were cultured, and protein lysates were prepared to perform Western blot analysis for protein expression. As part of the cGMP pathway components, the three different NOS isoforms responsible for generating NO under physiological conditions were also included in the analysis. The expression of nNOS and eNOS appeared variable among the different cell lines, while iNOS was not detected in any of the tested lines (**Figure 12A** and **Figure S3**). Regarding nNOS, the antibody specificity was doubtful among the breast cancer cell lines, showing several bands. Heterogeneous expression was also observed for the cGMP generators GC-B and NO-GC, as well as the main cGMP effector cGKI and the degrader PDE5. Interestingly, while PDE5 expression varied among all the different cell lines, GC-B, NO-GC, and cGKI were detected only in some of the TNBC cell lines (**Figure 12A** and **Figure S3**).

In accordance with the Western blot analysis, we did not detect an increase of cGMP in the human MCF-7, T47D, SK-BR-3, and MDA-MB-231 tumor cells upon stimulation with ANP, CNP, or the NO-donor DEA/NO during FRET imaging (**Figure 12B**). To ensure the reliability of the cGMP imaging setup, cells were permeabilized with β-escin at the end of the experiment (shown as dashed red line in **Figure 12B**), and then cGMP was directly applied to induce changes in the ratio traces (**Figure 12B**). Concordantly to GC-B expression, cGMP production was observed in BT549, Hs578T and 4T1 upon stimulation with CNP (**Figure 12C** and **D**).

Interestingly, a CNP stimulus also increased cGMP in the MDA-MB-157 cells (**Figure 12C**) despite the Western blot analysis did not show the expression of GC-B (**Figure 12A** and **Figure S3**). This contradictory result might be linked to a low GC-B expression in the MDA-MB-157 cells that was undetectable via Western blot. Additionally, DEA/NO increased intracellular cGMP level in MDA-MB-157, BT549 and Hs578T cells (**Figure 12C**). Of note, the cGMP production correlated well with the NO-GC expression levels, with a strong NO-induced cGMP increase in MDA-MB-157 and a milder one in BT549 and Hs578T cells (**Figure 12A**, **C** and **Figure S3**). On the other hand, MDA-MB-468 cells did not increase cGMP levels upon a DEA/NO stimulus (**Figure 12B**), although weak NO-GC expression was observed by Western blot analysis (**Figure 12A** and **Figure S3**). This might be explained by the presence of an inactive NO-GC enzyme or the use of an inadequate DEA/NO concentration to activate the enzyme. However, the same DEA/NO concentration was able to trigger cGMP production in BT549 and Hs578T cells (**Figure 12C**), which showed similar expression levels of NO-GC compared to the MDA-MB-468 (**Figure 12A** and **Figure S3**). Similarly, E0771 cells did not react to a CNP stimulus, despite the Western Blot analysis showed a band for GC-B (**Figure 12A** and **Figure S3**). Still, this band was not running at the same height as the bands of the positive control or the CNP responding cells (**Figure 12A**). Lastly, the ANP stimulus induced a weak increase of cGMP in the human MDA-MB-157 and the murine 4T1 cells (**Figure 12C** and **D**), suggesting the presence of an active ANP/cGMP pathway. However, the relatively high ANP concentration used (500 nM) could also lead to cross-activation of the CNP receptor, GC-B, which is also present in these cells. To sum up, MCF-7, T47D, SK-BR-3, MDA-MB-231, MDA-MB-468, and E0771 cell lines were classified as cGMP-insensitive, while MDA-MB-157, BT549, Hs578T and 4T1 cell lines were cGMP-sensitive.

It should be noted that the differences in cGMP responses can be observed between and within the breast cancer cell lines that exhibited a reaction (**Figure 12D**). For instance, albeit the MDA-MD-157, BT549, Hs578T, and 4T1 breast cancer cell lines displayed an increase in intracellular cGMP upon CNP stimulation, the percentage of responding cells to this stimulus was variable between cell lines (10% MDA-MB-157, 14% BT549, 48% Hs578T, and 66% 4T1, **Figure 12D**). DEA/NO stimulation, on the other hand, elicited cGMP production in the human breast cancer cell lines but not in the murine ones, again showing different percentage of reacting cells (58% MDA-MB-157, 19% BT549, and 32% Hs578T, **Figure 12D**). To summarize, Hs578T and 4T1 cell lines exhibited a preference for increasing intracellular cGMP in response to CNP stimulation, whereas the MDA-MB-157 cell line showed a stronger inclination towards a DEA/NO stimulus (**Figure 12C** and **D**). Regarding the BT549 cells, despite they showed a stronger cGMP increase after DEA/NO than CNP stimulus (**Figure 12C**), a high portion of the cell population did not react to any stimulus (**Figure 12D**).

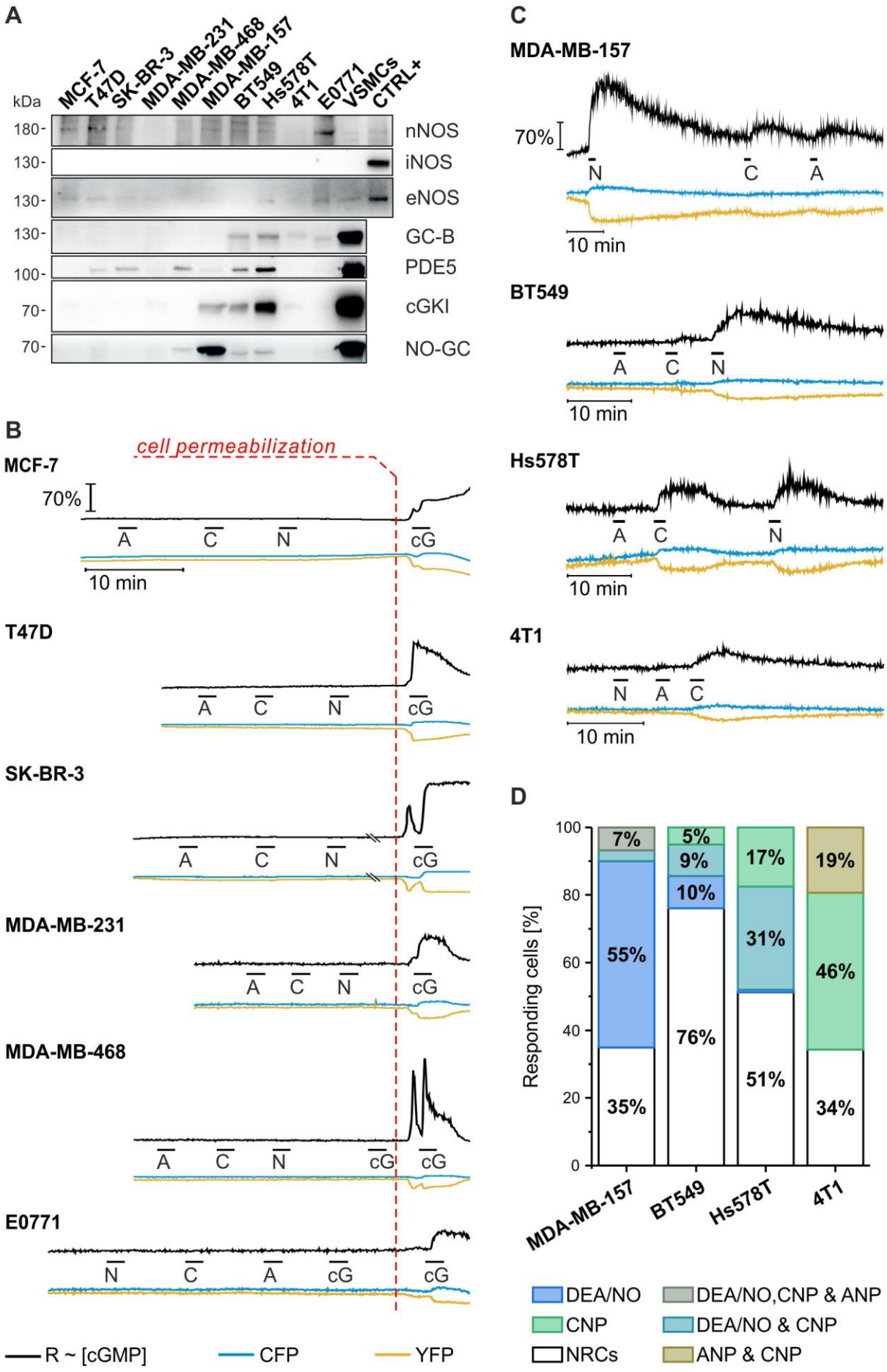
A
MCF-7
T47D
SK-BR-3
MDA-MB-231
MDA-MB-468
MDA-MB-157
BT549
Hs578T
4T1
E0771
VSMCs
CTRL+
kDa
180-
130-
130-
130-
100-
70-
70-
nNOS
iNOS
eNOS
GC-B
PDE5
cGKI
NO-GC
B
cell permeabilization
MCF-7
70%
A
C
N
cG
10 min
T47D
SK-BR-3
MDA-MB-231
MDA-MB-468
E0771
R ~ [cGMP]
CFP
YFP
C
MDA-MB-157
BT549
Hs578T
4T1
D
Responding cells [%]
100
80
60
40
20
0
7%
55%
35%
5%
9%
10%
76%
17%
31%
51%
19%
46%
34%
MDA-MB-157
BT549
Hs578T
4T1
DEA/NO
DEA/NO,CNP & ANP
CNP
DEA/NO & CNP
NRCs
ANP & CNP

Figure 12. Characterization of the expression and activity of the cGMP pathway in different breast cancer cell lines. A, Western blot was used to detect cGMP pathway components in the protein lysates from various breast cancer cell lines. Brain, dendritic cells, and kidney lysates were used as positive controls (CTRL+) for the detection of nNOS, iNOS, and eNOS, respectively, while VSMC lysate was used as a positive control for other proteins. Respective GAPDH for each blot can be found in **Figure S3**. **B** and **C**, Real-time FRET/cGMP imaging was performed upon transfection with the pCMV-cGi500 biosensor plasmid. Cells were stimulated with ANP (A, 500 nM), CNP (C, 500 nM), and DEA/NO (N, 1µM). Representative R~ [cGMP], CFP, and YFP traces of a single cell are shown. The scale on the left of the first ratio trace indicates the 70% change of the ratio trace relative to the baseline. In **B**, cells were permeabilized with β-escin (red dashed line, 0.1 mM) before applying cGMP (cG 100 µM). **D**, The percentage of responding and non-responding cells (NRCs) to ANP, CNP, and DEA/NO stimuli (n ≥ 93 cells from n ≥ 3 independent experiments per cell lines).

The identification of an active NO/cGMP pathway in the TNBC MDA-MB-157, BT549, and Hs578T cell lines provided an opportunity to examine the effects of the NO-GC stimulator riociguat on cGMP production, both individually and in combination with the DEA/NO stimulus. To prevent saturation of the cGMP response and enable the detection of potential riociguat effects, lower concentrations of DEA/NO than before were used (10 or 100 nM compared to 1 µM). This new setup further emphasized the heightened sensitivity of MDA-MB-157 cells to the DEA/NO stimulus compared to BT549 and Hs578T cells. In fact, while 10 nM was sufficient to stimulate MDA-MB-157 cells, ten times more (100 nM) was required for the other two cell lines (**Figure 13**). Notably, the co-stimulation with DEA/NO and riociguat led to a significant increase in cGMP across all three breast cancer cell lines in comparison to the single DEA/NO stimulus (**Figure 13A** to **C**). Likely due to the high expression of NO-GC in the MDA-MB-157 cells (**Figure 12A**), riociguat alone could induce a modest increase in cGMP in these cells (**Figure 13A**), while no change in the ratio trace was recorded after the riociguat stimulus in BT549 and Hs578T cells (**Figure 13B** and **C**). Furthermore, the riociguat vehicle DMSO did not induce any changes in the ratio traces, thus, validating the drug's specific effect (**Figure 13A** to **C**). These results collectively indicate that the NO-GC stimulator riociguat can potentiate NO-induced cGMP signals in the TNBC MDA-MB-157, BT549, and Hs578T cell lines, and this might induce changes in the breast cancer cell behavior and consequently in tumor growth and progression.

Taken together, these findings showed that NO/cGMP and CNP/cGMP signaling pathways are present in some of the examined human and murine breast cancer cells, while assessing the presence of the ANP/cGMP signaling pathway requires further analysis. Moreover, these results indicated that the cGMP signaling pathway might be particularly relevant in TNBC cells. Interestingly, the NO/cGMP pathway in the human TNBC cell lines can be targeted and modulated by the NO-GC stimulator riociguat. Thus, these results suggested that the cGMP pathway could be a potential target for developing specific therapies that are currently lacking for TNBC patients.

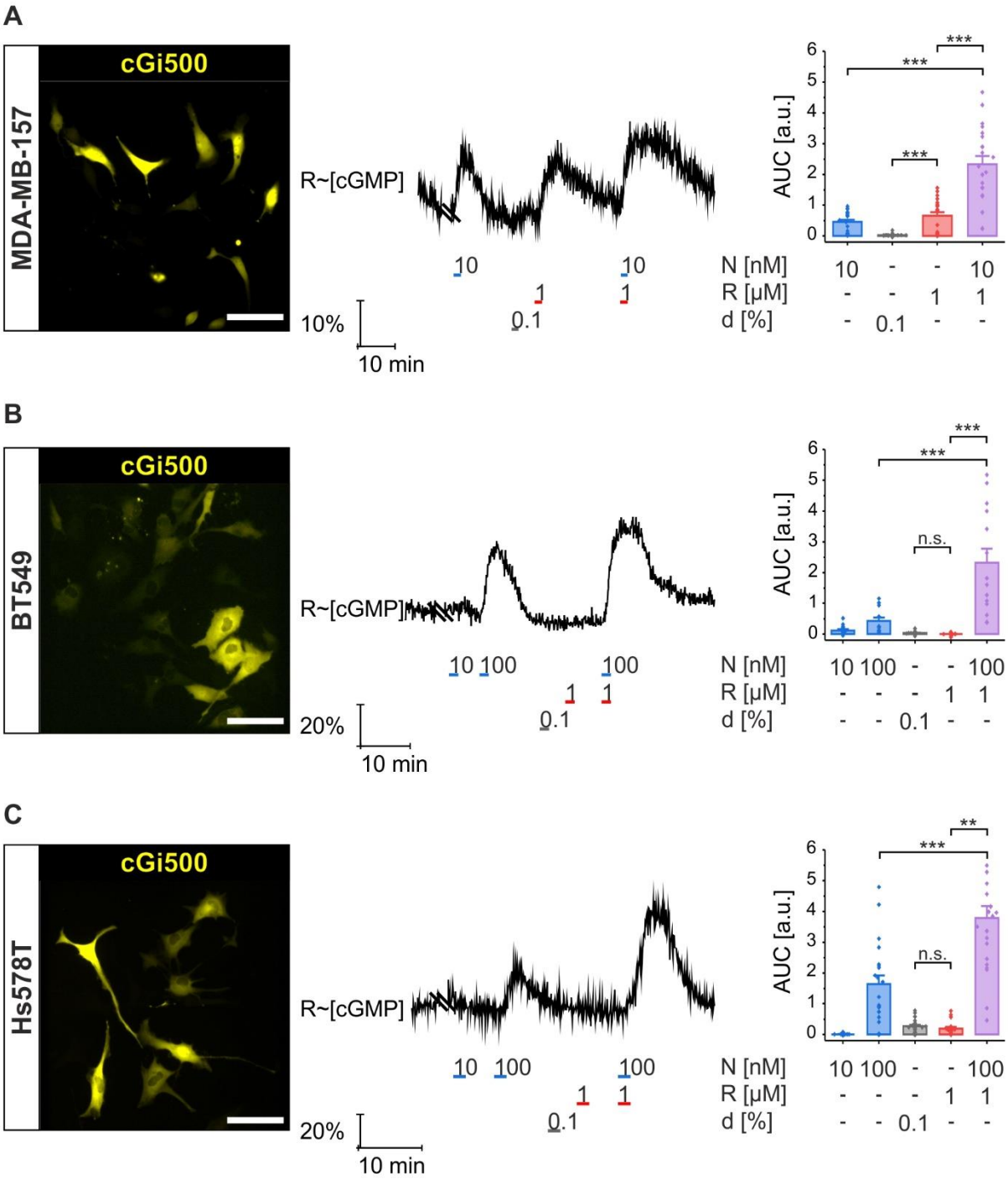

Figure 13. Effect of the NO-GC stimulator riociguat on the DEA/NO stimulus in NO-responsive breast cancer cells. Real-time FRET/cGMP imaging was performed upon transfection with the pCMV-cGi500 biosensor in MDA-MB-157 (**A**), BT549 (**B**), and Hs578T (**C**) cells. During the measurements, DEA/NO (N), riociguat (R), DMSO (d, riociguat vehicle) or a combination of DEA/NO and riociguat were superfused for 2 minutes each (concentration as indicated in the figure). The panels show (from left to right) the fluorescence images of the transfected cells, a representative ratio trace R~[cGMP] of a single representative cell and the statistical analysis of the AUC of cGMP signals recorded after each application. Yellow color shows YFP fluorescence of cGi500, not cGMP. Data represent mean ± SEM of n ≥ 15 cells per condition from one of three representative measurements.

4.1.2. Functional effects of the cGMP pathway in the Hs578T cell line

To understand the functional role of the cGMP signaling pathway in breast cancer cells, the influence of the pathway stimulation on cell growth and migration was investigated (**Figure 14**). Special attention was given to the cGMP-sensitive Hs578T cells, which expressed the vasodilator-stimulated phosphoprotein (VASP, data not shown), a well-known target of cGKI. To assess the activity of cGKI in these cells, the cGKI-specific phosphorylation of VASP at residue Ser239 was examined using a phospho-specific antibody following pathway stimulation with GC ligands ANP, CNP, and the NO-donor DETA/NO. Additionally, cGMP and the cGMP analog 8Br-cGMP were included as negative and positive controls, respectively. Indeed, cGMP is unable to diffuse through the cell membrane due to its high negative charge, unless in the presence of special transporters. On the other hand, 8Br-cGMP is a cell-permeable analog which directly activates cGKI. In Hs578T lysates, p239-VASP phosphorylation was detected after stimulation with 8Br-cGMP, as well as after CNP, ANP, and DETA/NO stimulations (**Figure 14A**). In contrast, unstimulated and cGMP-stimulated cell lysates did not show any basal level of p239-VASP (**Figure 14A**). The magnitude of the post-translational modification induced by the different compounds might be related to the varying expression of the GCs in this cell line. As shown in **Figure 12D**, Hs578T cells responded preferably to the CNP stimulus in comparison to NO stimulus. Additionally, it has to be considered that the loading of the DETA/NO-stimulated sample was less than the other conditions (**Figure 14A**), making difficult the comparison between NO stimulus and the other conditions. However, the weak ANP-induced VASP phosphorylation was in contrast with the previous FRET/cGMP results, where the ANP stimulus did not increase intracellular cGMP levels (**Figure 12C**). This discrepancy might be explained by the unspecific activation of GC-B, as hypothesized for the weak FRET signal recorded after the ANP stimulus in the MDA-MB-157 and 4T1 cell lines. Altogether, these results demonstrated that the downstream cGMP/cGKI pathway is functionally present in Hs578T cells, and upon stimulation, cGKI can phosphorylate its targets.

Next, we explored the impact of cGMP pathway activation on Hs578T cell growth. We stimulated the cells with 8Br-cGMP over a one-week period and cell growth was constantly monitored via the xCELLigence RTCA DP system. Significantly, the Hs578T cells demonstrated a marked decrease in growth upon treatment with 8Br-cGMP, compared to the control group. This reduced growth rate became notably significant after seven days of continuous stimulation (**Figure 14B**).

We then investigated whether cell migration might also be influenced by cGMP stimulation using the scratch assay. To add another layer to the investigation, we incorporated pharmacological modulation of the cGMP signaling pathway by treating the cells with the

NO-GC stimulator riociguat. As demonstrated in **Figure 13C**, riociguat significantly potentiated the DEA/NO-induced cGMP increase. However, after 24 hours, the scratch was completely closed, and no differences in cell migration were observed between the tested conditions (**Figure 14C**).

These results imply that the stimulation of Hs578T cells with CNP and NO has the potential to activate the cGMP effector cGKI. Interestingly, direct activation of cGKI with 8Br-cGMP appeared to influence cell growth, although it did not affect cell migration. Nonetheless, a more comprehensive investigation is necessary to fully elucidate the role of the cGMP signaling pathway within the context of Hs578T cells and other breast cancer cell lines, especially its potential to influence tumor cell migration.

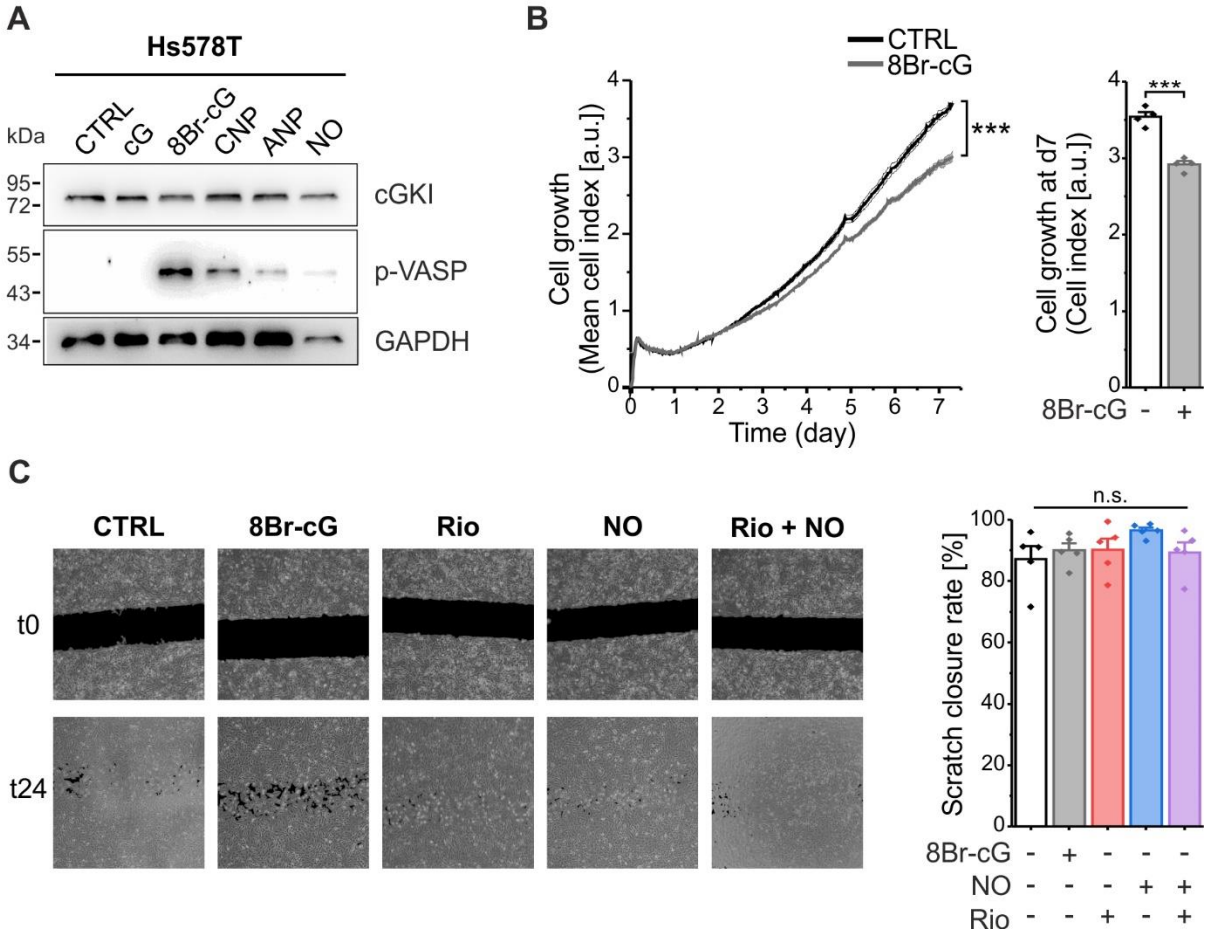

Figure 14. Activation of the cGMP pathway in Hs578T cells. A, Western blot analysis of cGKI, phospho(Ser239)-VASP (p-VASP), and GAPDH (as housekeeping gene) in Hs578T cells after 10 minutes of stimulation at 37°C and 6% CO_2 with cGMP (cG, 100 nM), the cell-permeable cGMP analog 8Br-cGMP (8Br-cG, 500 µM), CNP (250 nM), ANP (250 nM), or DETA/NO (10 µM). This analysis was performed in 2 independent experiments. **B**, Hs578T cell growth with and without 8Br-cG (500 µM) is illustrated as an xCELLigence growth curve (left) and cell index at day 7 (right) of n = 4 wells per condition of one out of three representative experiments. **C**, Analysis of cell migration using the scratch assay. Representative images of the scratch at time 0 (t0) and after 24 hours (t24) on the left, and quantification of the scratch closure rate of n = 5 experiments on the right. The cells were stimulated with 8Br-cG (500 µM), riociguat (Rio, 1 µM), DETA/NO (NO, 10 µM) or a combination of Rio (1 µM) and NO (10 µM). Data represent mean ± SEM.

4.1.3. Stimulation of the cGMP pathway in 4T1 cells and influence of 4T1 tumor-conditioned medium on VSMC migration

Among the cell lines utilized in this study, the 4T1 cells were unique in that they exhibited only a single cGMP pathway, namely the CNP/cGMP pathway. Previous research has highlighted the involvement of this pathway in the growth of murine melanoma B16F10 cells (Dhayade et al., 2016). Thus, it became imperative to investigate if this pathway might perform similar functions in different types of cancer.

The unknown CNP/cGMP pathway effectors present in the 4T1 cell line were activated through either physiological CNP stimulation or direct application of the cGMP analog 8Br-cGMP. However, intriguingly, the stimulation of the cGMP signaling pathway in 4T1 cells did not influence their growth or migration (**Figure 15A** and **B**).

That said, the stimulation of the cGMP signaling pathway could potentially lead to intracellular modifications, impacting not only phenotypical characteristics but also interactions with other cells present in the TME. Thus, we established a simplified system to investigate potential interactions between the 4T1 cancer cells and potential stromal cells. In particular, we examined the impact of the TCM from 4T1 cells on the migration of VSMCs.

As outlined in section **3.4.2**, to produce the TCM, 4T1 cells were seeded and allowed to grow until confluence was achieved. Subsequently, the 4T1 cells were incubated for 72 hours with FBS-free medium, which was then collected and filtered to treat VSMCs (see timeline in **3.4.2**). Remarkably, the resulting 4T1 TCM significantly enhanced VSMC migration compared to both FBS-free medium (FM) and VCM, the conditioned medium derived from incubation of VSMCs with FBS-free medium (**Figure 15C**). The absence of a migratory effect induced by VCM further attested the migration-enhancing effect provided specifically by the TCM, indicating the involvement of a factor secreted by the 4T1 cancer cells.

The next phase of our investigation was to explore whether activating the cGMP signaling pathway in 4T1 tumor cells might alter the composition and effect of the TCM derived from them. Thus, we stimulated the 4T1 cells with 8Br-cGMP or CNP for 48 hours, prior to the 72-hour incubation with FBS-free medium, ensuring no residual drug-containing medium remained in the plates (see timeline in **3.4.2**). Interestingly, the TCM derived from 4T1 cells pre-stimulated with 8Br-cGMP (4T1 TCM 8Br-cG) significantly attenuated the pro-migratory effect induced by 4T1 TCM in VSMCs (**Figure 15C**). A similar trend (P-value 0.08) was observed with the TCM derived from CNP pre-stimulated 4T1 cells.

These results imply that while stimulation of the cGMP signaling pathway may not directly influence 4T1 cell growth or migration, it could provoke alterations in the secretion of factors by these tumor cells, thus, affecting the behavior of other cells in the tumor stroma. In

particular, this secreted factor(s) seemed to influence the migration of VSMCs, which might influence vessel formation and function *in vivo*. However, further investigation is required to unravel the molecular mechanism governing this intercellular crosstalk, including the identification of both the cGMP effector and the yet-to-be-determined secreted factor.

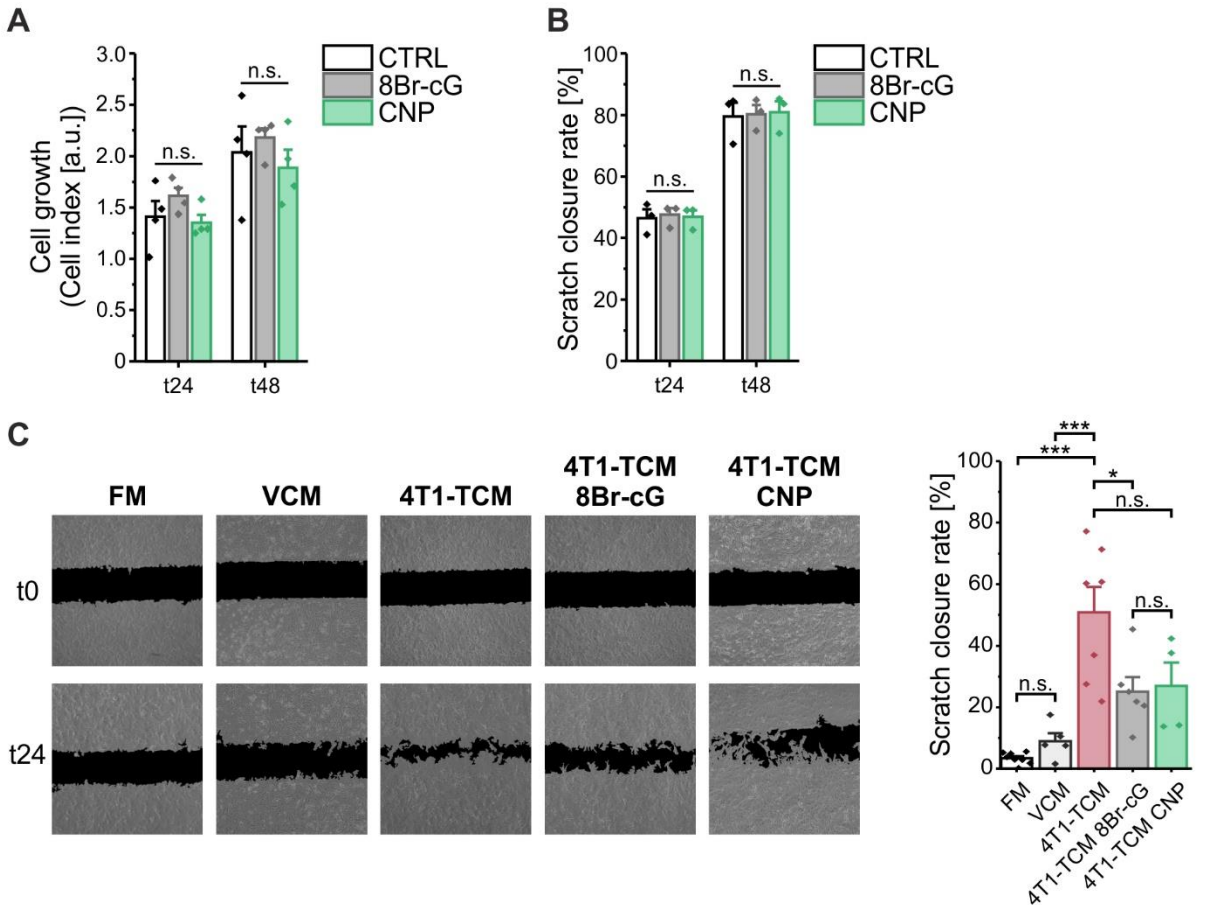

Figure 15. Activation of the cGMP pathway in 4T1 cells and its effect on the 4T1 TCM. A, 4T1 cell growth as cell index at 24 and 48 hours of n = 4 wells per condition of one out of three representative experiments. **B**, Quantification of 4T1 cell migration based on the scratch closure rate at 24 and 48 hours of n = 3 experiments. **C**, Effect of TCM from 4T1 cells on the migration of VSMCs. Representative images of the scratch at time 0 (t0) and after 24 hours (t24) on the left, and quantification of the scratch closure rate after treatment with FBS-free medium (FM), VSMC conditioned medium (VCM), 4T1 tumor conditioned medium (4T1-TCM), TCM of 4T1 cells pre-stimulated with 8Br-cGMP (4T1-TCM 8Br-cG) or CNP (4T1-TCM CNP) on the right (n ≥ 4 experiments). In the experiments shown in this figure, the 4T1 cells were stimulated with 8Br-cGMP (8Br-cG, 500 µM) or CNP (100 nM) as indicated. Data represent mean ± SEM.

4.2. The cGMP signaling pathway in patient samples

4.2.1. Effect of NO-GC stimulator on TNBC patient-derived organoids

The characterization of the different breast cancer cell lines showed that the cGMP signaling pathway seems to be active in some, but not all, TNBC cell lines (**Figure 12**) and might influence the cancer cell growth (**Figure 14B**). Furthermore, riociguat potentiated the NO-induced cGMP signals in the three human TNBC cell lines expressing NO-GC (**Figure 13**). As mentioned in **1.3.4**, organoids are a suitable tool to investigate drug efficacy in a context closer to human diseases. For this reason, we tested whether the modulation of the cGMP signaling pathway might influence the behavior of TNBC patient-derived organoids. Organoids were cultivated for 7 days in presence of 8Br-cGMP, riociguat, DETA/NO, or a combination of riociguat and DETA/NO. Then, they were collected, and protein lysates were prepared for Western blot analysis as described in **3.3.1** and **3.10.1.2**. The imaging of organoids prior to lysis revealed morphological differences between the riociguat-treated and the control samples. Organoids treated with riociguat alone or in combination with DETA/NO showed a less defined border than the control (**Figure 16A**), suggesting an effect on cell viability.

First, the patient-derived organoid line was characterized by the presence of the cGMP pathway components. Expression of NO-GC was detected via Western blot analysis, validating the presence of the riociguat target in this patient-derived organoid line (**Figure 16B**). However, it was not possible to detect cGKI (**Figure 16B**), leaving an uncertainty regarding the cGMP effector present in these organoids.

As we observed a difference in organoid culture morphology (**Figure 16A**), we further analyzed if apoptosis was affected by the treatment. Western blot analysis showed a trend for increasing Caspase 3 expression in the treated groups in comparison to the control (**Figure 16B**), reaching a significant difference for the riociguat-treated condition (**Figure 16C, left bar graph**). The combination of riociguat and DETA/NO did not lead to any potentiated effect (**Figure 16B** and **C**). However, detection of the full-length Caspase 3 is not indicative of its activity. For this reason, its downstream target PARP was checked, which once cleaved leads to apoptosis (Mashimo et al., 2021). PARP expression appeared to be slightly higher in the treated conditions compared to control (**Figure 16B**). However, looking at the ratio of the cleaved PARP over the full-length PARP showed that organoids treated with riociguat or DETA/NO might had less cleaved PARP in comparison to the control, although no statistical significance was reached (**Figure 16C, right bar graph**). Thus, the higher Caspase 3 expression in the treated groups might indicate a decrease in active Caspase 3, consequently leading to less cleaved PARP and apoptotic events. Taken together, these results showed that these patient-derived organoids express NO-GC and modulation of the cGMP signaling pathway might decrease apoptosis in a cGKI-independent manner.

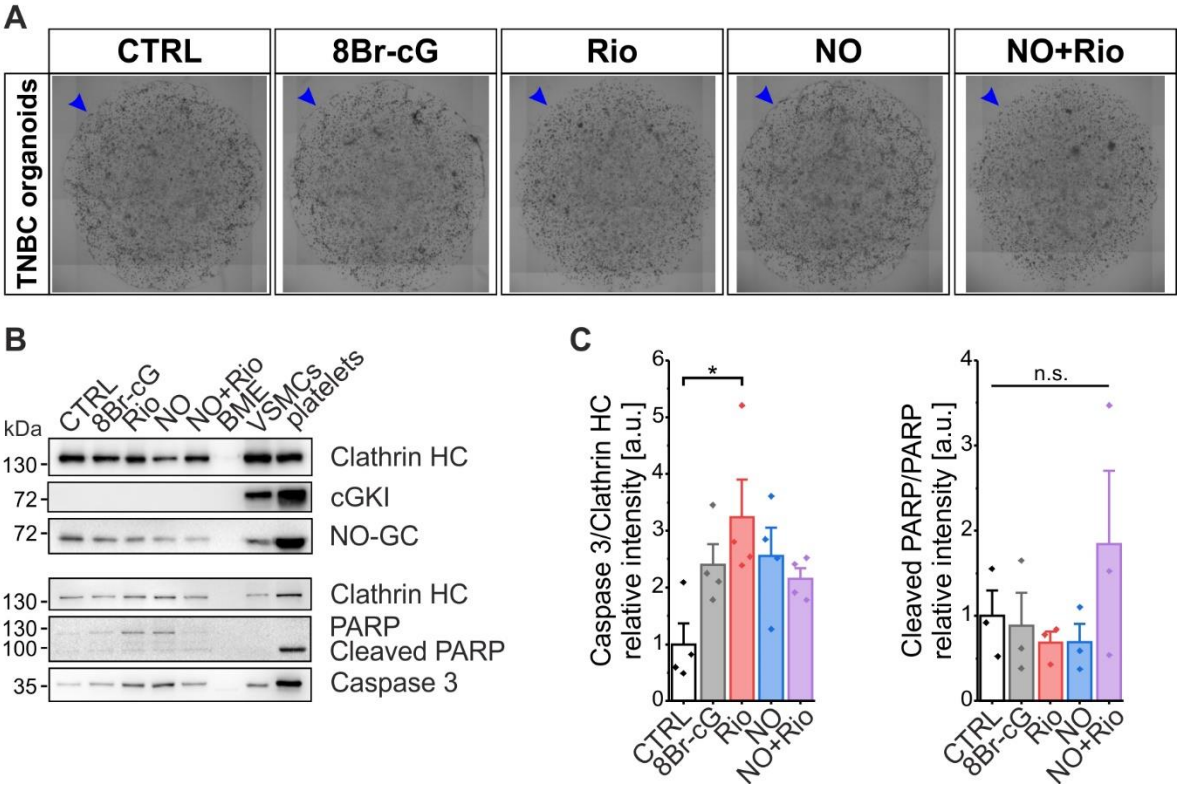

Figure 16. Stimulation of the cGMP pathway in TNBC patient-derived organoids. A, Representative brightfield images of patient-derived TNBC organoids after 7 days stimulation with 8Br-cGMP (8Br-cG, 2 mM), riociguat (Rio, 10 µM), DETA/NO (NO, 10 µM) or a combination of Rio (10 µM) and NO (10 µM). Blue arrowheads indicate organoid culture borders. **B**, Western blot analysis of cGKI, NO-GC, PARP, Cleaved PARP, Caspase 3 and Clathrin heavy chain (HC, as housekeeping gene) in organoid lysates. Matrigel (BME) was included as negative control, while VSMC and platelet lysates were used as positive controls. **C**, Densitometric analysis of Western blot bands. Data represent mean ± SEM of n ≥ 3 experiments with the same organoid line.

4.2.2. Localization of cGMP pathway components in human breast cancer biopsies

In our efforts to understand the role of the cGMP pathway in breast cancer, we investigated not only cell lines and organoids but also human biopsy samples. The analyzed samples were representative of 4 different breast cancer subtypes: TPBC, ER+PR+, HER2+, and TNBC. This set of samples provided us with a more comprehensive representation of the disease in real-world clinical scenarios and allowed us to visualize the heterogeneity in terms of cGMP pathway expression among breast cancer subtypes. We performed IF staining to identify the expression and spatial distribution of NO-GC and cGKI in both the cancer cells and the surrounding stromal cells. To differentiate more effectively between cancer and stromal cells, as well as to visualize the tumor vasculature, we co-stained the sections with CD31 and SMA. CD31 is a marker of endothelial cells, while SMA serves as a marker for perivascular cells, such as pericytes and smooth muscle cells.

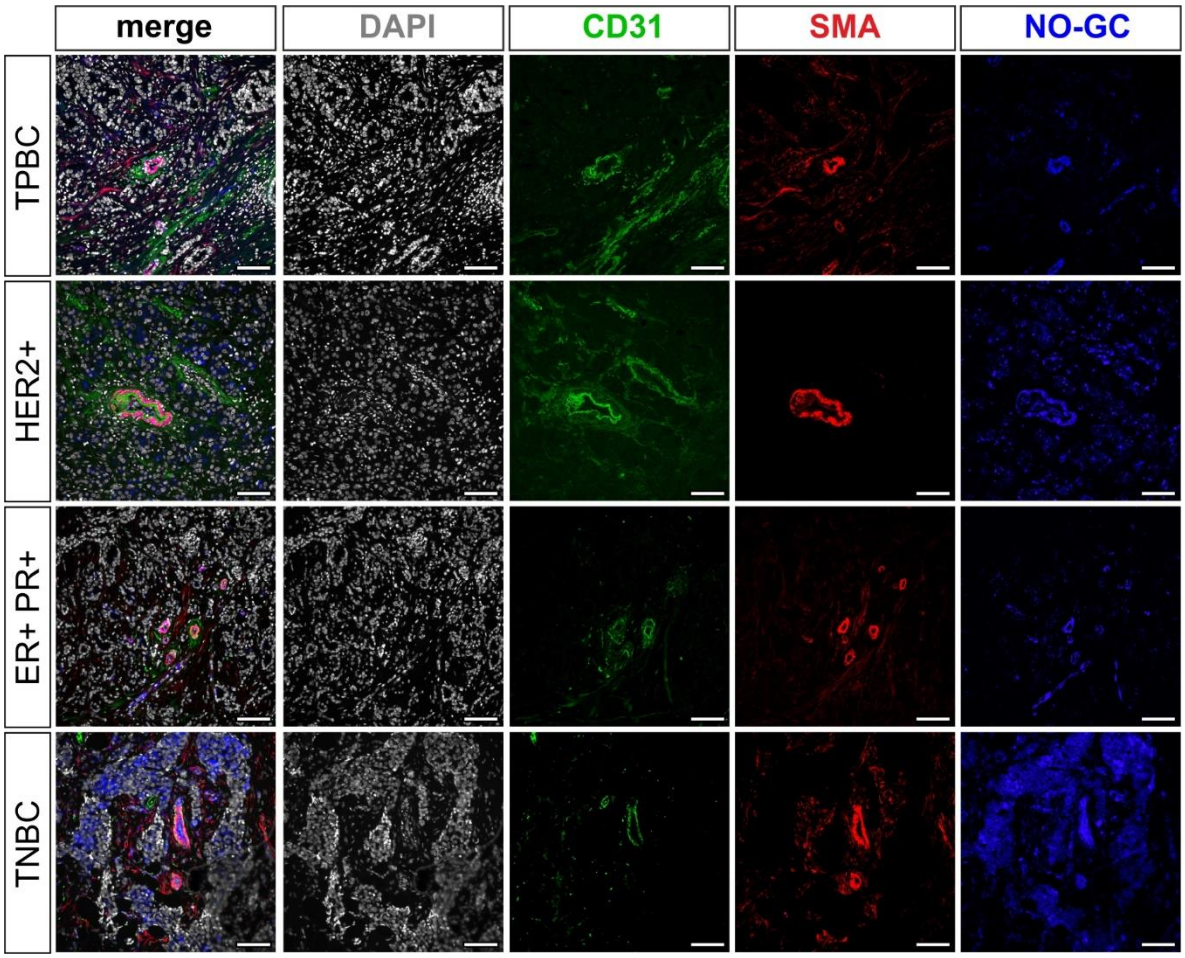

Figure 17. Expression of NO-GC in human biopsies of different breast cancer subtypes. TPBC, HER2+, ER+ PR+, and TNBC patient-derived 2.5 µm paraffin-embedded sections underwent IF staining using DAPI as a nuclear marker, CD31 as an endothelial marker, SMA as a smooth muscle/pericyte marker, and NO-GC to determine its localization. The panels display (left to right) for each breast cancer subtype a merged image (Gray: DAPI; Green: CD31; Red: SMA; Blue: NO-GC) and the four distinct single channels. The images are representative for n = 1 patient biopsy per breast cancer subtype. Scale bars, 100 µm.

The IF staining demonstrated a heterogeneous expression of NO-GC across various breast cancer subtypes. Specifically, no NO-GC expression was detected in the cancer cells of the TPBC and ER+PR+ subtypes. In contrast, cancer cells showed a weak expression in the HER2+ subtype and a notably strong expression in TNBC (**Figure 17**). This last result further supported our *in vitro* data about the importance of the cGMP signaling pathway in TNBC. However, despite the heterogeneous NO-GC expression among cancer cells, the stromal compartment exhibited a more consistent expression of NO-GC, which could be observed in SMA-positive ring or tubular structures (**Figure 17**). These structures were identified as pericytes/smooth muscle cells of either blood vessels, when they were in close proximity to CD31 staining, or mammary ducts, when they were not adjacent to any CD31 staining.

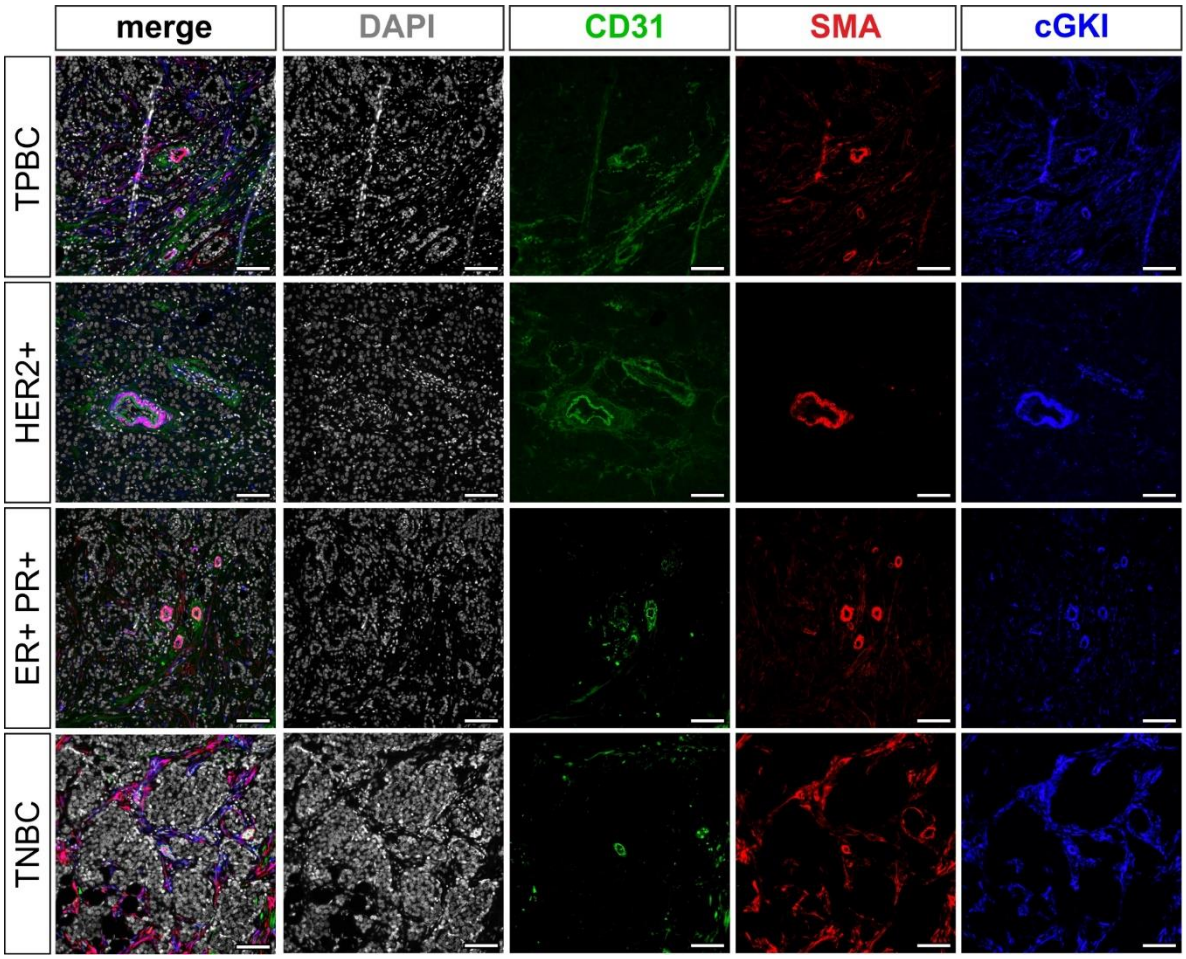

Figure 18. Expression of cGKI in human biopsies of different breast cancer subtypes. TPBC, HER2+, ER+ PR+, and TNBC patient-derived 2.5 µm paraffin-embedded sections underwent IF staining using DAPI as a nuclear marker, CD31 as an endothelial marker, SMA as a smooth muscle/pericyte marker, and cGKI to determine its localization. The panels display (left to right) for each breast cancer subtype a merged image (Gray: DAPI; Green: CD31; Red: SMA; Blue: cGKI) and the four distinct single channels. The images are representative for n = 1 patient biopsy per breast cancer subtype. Scale bars, 100 µm.

cGKI expression did not localize in the cancer cell areas of the different tumor biopsies, but rather in the stroma cells sharing strong colocalization with SMA (**Figure 18**). Similar to NO-GC, cGKI was found in blood vessels and mammary ducts. However, it should be noted that these results are based on a limited sample number. Given the observed heterogeneity in the cGMP pathway expression in breast cancer cell lines, further investigations with more biopsies from different patients are needed to fully understand the potential of this pathway as target in breast cancer cells.

Nevertheless, these findings suggest that modulation of the cGMP signaling pathway may not be limited to target cancer cells, but rather to act on the TME. This is particularly relevant given the growing recognition of the TME role in cancer progression and response to therapy. The expression of NO-GC and cGKI in stromal cells, including blood vessels, highlights the potential of targeting this pathway to affect angiogenesis and vascular permeability.

4.3. The E0771 breast cancer mouse model

4.3.1. Localization of the eNOS/NO-GC/cGKI pathway in the breast cancer TME

The aforementioned results underscore the fact that murine E0771 breast cancer cells do not exhibit any cGMP pathway activity, making them an optimal choice for developing a mouse model aimed at studying the influence of modulating the cGMP signaling pathway in stromal cells. By implanting E0771 cells into the 3rd mammary fat pad of wildtype Bl6 female mice, murine breast cancer tumors were formed in immune competent mice. These tumors could be examined for the presence of proteins associated with the cGMP signaling pathway within the breast cancer TME.

Nowadays, breast cancer therapies are focusing on targeting the TME, especially the tumor vasculature, in order to induce changes which might help in the delivery of chemotherapeutic or immunotherapeutic drugs (Patel et al., 2023). In the past years, NO-GC stimulators evoked a growing pharmacological interest targeting the cardiovascular system and relieving diseases such as heart failure and pulmonary hypertension (Sandner et al., 2021). Thus, with the purpose to test how these drugs can impact breast cancer growth, we first of all investigated the localization of their target, the NO-GC/cGKI pathway in the breast cancer TME. Furthermore, we looked at the expression and localization of eNOS, which might be the main NO producer in the breast cancer TME. As per the literature (Lehners et al., 2018; Förstermann & Sessa, 2012) and recent studies on melanoma conducted by our research group (Stehle, 2022), the NO/cGMP pathway is generally expressed in both healthy and abnormal blood vessels. To verify if this holds true for the breast cancer vasculature, E0771-derived tumors were allowed to grow for around 25 days to reach a final size of ~1000 mm^3 before excision, fixation, and sectioning into 10 µm sections.

The tumor sections were stained for the proteins of interest, as well as for CD31 and SMA, the endothelial cell and pericyte/smooth muscle cell markers already mentioned in **4.2.2**. Together, CD31 and SMA expression revealed the presence of an irregular vasculature within the TME, featuring small tumor blood vessels with diameters between 10-100 µm (data not shown).

The expression of eNOS was found in tubular structures resembling vessels and displayed a significant overlap with CD31 staining (**Figure 19**). In contrast, only minor overlap was observed between eNOS and SMA (**Figure 19**). Contrary to the Western blot analysis (**Figure 12A**), in which cultured E0771 cells exhibited a faint eNOS band, IF staining did not reveal any expression of this protein in CD31- and SMA-negative areas, predominantly consisting of E0771 cancer cells (**Figure 19**).

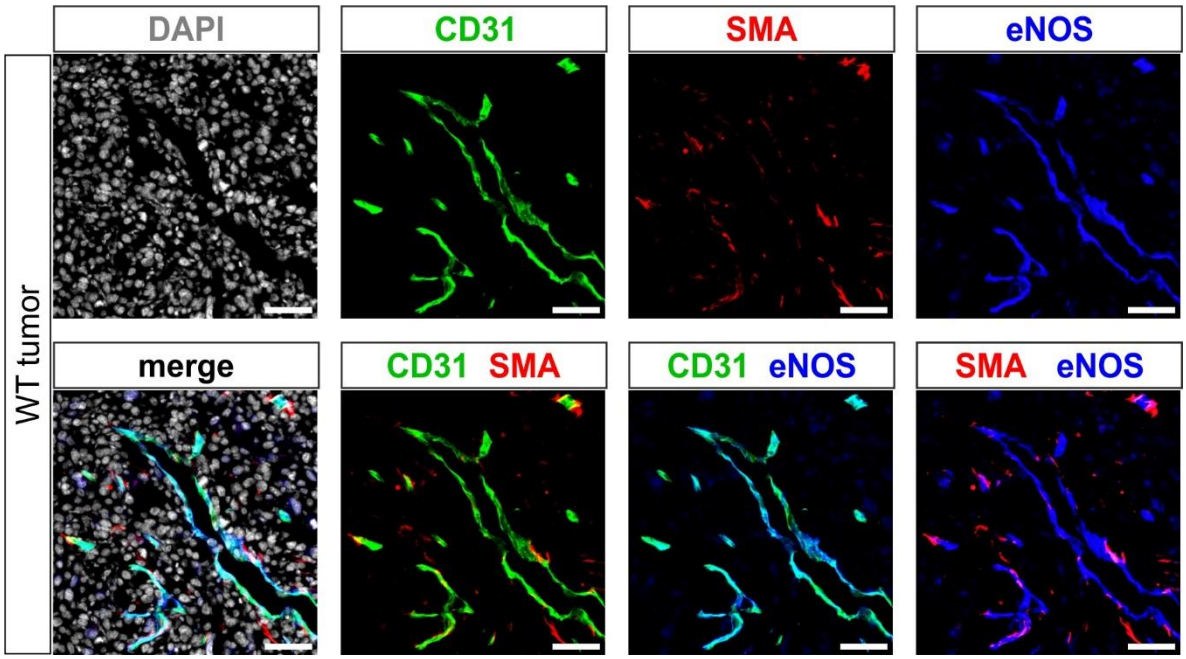

Figure 19. Localization of eNOS in the breast cancer TME. E0771 cells were implanted into the 3rd left mammary fat pad of female Bl6 wildtype mice. Following resection, tumors were fixed and sectioned into 10 µm slices. Frozen sections underwent IF staining using DAPI as a nuclear marker, CD31 as an endothelial marker, SMA as a smooth muscle/pericyte marker, and eNOS to determine its localization. The panels display single-channel staining (Gray: DAPI; Green: CD31; Red: SMA; Blue: eNOS) and merged images of all or pairs of channels to assess colocalization (nuclei without associated immunostaining are likely to belong to tumor cells). Colocalization can be observed as regions in Yellow (Green + Red), Cyan (Green + Blue) or Magenta (Red + Blue) in the pairs of channels. The images are representative of n ≥ 6 tumors dissected from ≥ 6 mice. Scale bars, 50 µm.

In contrast to the pattern observed with eNOS staining, NO-GC expression was detectable in a subset of cells located closely adjacent to blood vessels, displaying finger-like protrusions, a feature typically associated with pericytes. Only minimal overlap was found between NO-GC and CD31 staining (**Figure 20A**). This overlap was primarily attributable to the positioning of NO-GC-positive cells in direct contact with the endothelium of the tumor blood vessels (**Figure 20A**). On a different note, a distinct colocalization was evident between SMA and NO-GC staining (**Figure 20A**). The vast majority of the NO-GC-positive cells within the tumor vasculature were also SMA-positive, suggesting that NO-GC expression in breast cancer tumors is largely localized to pericytes/smooth muscle cells within the tumor vasculature.

However, we also noted the presence of some SMA-positive cells that lacked NO-GC staining, and reciprocally, some NO-GC positive cells that were not SMA-positive. This observation suggested the presence of distinct subpopulations of tumor pericytes within the breast cancer TME.

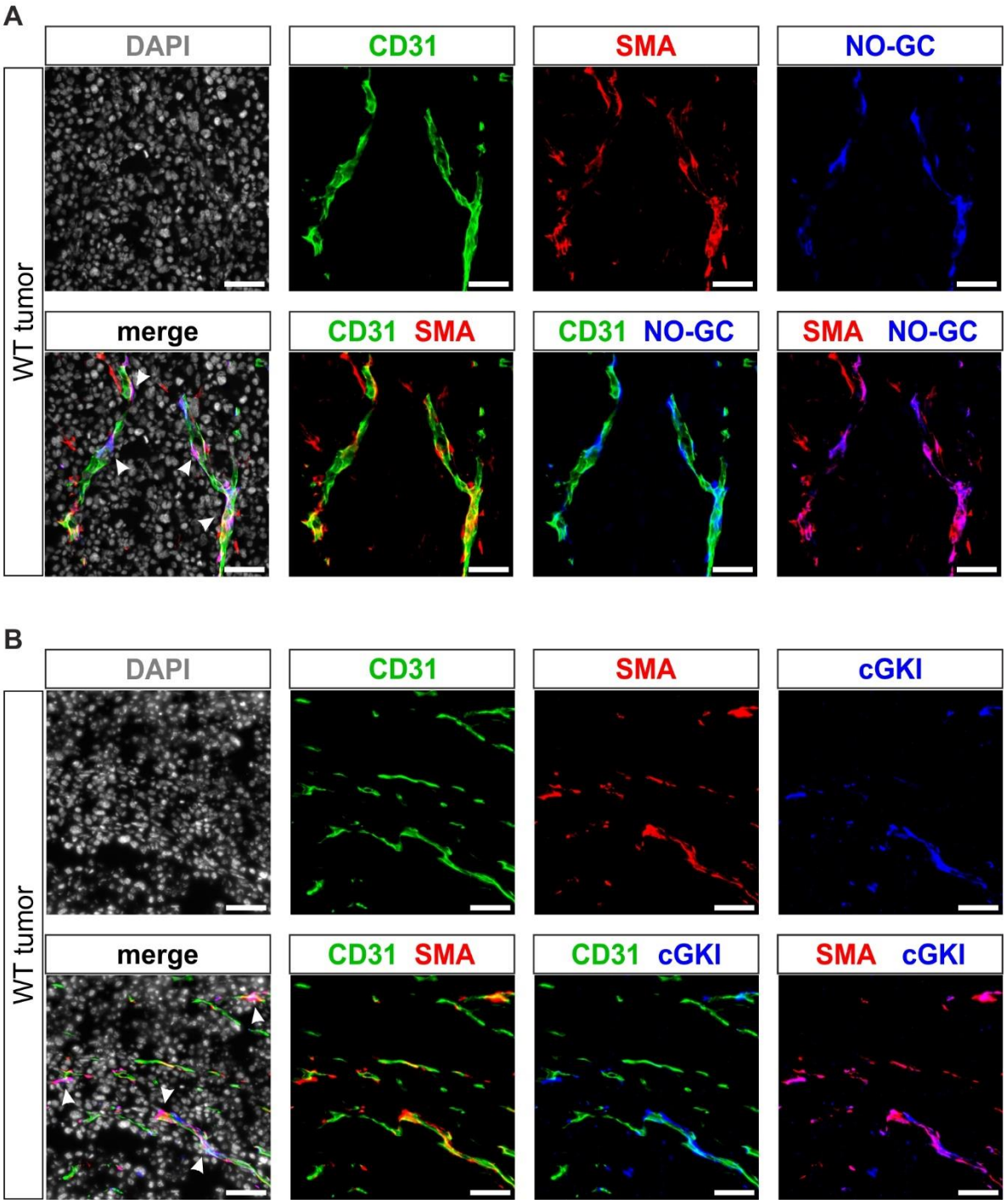

Figure 20. Localization of NO-GC and cGKI in the breast cancer TME. E0771 cells were implanted into the 3rd left mammary fat pad of female Bl6 wildtype mice. Following resection, tumors were fixed and sectioned into 10 µm slices. Frozen sections underwent IF staining using DAPI as a nuclear marker, CD31 as an endothelial marker, SMA as a smooth muscle/pericyte marker, and NO-GC (**A**) or cGKI (**B**) to determine their localization. The panels display single-channel staining (Gray: DAPI; Green: CD31; Red: SMA; Blue: NO-GC or cGKI) and merged images of all or pairs of channels to assess colocalization (nuclei without associated immunostaining are likely to belong to tumor cells). Arrows in the merged images indicate colocalization of SMA with NO-GC (**A**) or cGKI (**B**). Colocalization can be observed as region in Yellow (Green + Red), Cyan (Green + Blue) or Magenta (Red + Blue) in the pairs of channels. The images are representative of n ≥ 6 tumors dissected from ≥ 6 mice. Scale bars, 50 µm.

Lastly, due to the important role of cGKI as main effector of the cGMP signaling pathway, its localization in the TME of breast cancer was investigated. Similar to NO-GC staining, the expression of cGKI was found in cells on top of the endothelium, but not overlapping with CD31-positive regions (**Figure 20B**). Indeed, cGKI-positive cells strongly colocalized with SMA (**Figure 20B**), suggesting that pericytes of the TME expressed also cGKI. As with NO-GC, the population of cGKI-positive cells did not fully overlap with the SMA-positive cells, supporting the hypothesis of different pericytes populations.

In accordance with the Western Blot analysis (**Figure 12A**), IF did not detect NO-GC or cGKI in regions of the tumor that were CD31- and SMA-negative, where E0771 breast cancer cells were predominantly located (**Figure 20A** and **B**).

Collectively, these data indicate that an eNOS/NO-GC/cGKI pathway is present in the vasculature of the TME of the murine E0771 breast cancer tumor. While the expression of eNOS is confined to the endothelium, NO-GC and cGKI are expressed by a subpopulation of pericytes and absent in endothelial cells and breast cancer cells. The use of more elegant techniques, which aim to understand whether this pathway is indeed active and able to produce cGMP, is described in the following paragraph.

4.3.2. Real-time FRET/cGMP imaging ex vivo on breast tumor slices

To investigate the mechanism(s) of action of cGMP signaling in the context of breast cancer, *in situ* real-time FRET/cGMP imaging was carried out on freshly prepared tumor slices. This method maintained both spatial and temporal information on cGMP production, allowing for the comparison of cGMP signaling in various structures and cell types within the tumor under controlled conditions, such as with or without drug treatments. For these experiments, E0771 cells were implanted into the 3rd left mammary fat pad of global (global cGi500) or smooth muscle/pericyte-specific (SMA-cGi500 or SM22-cGi500) cGMP sensor mice.

In tumors from the global cGi500 mouse line, all mouse-derived cells, including vascular and stromal cells, constitutively expressed the cGMP biosensor. Instead, in tumors derived from both SMA-cGi500 and SM22-cGi500 mice, only the host recombinant cells exhibited the biosensor expression (see sections **1.2** and **3.7.2**). On the other hand, the injected E0771 tumor cells were always cGi500-negative. In all experiments, primary tumors were allowed to grow until they reached a final size of approximately 1000 mm³ (~25 days after cell implantation) before being dissected. To facilitate the success of the real-time FRET/cGMP imaging, the viability of the tumors was ensured by incubating them in glucose-supplemented imaging buffer on ice (as described in **3.9.3**). Changes of the intracellular cGMP concentration were recorded in response to stimuli with the physiological GC ligands ANP, CNP and NO, as well as the NO-GC stimulator vericiguat.

Expression of the cGMP sensor could be detected in the TME of E0771 tumors from global cGi500 mice (**Figure 21A**). Host-derived cells expressing the sensor were mainly organized in tubular structures, resembling tumor blood vessels or mammary ducts. The cGMP increases were recorded mainly in the vessel-like regions (**Figure 21A**). Due to the feature of the global cGi500 mice and the small size of the vessels present in the breast cancer tumors, even after the identification of vessel-like structures, it was not possible to distinguish between endothelium and perivascular cells. Nevertheless, FRET imaging of cGi500 tumor slices showed active cGMP pathways in these vessel-like structures. Interestingly, the intracellular cGMP concentration increased in response to both ANP and DEA/NO stimuli, while CNP did not induce any cGMP changes (**Figure 21A** middle-right panel).

To further understand which cell type(s) were responsible for the cGMP generation in tumor vessels, tumor pericytes, which were identified to express NO-GC (**Figure 20A**), were studied. To analyze this cell type, two specific pericyte/smooth muscle cell-specific cGMP sensor mice were used, the SMA-cGi500 and the SM22-cGi500 (**Figure 21B** to **D**). The YFP fluorescence of the cGMP sensor in SMA-cGi500 and SM22-cGi500 mice appeared in scattered single cells with finger-like extensions, resembling pericyte morphology. Supporting their pericyte identity, these YFP-positive cells were wrapped around mT-expressing vessel-like structures resembling vascular endothelium. Furthermore, IF staining on tumor sections derived from both SMA-cGi500 and SM22-cGi500 mice confirmed the localization of recombinant cells in close proximity to, but not overlapping with the endothelium (CD31-positive areas), and colocalized with the pericyte marker NG2 (**Figure S4A** and **B**).

In both mouse lines, FRET/cGMP imaging on these cells showed again an insensitivity to the CNP stimulus (**Figure 21B** and data not shown). Similar to CNP, ANP also did also not elevate cGMP in tumor pericytes (**Figure 21B** and data not shown). In line with the NO-GC immunostaining (**Figure 20A** and **Figure S4C**), the DEA/NO stimulus significantly increased cGMP levels in these pericyte-like cells and this effect was further potentiated by the NO-GC stimulator vericiguat (**Figure 21C**). Vericiguat alone was able to increase cGMP levels in pericytes of both cGMP sensor mouse lines (**Figure 21C** and **D**). Vericiguat vehicle DMSO did not induce any changes in the intracellular cGMP concentration, confirming the specificity of the effect of the drug treatment (**Figure 21C** and **D**).

Additionally it was also possible to detect cGKI expression in the recombinant cells (**Figure S4D**), supporting the data shown in **4.3.1**.

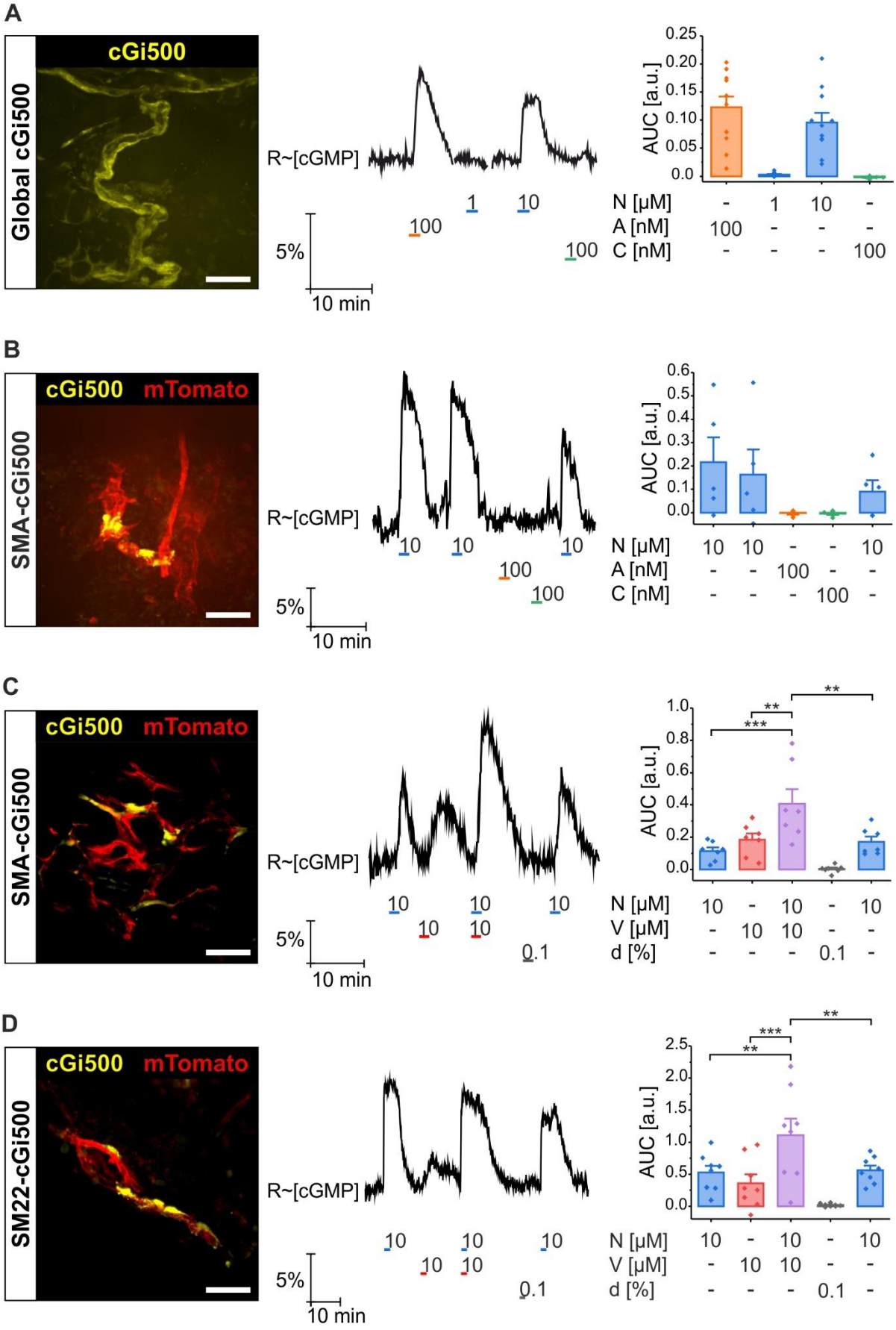
A
Global cGi500
cGi500
R~[cGMP]
5%
10 min
1
10
100
100
AUC [a.u.]
0.25
0.20
0.15
0.10
0.05
0.0
N [µM] - 1 10 -
A [nM] 100 - - -
C [nM] - - - 100
B
SMA-cGi500
cGi500 mTomato
R~[cGMP]
5%
10 min
10
10
10
100
100
AUC [a.u.]
0.6
0.5
0.4
0.3
0.2
0.1
0.0
N [µM] 10 10 - - 10
A [nM] - - 100 - -
C [nM] - - - 100 -
C
SMA-cGi500
cGi500 mTomato
R~[cGMP]
5%
10 min
10
10
10
10
10
0.1
AUC [a.u.]
1.0
0.8
0.6
0.4
0.2
0.0
**
***
**
N [µM] 10 - 10 - 10
V [µM] - 10 10 - -
d [%] - - - 0.1 -
D
SM22-cGi500
cGi500 mTomato
R~[cGMP]
5%
10 min
10
10
10
10
10
0.1
AUC [a.u.]
2.5
2.0
1.5
1.0
0.5
0.0
**
***
**
N [µM] 10 - 10 - 10
V [µM] - 10 10 - -
d [%] - - - 0.1 -

Figure 21. Real-time FRET/cGMP imaging in cells of the breast cancer TME. E0771 tumor cells were implanted into the 3rd left mammary fat pad of female mice expressing the cGi500 biosensors in different cell types. After tumor resection, slices were prepared and subjected to real-time FRET/cGMP imaging. During the measurements ANP (A), CNP (C), DEA/NO (N), vericiguat (V), DMSO (d, vericiguat vehicle), or a combination of DEA/NO and vericiguat were superfused for 2 minutes each (concentration as indicated in the figure). Shown are (from left to right) the fluorescence images of the tumor slices, a representative ratio trace R~[cGMP], and the statistical analysis of the AUC of cGMP signals recorded after each application. **A**, FRET/cGMP imaging in tumors from the global cGi500 mice. Genotype: cGi500(L1)$^{+/L1}$. Yellow color shows YFP fluorescence of cGi500, not cGMP. **B** to **D**, FRET/cGMP imaging in tumor slices from two models of pericyte/smooth muscle cell-specific cGMP sensor mice, SMA-cGi500 and SM22-cGi500 mice. Genotypes: SMA-CreERT2$^{tg/+}$ mT/cGi500(L2)$^{+/L2}$ and SM22CreER$^{tg/+}$ mT/cGi500(L2)$^{+/L2}$. SMA-cGi500 mice were tamoxifen injected starting 6 weeks before tumor cell injection, as for the protocol described in section **3.7.4**. Yellow color shows YFP fluorescence of cGi500 in the recombinant stromal cells and red color shows mT fluorescence of the non-recombinant stromal cells. **C** and **D**, Vericiguat effect on the cGMP level alone and together with a DEA/NO stimulus. Data represent mean ± SEM of a representative measurement of a single slice (n ≥ 5 region/cells per slice). FRET/cGMP imaging was repeated on n ≥ 3 tumor slices from ≥ 2 mice. Scale bars, 50 µm.

Thus, within the breast cancer TME, changes in cGMP were observed upon stimulation of the ANP/cGMP and NO/cGMP signaling pathways, but not in response to CNP. The specific cell type generating cGMP in response to ANP stimulus remains uncertain. Based on the morphological structure, it is hypothesized to be endothelial cells. Further analysis, using endothelial cell-specific cGMP sensor mice, is needed to confirm this assumption. Using cell type-specific sensor mice, we identified an active NO/cGMP pathway in vascular pericytes within the tumor stroma. Vericiguat application, in turn, was able to generate a mild cGMP increase and to potentiate the NO-induced cGMP generation in these cells. These findings suggest that, at least in our E0771 breast cancer mouse model, NO-GC stimulators act as a potent tool for targeted stimulation of the cGMP pathway in vascular pericytes, without impacting cGMP levels in tumor cells.

4.3.3. Pharmacological targeting of NO-GC in the breast cancer mouse model

The results obtained thus far showed that in the E0771 breast cancer mouse model: (1) the implanted E0771 cells did not express any of the tested proteins of the cGMP signaling pathway, and no elevated cGMP levels were observed following ANP, CNP, or DEA/NO stimuli, classifying them as cGMP-insensitive (**Figure 12A** and **B**); (2) expression of NO-GC was localized in pericytes (**Figure 20A**), which also exhibited NO-triggered cGMP signals that were potentiated by vericiguat co-application (**Figure 21C** and **D**). Moreover, (3) vericiguat did not influence E0771 cell growth or migration (**Figure S6**). Collectively, these findings highlight the potential of targeting the NO/cGMP signaling pathway in pericytes of the breast cancer TME through systemic administration of vericiguat, leading to a specific focus on tumor vascularization, thereby impacting tumor growth and progression.

To investigate the effects of the pharmacological modulation of NO-GC in tumor pericytes, Bl6 female mice were fed with either vericiguat-supplemented or control diets. Vericiguat was added to both high-fat diet (HFD) and normal diet (ND) across two distinct cohorts. Two days following diet exchange, E0771 cells were implanted into the 3rd left mammary fat pad of each mouse (see **3.8.3** for the timeline). Tumor growth was monitored daily, and approximately 3 weeks post tumor cell implantation, the experimental animals were euthanized, with tumors weighed and collected for further analysis.

Considering the systemic administration of vericiguat, it was crucial to assess its presence in the plasma of treated animals and its impact on physiological parameters, such as blood pressure. Ongoing research on the effect of vericiguat in atherosclerosis within our group has demonstrated the presence of vericiguat in the plasma of female and male animals fed a vericiguat-supplemented HFD for 16 weeks, with a small, not significant drop in blood pressure following drug administration for both sex (Roessing et al., *unpublished*). The current study showed comparable results (**Table 10, Figure 22, Table S2** and **Figure S5**). In fact, the plasma concentrations of vericiguat revealed an increase in both the total drug and unbound fraction concentrations in the treated groups of each cohort, while insignificant (possibly caused by sample preparation) or no traces of the drug were detected in any of the control groups (**Table 10**).

Table 10. Concentration of vericiguat in the plasma of experimental animals.

Group	Total vericiguat [pmol/mL]	Unbound vericiguat [pmol/mL]
1st cohort of experimental animals		
ND (n = 4)	4.8 ± 1.7	Not detected
HFD (n = 6)	Not detected	Not detected
HFD + V (n= 7)	2648 ± 354	51.1 ± 5.2
2nd cohort of experimental animals		
ND (n = 7)	15.6 ± 10.3	Not detected
ND + V (n = 6)	3882 ± 162	79.0 ± 5.1

Footnotes: Concentration of total (left) and unbound (right) vericiguat in the plasma on the day of tumor resection for the 1st and 2nd cohort of animals. In the 1st cohort, animal groups received normal diet (ND), high-fat diet (HFD) or vericiguat-supplemented HFD (HFD + V). In the 2nd cohort, animal groups received normal diet (ND) or vericiguat-supplemented ND (ND + V). Data represent mean ± SEM.

In accordance with the literature and the aforementioned findings in our group, vericiguat-treated female animals exhibited a slight, albeit not significant, reduction of mean blood pressure by approximately 10 mmHg at the day of intended tumor cell injection (before diet exchange: 94.8 ± 6.3 mmHg versus after diet exchange: 81.1 ± 6.6 mmHg), compared to the control in a normal diet context (before diet exchange: 97.7 ± 5.7 mmHg versus after diet

exchange: 92.7 ± 3.3 mmHg) (**Figure 22A** and **Table S2**). Similar results were obtained also in male mice (**Table S2** and **Figure S5A**). This vericiguat-induced mild hypotensive state remained relatively constant throughout the duration of the experiment (**Figure 22B** and **Figure S5B**).

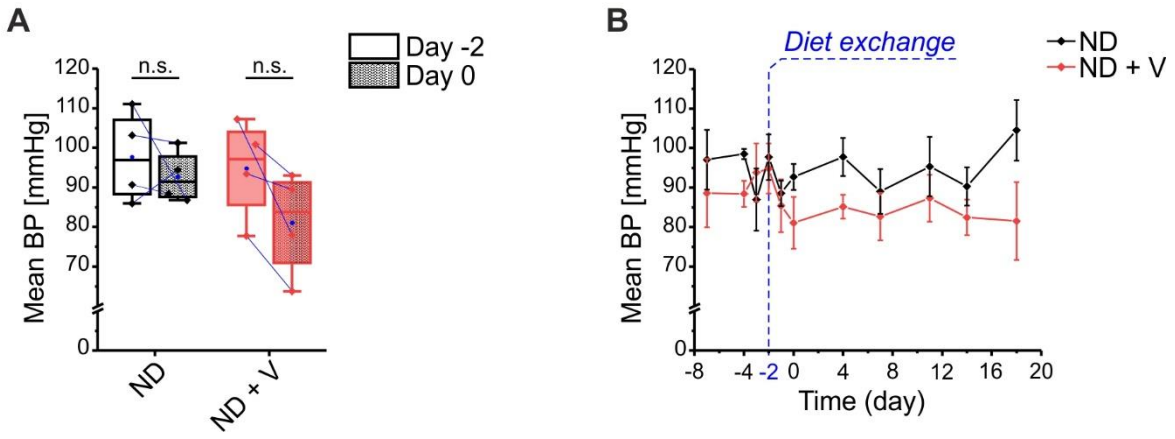

Figure 22. Effect of vericiguat on blood pressure in female mice. A, Mean blood pressure (BP) recorded at day -2 (before diet exchange) and at day 0 (formal tumor cell injection day) for both control (ND) and vericiguat-treated (ND + V) groups. Boxes indicate 25%–75% interquartile range; horizontal lines in boxes, median; blue dots in boxes, mean; whiskers, 5%–95% range; dots, n = 4 female animals per condition; blue lines, data points connectors. **B**, Mean BP over time for both control (ND) and vericiguat-treated (ND + V) groups. Data represent mean ± SEM of n = 4 animals. Time on X axis considered the cell injection day as 0. Note that these mice did not receive tumor cells.

Focusing on the effects of vericiguat on breast cancer, tumor growth was examined in the E0771 mouse model. In the 1st cohort of animals, vericiguat was supplemented in HFD, and two control diets, HFD and ND, were included. At the time of tumor resection, tumors from vericiguat-fed mice were visibly larger in size compared to both HFD and ND groups (**Figure 23A**). Daily monitoring of tumor growth revealed a difference in tumor volume between the vericiguat-treated and control groups beginning at day 12 post tumor cell implantation, with the maximum difference observed on the resection day. Both control groups displayed similar growth patterns over time, with no discernible differences in tumor growth attributable to the diets (**Figure 23B**). Consistent with the volume, the tumor weight post-resection was significantly higher in the vericiguat-treated group compared to the HFD group (**Figure 23C**). A similar tendency was observed between the ND and the vericiguat-treated group, albeit it was not statistically significant (**Figure 23C**).

Comparable results were obtained in the 2nd cohort, where vericiguat was supplemented in the normal diet. Although the variability within the group was higher than in the previous cohort, tumors from vericiguat-treated animals were larger than those from the control group at the time of resection (**Figure 23D**). The difference in tumor volume between groups started around day 10, similar to the above-mentioned results, although the difference did not reach the same

magnitude like in the 1st cohort at the end of the experiment (**Figure 23E**). Surprisingly, there was no significant difference in tumor weight. Although the tumors in the vericiguat group exhibited larger volumes, their weights were similar to tumors from mice fed the normal diet without drug (**Figure 23F**). Of note, the relative increase in tumor volume in the vericiguat supplement HFD group was much higher in comparison to their increase in tumor weight (**Figure 23B** and **C**). These results may suggest a difference in the composition of the TME, leading to an increased proportion of the ECM or bigger necrotic cores within the vericiguat-treated tumors. However, further analysis is needed to validate this hypothesis.

To sum up, these results showed that vericiguat treatment causes an increase in breast tumor growth in our preclinical mouse model, presumably affecting the establishment and/or regulation of the tumor vasculature via targeting of the NO/cGMP signaling cascade in tumor-associated pericytes.

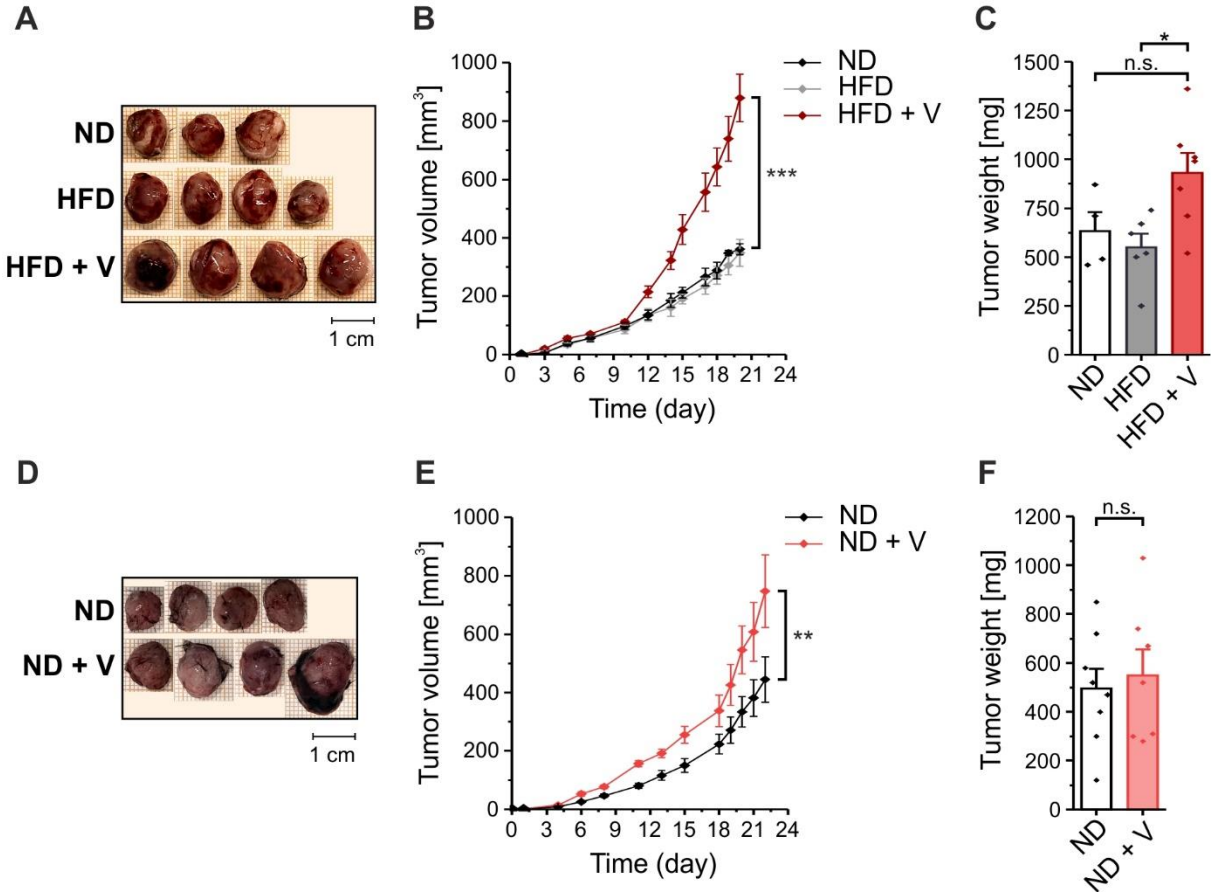

Figure 23. Breast tumor growth under pharmacological stimulation of NO-GC with vericiguat. E0771 cells were implanted into the 3rd left mammary fat pad of female Bl6 mice, 2 days after diet exchange. In the 1st cohort (**A** to **C**), animal groups received normal diet (ND), high-fat diet (HFD) or vericiguat-supplemented HFD (HFD + V). In the 2nd cohort (**D** to **F**), animal groups received normal diet (ND) or vericiguat-supplemented ND (ND + V). Tumor size was determined every second/third day, and tumors were resected approx. 20 days after tumor cell injection. **A** and **D**, Images of representative tumors for each condition after dissection on day 20 (**A**) and 22 (**D**). **B** and **E**, Tumor growth over time under the different conditions. **C** and **F**, Tumor weight after dissection on day 20 (**C**) and 22 (**F**) for each condition. Data represent mean ± SEM (n ≥ 4 tumors dissected from ≥ 4 mice per condition).

5. Discussion

Breast cancer is the most common type of cancer among women worldwide, leading to about 40,000 deaths per year only in the United States (Siegel et al., 2023). Breast cancer originates in the breast tissues, and it is characterized by a strong heterogeneity based on its localization of origin (duct or lobule) and marker expression (Nolan et al., 2023). The cGMP signaling pathway has been reported to be implicated in breast cancer, where its dysregulation can impact cell growth, proliferation, and metastasis (Stehle et al., 2023). As discussed in **1.4**, while elevated cGMP levels have been associated with anti-tumorigenic effects through inhibiting proliferation, inducing apoptosis, and modulating immune responses, cGMP signaling can also exhibit pro-tumor effects, leading to tumor progression (Stehle et al., 2023). Thus, the role of cGMP in breast cancer appears to be complex, and further research was required to fully comprehend its implications and develop potential therapeutic interventions.

The present study aimed to shed light on the role of the cGMP signaling pathway in both tumor and stromal cells of breast cancer. To investigate the dynamic behavior of cGMP, we used the cGi500 biosensor, which enabled us to precisely define the spatiotemporal profile of cGMP signals in live cells and tissues. Our novel findings contributed significantly to our understanding of the distribution of various cGMP generators and effectors among different subtypes of breast cancer and cells within the TME. Of note, our results are consistent with a previous study conducted on a melanoma model (Stehle, 2022), as we observed a potentiation effect of NO-GC stimulators, such as riociguat and vericiguat, on NO-induced cGMP production in breast cancer cells *in vitro* and breast tumor slices *ex vivo*. These findings further strengthen the relevance of the cGMP pathway in breast cancer research.

5.1. Heterogeneity of cGMP pathway expression in breast cancer

In recent years, numerous studies have shed light on the significance of the cGMP signaling pathway in the development and progression of various cancer types, including breast cancer (Stehle et al., 2023; Di Iorio et al., 2021; Windham & Tinsley, 2015). However, despite the wealth of available data, the precise role of this pathway in breast cancer remains a topic of ongoing debate. Arguments have emerged regarding its potential pro- or anti-tumor effects (section **1.4**).

In our study, we conducted an in-depth analysis of multiple breast cancer cell lines, revealing a striking variability in terms of the presence of cGMP pathway components and cGMP production (**Figure 12**). Surprisingly, out of the 10 tested breast cancer cell lines, only four demonstrated responsiveness to cGMP signaling. Categorizing these cell lines based on breast cancer subtypes, we observed that all tested ER+PR+ and HER2+ cell lines exhibited

insensitivity to cGMP, whereas within the TNBC subtype, both cGMP-insensitive and cGMP-responsive lines were present (**Figure 12** and **Table 11**).

Further investigations uncovered that the human cell lines MDA-MB-157, BT549, and Hs578T displayed an active CNP/cGMP/cGKI pathway as well as a NO/cGMP/cGKI pathway, whose cGMP production could be potentiated by the NO-GC stimulator riociguat (**Figure 13**). On the other hand, the murine 4T1 cell line expressed solely the CNP/cGMP pathway, likely mediated through cGKI, albeit its expression was relatively faint (**Figure 12A** and **C**). Additionally, it would be intriguing to investigate whether the *BRCA1* and *BRCA2* status correlates with cGMP pathway expression and activity, as all the tested cell lines were confirmed to be at least *BRCA1* wildtype (Elstrodt et al., 2006).

Some of our findings appear to be in conflict with existing literature, which has documented cGMP-dependent alterations in the behavior of cell lines such as MCF-7, T47D, SK-BR-3, MDA-MB-231, and MDA-MD-468 (Catalano et al., 2016; Saravani et al., 2012; Tinsley et al., 2009). These studies explored the impact of PDE inhibitors, such as sildenafil and sulindac for PDE5, and BAY73-6691 for PDE9. Curiously, in our study, we were unable to detect PDE5 expression in MCF-7 and MDA-MB-231 cells through Western blot analysis (**Figure 12A**). PDE9 was not evaluated by us. Moreover, in these cell lines, we could not detect the expression of cGMP generators using Western blot analysis, nor observe cGMP production using FRET/cGMP imaging (**Figure 12A** and **B**). Thus, due to the absence of cGMP production, PDE inhibitors could not induce an increase in cGMP levels in these cell lines. These discrepancies could potentially be attributed to the usage of different batches of cell lines in laboratories worldwide. Ben-David et al. (2018) examined 27 batches of MCF-7 cell lines obtained from different research groups and identified variations in gene expression, including the tumor suppressor PTEN, leading to noticeable disparities in cell morphology and proliferation. Furthermore, these cell line batches exhibited heterogeneous responses to treatment with diverse anti-cancer compounds, ranging from significant growth inhibition to complete ineffectiveness (Ben-David et al., 2018). Therefore, it would not be surprising if the differences between our study and others were linked to genetic drift occurring in cell culture. Moreover, it is worth noting that most of the studies cited in section **1.4** did not assess the protein expression of cGMP pathway components, raising questions about the specificity of drug targets. Hence, a comprehensive understanding of the cGMP signaling pathway's involvement in breast cancer warrants further investigations, considering the genetic variations within cell lines, and conducting thorough assessments of protein expression.

Table 11. Summary of cGMP signaling in different breast cancer cell lines.

		Protein expression							cGMP Imaging			
	Cell line	nNOS	iNOS	eNOS	GC-B	NO-GC	cGKI	PDE5	ANP	CNP	NO	
ER+PR+	MCF-7	?	-	+	-	-	-	-	-	-	-	Human
	T47D	?	-	+	-	-	-	+	-	-	-	
HER2+	SK-BR-3	-	-	+	-	-	-	+	-	-	-	
TNBC	MDA-MB-231	-	-	+	-	-	-	-	-	-	-	
	MDA-MB-468	-	-	-	-	+	-	+	-	-	-	
	MDA-MB-157	?	-	+	-	+	+	-	+/?	+	+++	
	BT549	?	-	+	+	+	+	+	-	+	++	
	Hs578T	?	-	+	+	+	+	+	-	+++	+	
	4T1	-	-	-	+	-	?	-	+/?	+++	-	Murine
	E0771	?	-	?	?	-	-	-	-	-	-	

Footnotes: "+," protein detected/cGMP level increase; "-", protein undetected/no cGMP level changes; "?", uncertain result.

In line with the *in vitro* findings obtained from cell culture experiments, our analysis of human samples derived from TNBC patients showed expression of NO-GC (**Figure 16B** and **Figure 17**). Indeed, we were able to detect NO-GC protein in lysates of human TNBC organoids (**Figure 16B**), and immunostaining of TNBC biopsies localized the protein also in the cancer cell areas (**Figure 17**). Interestingly, NO-GC was also observed to be expressed, although weakly, in the cancer cells of a HER2+ biopsy (**Figure 17**). Notably, in all patient biopsies, both NO-GC and cGKI were detected in the stromal compartment, including tumor blood vessels. In this regard, the presence of NO-GC in organoids may also originate from pericytes or other stromal cells, as organoids are derived from tumor biopsies and resemble the cellular composition of the tumor of origin (Porter et al., 2020).

IF staining of human biopsies highlighted the substantial presence of the NO-GC and cGKI within the TME of breast cancer patients (**Figure 17** and **Figure 18**), regardless of breast cancer subtype. In particular, NO-GC and cGKI showed strong colocalization with SMA in regions closely adjacent to the areas stained with CD31, suggesting their expression in tumor-associated pericytes. Thus, the focus of this study moved to investigate the presence of the cGMP pathway within the breast cancer TME and its influence on tumor growth and progression. To achieve this goal, we established a TNBC mouse model by implanting cGMP-insensitive E0771 murine breast cancer cells into the 3rd mammary fat pad of female mice. Indeed, the E0771 breast cancer cells do not produce cGMP in response to ANP, CNP, or NO (**Figure 12B**). Furthermore, when implanted into the mammary fat pad of female cGMP sensor mice, E0771 cells do not express the cGi500 sensor, which is present in the host stromal cells. This specific set up allowed for an *in situ* characterization of the cGMP pathway

in acute tumor slices, allowing us to identify the presence of two distinct cGMP signaling pathways inside the breast cancer TME: the ANP/cGMP and the NO/cGMP pathways.

Although the exact cell population remains uncertain, we detected an active ANP/cGMP pathway within the TME (**Figure 21A**). The ANP/GC-A pathway is predominant in the endothelium, where it plays a role in both pro- and anti-angiogenic processes (Kuhn, 2012). Furthermore, a previous study conducted by our working group demonstrated that ANP stimulation induced cGMP production in melanoma tumor slices of endothelium-specific sensor mice (Stehle, 2022). Therefore, it is reasonable to hypothesize that the ANP-induced cGMP production in breast tumor slices is also localized to the tumor endothelium. On the other hand, using IF staining and cell type-specific cGMP sensor mice, the NO/cGMP pathway was found in pericytes/smooth muscle cells of the TME. These cells exhibited robust cGMP production in response to NO but not ANP or CNP (**Figure 21B**). Additionally, *ex vivo* application of the NO-GC stimulator vericiguat significantly increased the NO-induced cGMP generation in these cells (**Figure 21C** and **D**). Supporting the FRET data, NO-GC immunostaining indicated that the expression of NO-GC within E0771 breast tumors is primarily limited to pericytes (**Figure 20A**). Similar results were obtained also for cGKI expression (**Figure 20B**).

In conclusion, our data revealed a new layer of inter- and intra- heterogeneity in breast cancer. Indeed, breast cancer is commonly recognized to be an heterogeneous disease with differences between breast tumor types and within the cells of the same subtype, which has clinical applications in terms of effective diagnostics as well as prognostic and therapeutic strategies (Turashvili & Brogi, 2017). Here, we showed that the cGMP signaling pathway in breast cancer is differently expressed not only between different cancer cell subtypes but also among the cells of the TME (**Figure 24**). The analysis of 10 different breast cancer cell lines showed that CNP/cGMP/cGKI and NO/cGMP/cGKI pathways are expressed in some TNBC cell lines, while all the examined ER+ PR+ and HER2+ cell lines were cGMP-insensitive (**Figure 24 left**). Moreover, the NO/cGMP/cGKI pathway was also found in tumor-associated pericytes/smooth muscle cells (**Figure 24 right**). Additionally the analysis of the breast cancer TME revealed the presence of an active ANP/cGMP pathway presumably in the tumor endothelium, which was shown to express eNOS (**Figure 24 right**). Understanding which cGMP signaling pathway is expressed in the different cells of breast tumors provides insights into the targeted stimulation of the pathway in specific cell types without unwanted off-target effects. Previous studies investigating the potential of PDE5 inhibitors to treat breast cancer have primarily focused on treating tumors targeting cancer cells. However, PDE5 is broadly expressed among cancer and stromal cells (Catalano et al., 2019; Catalano et al., 2016). As a result, the drug does not specifically target a particular component of the tumor, potentially

enhancing undesired features such as cancer growth. Therefore, by deciphering the intricate dynamics of the cGMP pathway within the TME, we can develop more precise therapeutic strategies to optimize breast cancer treatment.

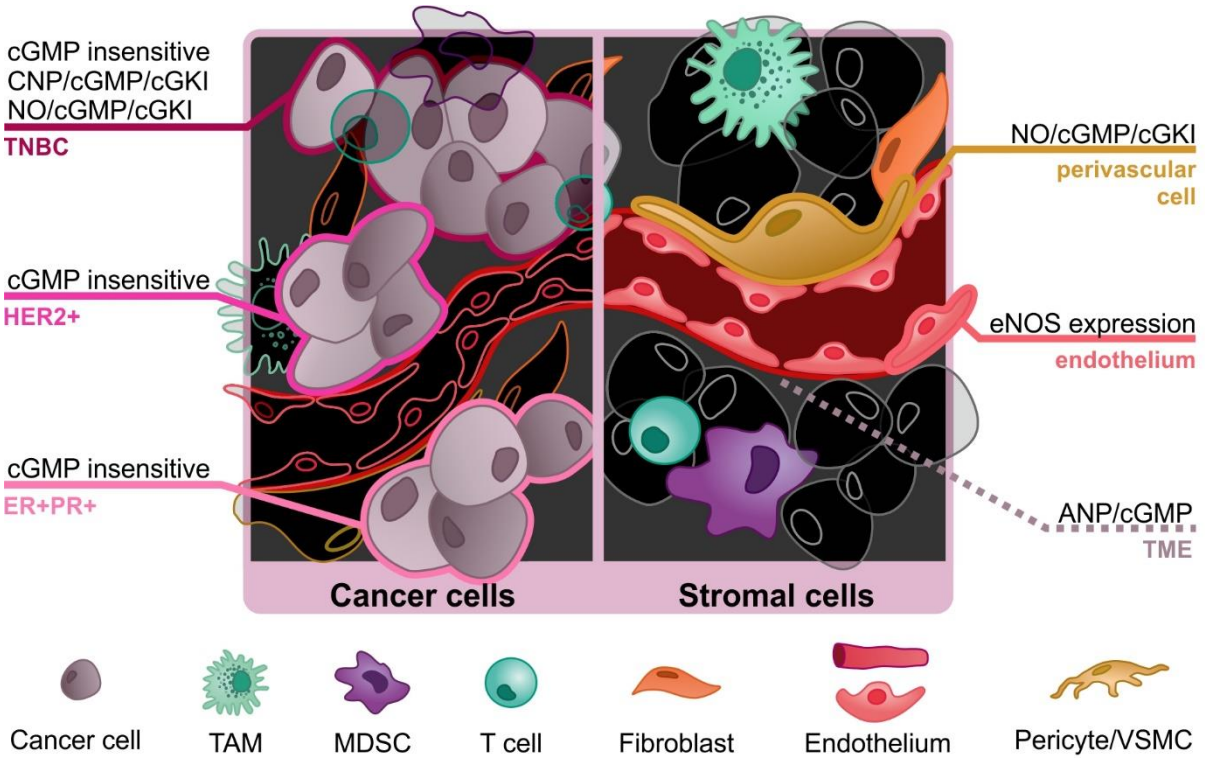

Figure 24. Heterogeneity of cGMP pathways in breast cancer. Schematic summary of the findings of the present study regarding the presence and ligand preference of the cGMP pathways in cancer and stromal cells of breast tumors. Our analysis of 10 different cultured breast cancer cell lines (on the left) belonging to different breast cancer subtypes classified the ER+PR+ and HER2+ cells as cGMP-insensitive, while the TNBC cell lines were a heterogeneous group, with cGMP-insensitive lines and lines with active CNP/cGMP/cGKI and NO/cGMP/cGKI pathways. In the breast cancer TME of the E0771 mouse model (on the right), it was possible to detect eNOS expression in the tumor endothelium, possibly also expressing an ANP/cGMP pathway. Importantly, perivascular cells like pericytes and VSMCs expressed and active NO/cGMP/cGKI pathway.

5.2. The role of the cGMP pathway in breast cancer and stromal cells

As discussed in the previous section **5.1**, the significant heterogeneity of the cGMP pathway among breast cancer subtypes and stromal cells raises questions about its potential functions depending on the cellular context. Preliminary insights into the effect of cGMP stimulation on breast cancer cell lines are shown in **Figure 14**. In our study, we observed an inhibitory effect of cGMP on human Hs578T cell growth following long-term treatment (7 days) with the membrane-permeable cGMP analog 8Br-cGMP. However, in the short term (24 hours), stimulation of the NO/cGMP pathway with 8Br-cGMP, DETA/NO, riociguat or combination of DEAT/NO and riociguat did not influence Hs578T cell migration. Similarly, in murine 4T1 cells expressing the CNP/cGMP pathway, stimulation with 8Br-cGMP or CNP did not have any

effect on cell growth or migration (**Figure 15A** and **B**). The differential effects on cell growth may depend on the specific cGMP pathway expressed, its activation and localization within the cells (Bork & Nikolaev, 2018) .

Recent findings indicated that a sulindac derivative inhibited the growth of Hs578T cells and other tumor cell lines by inhibition of PDE5, presumably leading to an increase of cGMP (Tinsley et al., 2023). The research group observed that the sulindac derivative induced an increase in the activity of Caspase 3 and 7, leading to apoptotic events. Hence, we can hypothesize that, similar to the findings of Tinsley et al. (2023), the decreased Hs578T cell growth caused by 8Br-cGMP stimulation in our study may be attributed to increased apoptosis.

In TNBC patient-derived organoids, stimulation of the NO/cGMP pathway induced changes in Caspase 3 and PARP expression (**Figure 16B** and **C**), potentially resulting in decreased apoptotic events. PARP plays a crucial role in promoting single-strand DNA repair, thereby preventing cell death (Helleday, 2011). PARP inhibitors have shown promise in increasing cancer cell death, particularly in TNBC cases with germline *BRCA1* and *BRCA2* mutations (Helleday, 2011). Similarly, Caspase 3 induces apoptosis by inhibiting PARP through cleavage into two parts, 89 kDa and 24 kDa. However, evidence suggested that full-length PARP or the 89 kDa PARP fragment could induce caspase-independent apoptosis (Mashimo et al., 2021; Zhou et al., 2021). Therefore, the changes induced by the stimulation of the cGMP pathway require further analysis to determine whether they have a pro- or anti-tumor effect. Additionally, it remains unclear which effector is mediating the cGMP response, as cGKI was not detected in the protein lysate of the tested human organoids (**Figure 16B**). A probable candidate is cGKII, as its mRNA has been detected in breast cancer cell lines *in vitro* (Karami-Tehrani et al., 2012). Collectively, these findings suggest that, at least *in vitro*, apoptosis in human breast cancer cells may be modulated by the stimulation of the NO/cGMP signaling pathway.

As discussed in section **1.3.2**, cancer cells and stromal cells in a tumor are closely interconnected, forming an intricate network of crosstalk and co-dependence. However, the role of the cGMP pathway in this cancer-to-stroma cell interaction, and vice versa, is poorly understood. Initial insights into cGMP-mediated crosstalk between cancer and stromal cells can be found in **Figure 15C**. Stimulation of primary isolated VSMCs with tumor conditioned medium (TCM) from 4T1 breast cancer cells significantly promoted VSMC migration. Interestingly, the pro-migratory effect of the TCM was influenced by pre-stimulation of the CNP/cGMP pathway in 4T1 cancer cells. Similarly, studies on stroma-to-cancer cell crosstalk have shown that breast CAFs promoted cancer cell growth both *in vitro* and *in vivo*. The pro-tumor factor identified in the CAF-conditioned medium was found to be a C-X-C motif chemokine 16 (CXCL16). Moreover, these mechanisms were likely PDE5-dependent, as specific PDE5 inhibitors not only reduced CXCL16 secretion but also inhibited CAF

proliferation (Catalano et al., 2019). Therefore, we can hypothesize that, similar to the findings of Catalano et al. (2019), the 4T1 cancer cells in our study may secrete chemokines that promote VSMC migration *in vitro* and potentially affect the organization of perivascular cells *in vivo*, consequently impacting the tumor vasculature. Importantly, we showed that the secretion of this pro-migratory factor is attenuated by activation of the cGMP pathway in the tumor cells (**Figure 15C**). However, it should be noted that the VSMCs used in this study were isolated from healthy aortae and may differ from perivascular cancer cells in the TME. Further analysis using perivascular cells isolated from breast tumors is necessary. Moreover, such a setup might provide insights into the mechanisms underlying the vericiguat-promoted growth of breast tumors *in vivo*, discussed in the following paragraph.

5.3. Influence of NO-GC stimulator on tumor growth and vasculature

As described in **1.3.2**, the role of the tumor vasculature in cancer progression and metastasis has recently become prominent, paving the way to therapeutic strategies which aim to induce vessel normalization and restoration of the tumor vasculature, and, therefore, improve standard care therapies (Patel et al., 2023).

Our preclinical E0771 breast cancer mouse model provided valuable insights into the pathophysiological relevance of the cGMP pathway in cancer progression, particularly focusing on its modulation within the TME. Given the robust expression of the NO/cGMP pathway in breast cancer pericytes in mouse and human as identified in this study (see section **4.2.2**, **4.3.1** and **4.3.2**), but not in the endothelium or cancer cells, we aimed to investigate the impact of cGMP stimulation in the pericytes of the TME on breast cancer growth. While the NO-GC stimulator vericiguat did not influence the growth or migration of E0771 cells (**Figure S6**), tumor growth in mice receiving vericiguat-supplemented food was significantly increased compared to the control group (**Figure 23**). This outcome might introduce a new risk factor for breast cancer patients taking vericiguat for cardiovascular diseases. However, as discussed below, vericiguat might also have potential as a tumor vessel normalizing agent acting on pericytes.

Pericytes are a crucial component of the vascular system. Their interaction with the endothelium is essential to stabilize blood vessels, regulating blood flow, and maintaining the vessel functionality, thereby significantly influencing tissue health and disease processes (Caporali et al., 2017; Ferland-McCollough et al., 2017). Previous studies have suggested that the recruitment of pericytes to tumor vessels is strongly dependent on the NO gradient generated by the endothelium via eNOS (Kashiwagi et al., 2008; Kashiwagi et al., 2005). While the specific mechanisms underlying pericyte recruitment have not been fully elucidated, several studies have reported the involvement of NO/cGMP in the growth and survival of

VSMCs (Lehners et al., 2018; R. Feil et al., 2005; Friedman, 1976). In our murine E0771 breast cancer model, pericytes in the TME exhibited expression of both NO-GC and cGKI (**Figure 20**), and NO stimulation resulted in cGMP generation in live tumor sections (**Figure 21B** to **D**). Additionally, eNOS was expressed by breast cancer endothelium (**Figure 19**). Taking all this in account, we hypothesize that the eNOS/NO/cGMP pathway plays a crucial role in the crosstalk between the endothelium and perivascular cells, presumably leading to the recruitment of pericytes to tumor vessels and promoting vascular normalization (**Figure 25**) (Stehle et al., 2023). *Ex vivo* stimulation of breast tumor sections with vericiguat significantly increased cGMP and potentiated NO-induced cGMP production in pericytes (**Figure 21C** and **D**), suggesting that *in vivo*, vericiguat may influence the interaction between pericytes and the endothelium, consequently impacting the stability and functionality of the tumor vasculature.

Of note, pericytes are recognized as one of the main regulators of the TME, playing a controversial role in processes such as angiogenesis and metastasis. A low pericyte density is often associated with increased metastasis. Indeed, low pericyte coverage promoted tumor cell invasiveness and metastasis formation in different tumor types, while a high coverage was correlated with a lowered rate of metastatic dissemination (Correa et al., 2016; Yonenaga et al., 2005). On the other hand, high pericyte coverage has been associated with stabilized tumor vasculature, leading to increased nutrient delivery, and therefore favored tumor growth (Furuhashi et al., 2004), which might explain the increased tumor growth under vericiguat seen in **Figure 23**.

Nevertheless, several benefits have been reached in cancer therapy though application of vessel normalizing agents. Indeed, while it may seem counterintuitive, vascular normalization, by improving the functionality of tumor blood vessels may not only promote tumor growth but may also contribute to anti-tumor therapy under certain conditions. This is because vascular normalization can enhance the delivery of anticancer therapies and improve immune surveillance within the tumor (Patel et al., 2023). It has been shown that bevacizumab, a monoclonal antibody against VEGF-A, improves the infiltration of immune cells, such as dendritic and T cells in TNBC patients, which supports the implementation of bevacizumab during neoadjuvant treatment to enhance the efficacy of immunotherapy (Boucher et al., 2021). Preclinical studies already highlighted the beneficial effect of combining vessel normalizing agents, such as an antibody blocking the VEGF pathway (Meder et al., 2018) to improve the outcome of immunotherapies in breast cancer.

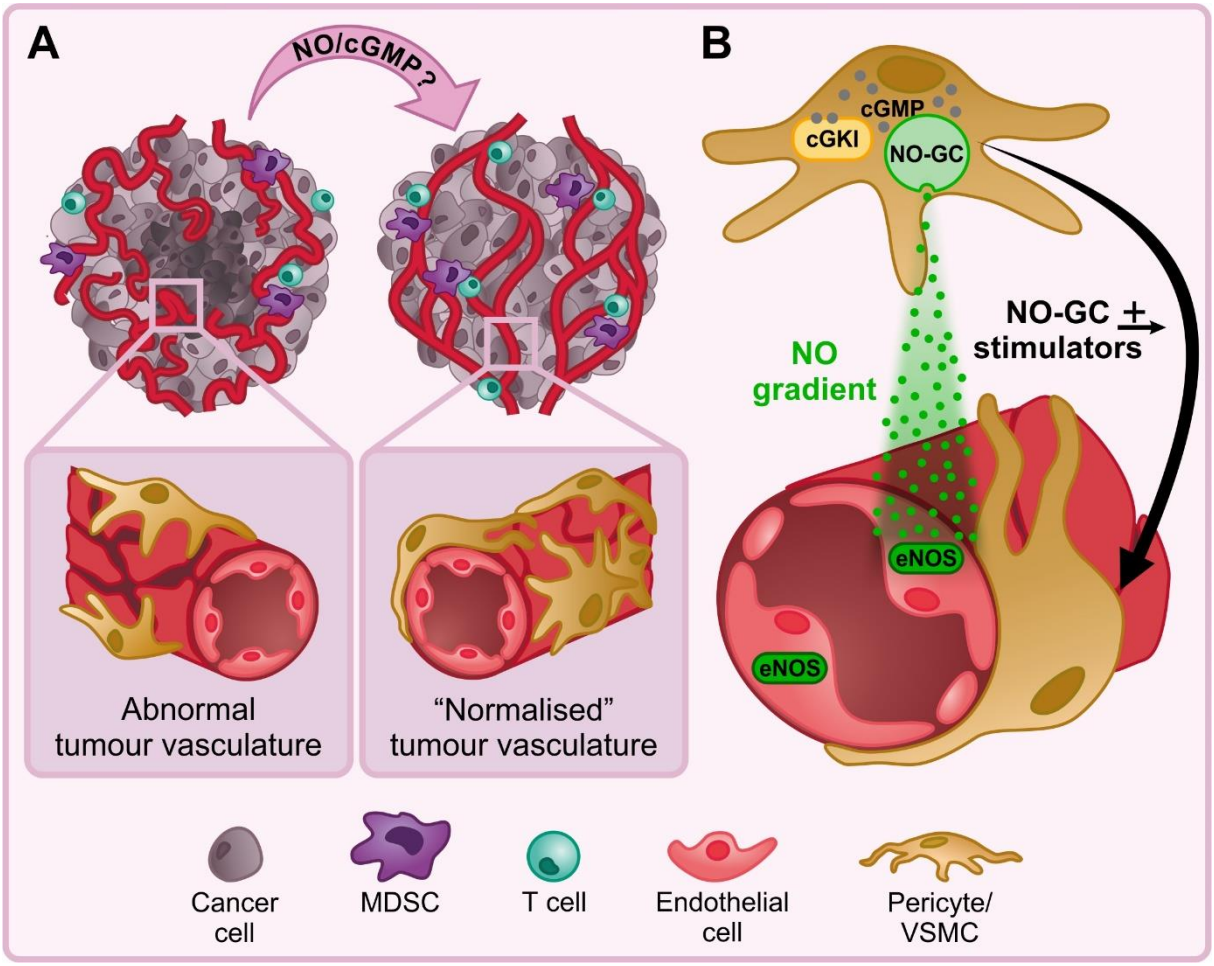

Figure 25. Hypothesis of NO/cGMP-mediated vascular normalization. A, The tumor vasculature typically presents a distorted and dysfunctional phenotype (left panel). The goal of vascular normalization is to reestablish the functionality of the tumor vasculature, thereby enhancing blood circulation and drug supply. The NO/cGMP signaling in perivascular cells has shown promise in aiding vascular normalization (right panel). **B**, Model of NO/cGMP-mediated vascular normalization. NO (green circles) is produced by eNOS in endothelial cells. The recruitment of pericytes on tumor vessel is dependent on the perivascular NO gradient. Thus, it might be modulated by the activation of the NO-GC/cGMP/cGKI axis in pericytes, which could be manipulated by NO-GC stimulators like vericiguat. Gray circles, cGMP; MDSC, myeloid-derived suppressor cell; VSMC, vascular smooth muscle cell. Figure from Stehle et al. (2023).

Interestingly, preclinical studies suggested that PDE5 inhibitors might also influence the breast cancer vasculature and improve drug delivery. Kumazoe et al. (2013) showed the interesting potential of combining vardenafil with an anti-tumor polyphenol derived from the green tea as treatment for breast cancer in a MDA-MB-231 xenograft model. Indeed, although single treatments showed no or adverse effect on tumor growth, the combination of the polyphenol together with vardenafil strongly inhibited tumor growth (Kumazoe et al., 2013). Additionally, improved delivery of the chemotherapeutic agent doxorubicin was obtained with co-administration of sildenafil in the 4T1 breast cancer mouse model (Greish et al., 2018). In both studies PDE5 inhibition *in vitro* did not influence MDA-MB-231 or 4T1 cell growth. Notably,

vardenafil alone increased tumor growth in the MDA-MB-231 xenograft model (Kumazoe et al., 2013), similarly to our results with vericiguat treatment (**Figure 23**).

It also has to be considered that vessel normalization and ECM remodeling are closely related (Martin et al., 2019). Indeed the hypoxia status inside tumors induces CAFs to produce excessive ECM, leading to solid stress which causes existing vessel compression, and angiogenesis, promoting tumor progression (Martin et al., 2019). Especially tumor angiogenesis is dependent on adhesion, migration, and degradation of the ECM, promoted by metalloproteinases. It has been shown that maintaining the integrity of the vascular basement membrane, part of the ECM, by inhibition of the metalloproteinase 14 induced vascular normalization and sensitivity to radiotherapy in a preclinical breast cancer model (Ager et al., 2015). Interestingly, findings showed that the NO-GC stimulators have anti-fibrotic effects in liver and kidney diseases (Hall et al., 2019; Schinner et al., 2017), which can induce ECM remodeling and influence tumor mass. Surprisingly, we did not observe a significant difference in tumor weight between normal diet control group and vericiguat-supplemented normal diet group (**Figure 23F**), while a significant difference was observed in the tumor volume between the two groups (**Figure 23E**). However, on a high-fat diet, the vericiguat-treated tumors were both larger in volume and heavier in weight in comparison to the control (**Figure 23B** and **C**). These findings might be linked to a different stroma composition in the absence and presence of vericiguat, influenced also by the different diet background and it needs to be studied in detail in the future.

Taken together, these findings support the hypothesis that the cGMP pathway plays a pivotal role in the organization and structure of the TME. Furthermore, we provided evidence that the pharmacological modulation of the NO/cGMP pathway influences tumor growth, probably because of an influence on the tumor vasculature and arrangement of the TME. Considering the application of vessel normalizing agents to augment standard of care therapies (Patel et al., 2023), cGMP-targeting drugs could be considered for this purpose. However, while it was evident that vericiguat exacerbated tumor growth, its potential role in vascular normalization still needs to be further elucidated. Additionally, we should consider that vericiguat was applied systemically and its effect on decreasing blood pressure (**Figure 22** and **Table S2**) might decrease nutrient and oxygen supply to the tumor, promoting hypoxia and thereby tumor growth.

5.4. Potential of targeting cGMP pathway components in the TME to treat breast cancer

As mentioned in section **1.1.2**, the cGMP signaling pathway's pharmacological importance is widely acknowledged. To date, this understanding has driven the development of various drugs to treat numerous conditions, including heart failure and pulmonary hypertension. Our research has made strides in identifying different components of this pathway in both tumor and stromal cells in breast cancer. Notably, the components found in the TME stand out, because they might become target for designing future therapies that can be beneficial to breast cancer patients independently on their breast cancer subtype.

In previous studies, the effects observed by cGMP modulation have been noted in stromal cells such as CAFs (Catalano et al., 2019) and MDSCs (Meyer et al., 2011; Serafini et al., 2006). The potential elevation of cGMP through PDE5 inhibition in these cell types has been associated with an anti-tumor response. This, however, was not the case in our current study. We observed that vericiguat treatment caused a pro-tumor response *in vivo* (**Figure 23**). Most likely this effect was mediated by intracellular cGMP increases in pericytes, which showed expression of NO-GC and cGKI through IF staining (**Figure 20**) and produced cGMP upon stimulation with DEA/NO and vericiguat (**Figure 21C** and **D**). However, we did not use PDE5 inhibitors nor explore PDE5 expression within human and murine breast tumors. Thus, we cannot exclude a different outcome in tumor response in our model if a PDE5 inhibitor is used. Furthermore, although FRET imaging did not indicate any cGMP production outside the tumor vasculature, it is still possible that other stromal cells could express cGMP generators and effectors at a very low but functional level, which could not be detected by our methodologies.

In the breast cancer TME, we managed to identify active ANP/cGMP and NO/cGMP pathways. The role of ANP/cGMP signaling in endothelial regulation is still a topic of ongoing debate (Kuhn, 2012). The consensus among most studies is that the ANP/cGMP pathway in endothelial cells plays a crucial part in controlling vascular permeability and angiogenesis. Nevertheless, the results of its modulation range from promoting to inhibiting these processes, depending on physiological or experimental parameters (Kuhn, 2012). Therefore, predicting the impact of ANP/cGMP pathway modulation on the endothelium of tumor vessels presents a significant challenge. Furthermore, we are only hypothesizing that the observed ANP-induced cGMP signal (**Figure 21A**) originates from the endothelium. Hence, our hypothesis can be validated using the broad spectrum of available Cre mouse lines, as discussed in section **1.2**. Notably, the presence of an active ANP/cGMP pathway in the tumor endothelium of B16F10 melanoma tumors has been demonstrated using endothelium-specific Cre mouse lines such as TIE2-Cre (Kisanuki et al., 2001) and CDH5-Cre (Sörensen et al., 2009), combined with the cGi500 mouse lines (Stehle, 2022).

Another crucial consideration is that confirming the presence of the ANP/cGMP pathway in the endothelium does not guarantee an easy path to specifically target it to influence tumor angiogenesis. This is because drugs capable of pharmacologically modulating this pathway remain limited. Until now, due to the absence of pharmacologically useful selective GC-A agonists, our interference with the ANP/cGMP pathway has been restricted to compounds that inhibit NP degradation, such as sacubitril. This drug, as discussed in section **1.1.2**, is typically used in conjunction with valsartan to treat chronic heart failure. However, it's worth noting that sacubitril/valsartan can influence the renin-angiotensin system, which has been shown to have a controversial role in tumor progression of various cancers (Almutlaq et al., 2021). Given this complexity, the opportunity of targeting the ANP/cGMP pathway in cancer treatment appears remote at the present stage. Yet, these challenges should not diminish the interest in further investigations about the role of the ANP/cGMP pathway in the breast cancer TME, which could lead to novel insights and potentially transformative therapeutic strategies.

Of potentially high importance was the identification of the NO/cGMP pathway in breast cancer pericytes in this study. Extensive discussion in **5.3** has highlighted the positive impact of NO on the tumor vasculature, which influences the arrangement of the TME and consequently impacts tumor growth and progression. Thus, NO has become pivotal in the design of precision therapies. For instance, a nanocarrier capable of supplying NO has been shown to induce vascular normalization and enhance the effectiveness of chemotherapy (Sung et al., 2019). It is reasonable to assume that similar results could be achieved using NO-GC stimulators such as riociguat and vericiguat, which have robustly demonstrated their potentiation effect in modulating NO-GC activity, as depicted in **Figure 13** and **Figure 21C** to **D**. Furthermore, the hypothesis developed in section **5.3** links the growth-promoting effect given by the pharmacological treatment with vericiguat in our preclinical model to vessel normalization.

The novel therapeutic approaches based on stimulation of NO/cGMP signaling in the TME may avoid adverse events associated with traditional anti-angiogenic therapies that utilize VEGF inhibitors. Although VEGF inhibitors have demonstrated considerable potential when incorporated into standard cancer therapies, they are also associated with severe, dose-dependent side effects, including hypertension (Versmissen et al., 2019). Moreover, also other cancer treatments, including specific types of chemotherapy and hormone therapies, can also contribute to the development or exacerbation of hypertension (Cohen et al., 2023). This poses significant risks for patients with co-existing health conditions.

This perspective underscores the potential of NO-GC stimulators as a co-treatment that could boost the potency of chemotherapy or immunotherapy, while concurrently mitigating their hypertensive effects. Vericiguat and other NO-GC stimulators target perivascular cells like VSMCs and pericytes, thereby modulating vessel function and contributing to vascular

relaxation. These characteristics enable them to affect blood pressure in a dose-dependent manner (Sandner et al., 2021). In this study, the concentration of vericiguat achieved in the experimental mice affected tumor growth without significantly altering blood pressure (**Figure 22** and **Table S2**). Consequently, this should not present any significant concerns for patients, and could even have a protective effect on chemotherapy-induced hypertension.

In conclusion, our study demonstrated the presence of the cGMP signaling pathway in the breast cancer TME, which might be useful targets to improve breast cancer therapies. Importantly, we hypothesize that vericiguat stimulation of the NO/cGMP pathway in pericytes of the TME can induce vascular normalization in breast cancer (**Figure 25**). This could potentially enhance the effectiveness of concurrent chemotherapy and immunotherapy. Moreover, the tendency of vericiguat to induce mild hypotension can counteract the hypertensive side effects caused by some standard cancer therapies.

5.5. Limitations of the study

In this study, we aimed to elucidate the role of the cGMP pathway in breast cancer, revealing a remarkable heterogeneity in its expression and activity among breast cancer and stromal cells. Despite the significant advancements made, our findings have also unveiled several unanswered questions that require further investigation.

First of all, the functional relevance of the cGMP pathway in the human Hs578T, BT549 and MDA-MB-157 and murine 4T1 breast cancer cell lines remains unclear. Although results on Hs578T cells seem to suggest a cGMP-induced anti-growth effect (**Figure 14B**), no change has been shown after cGMP pathway stimulation in 4T1 cells (**Figure 15A**). Thus, further analysis is required to evaluate changes in growth, migration, and apoptosis in all these cell lines. Furthermore, several questions need to be answered regarding the mechanism underling the pro-migratory effect induced by the 4T1 TCM on VSMCs (**Figure 15C**). TCM should be analyzed to define its composition and identify the unknown factor whose secretion is influenced by cGMP pathway stimulation.

As for the TNBC patient-derived organoids, results suggested that activation of the cGMP signaling pathway inhibits apoptosis (**Figure 16B** and **C**). However, to clarify the role of the cGMP pathway in apoptosis and its impact on Caspase 3 and PARP activity, specific apoptosis assays are necessary. Furthermore, the use of the cGi500 biosensor could be an appropriate tool to assess the presence of an active cGMP pathway in this system.

While the role of the cGMP pathway in breast cancer cells remains uncertain and may be linked to the cell batch, tumor subtype and stage, expression of the pathway in the stroma cells seems to be more robust and easier to analyze. Localization of components of the pathway,

such as NO-GC and cGKI, in the tumor stroma of different patients highlights a common target among breast cancer subtypes. The structures identified as NO-GC- and cGKI-positive in the stroma were part of the tumor vasculature (**Figure 17** and **Figure 18**). Although these data are supported by our preclinical mouse model (**Figure 20**), the number of analyzed patient biopsies needs to be increased to better understand the localization of the cGMP pathway components in human breast cancer.

The mechanism driving the vericiguat-induced tumor growth phenotype (**Figure 23**) remains unknown. A thorough analysis of the tumor vasculature is essential to understand if and how vericiguat affects pericytes within the tumor vascular network. This can be achieved through immunostaining of endothelial cells and pericytes within tumor sections or whole-mount samples, followed by detection using confocal or light-sheet microscopy, respectively. Moreover, potential differences in vessel integrity between conditions can be addressed through intravenous injection of markers like Evans blue-BSA, fluorescently labeled dextrans, and lectins (R. Jain et al., 2021). In line with our hypothesis that NO-GC activation in tumor pericytes leads to vascular normalization, it will be exciting to examine the co-therapy of vericiguat with standard care therapies, such as immunotherapy.

However, a crucial step is still required to conclusively substantiate our hypothesis. Although real-time cGMP imaging in breast cancer slices has shown that NO and vericiguat induce cGMP generation in tumor pericytes (**Figure 21B** to **D**), and we hypothesize that the primary target of vericiguat treatment within the tumor is the pericyte population, pericytes-specific knockout mice are needed. Both wildtype and pericyte-specific NO-GC knockout animals should be treated with vericiguat or placebo, followed by a comparative analysis of their tumor vasculature to confirm that the vericiguat-induced pro-tumor effect observed in this study was indeed mediated by NO-GC in pericytes.

Lastly, considering the high recurrence of metastatic breast cancer among patients, it would be interesting to investigate the role of the cGMP pathway for metastatic spread as well as in tumor pericytes of metastatic lesions. This could be done using mouse models for metastatic breast cancer, in which the primary tumor is resected after the initial growth phase (as described in **3.8.5**) to allow the development of lung metastases (**Figure S7**).

In summary, while our study has deepened the understanding of the cGMP pathway's involvement in breast cancer, numerous unanswered questions have emerged, emphasizing the need for further research to unravel its complexities and potential implications for diagnosis, treatment, and patient outcomes.

6. Conclusions and outlook

The present work has provided exciting new insights into the role of the cGMP signaling pathway in breast cancer. Through real-time cGMP imaging, we have elucidated which different GCs are activated by natural and pharmacologically derived ligands in cancer and stromal cells. Characterization of several human and murine breast cancer cell lines revealed a remarkable heterogeneity in the presence and activity of the cGMP pathway. Notably, our experiments revealed the presence of the CNP/cGMP and NO/cGMP pathway particularly in TNBC cells. *In vitro* approaches suggested that activation of the cGMP pathway in TNBC cancer cells might influence breast cancer growth and apoptosis, and also mediate crosstalk with stromal cells.

Shifting our focus to the analysis of the stroma of both breast cancer patients and a preclinical mouse model, we found consistent expression of the cGMP pathway in specific structures of the TME. In both human and murine stroma, components of the cGMP signaling pathway were associated with tumor vasculature. Specifically, NO-GC and cGKI expression was observed in tumor vessel-associated pericytes, suggesting a potential role of the NO/cGMP pathway in managing the tumor's blood supply.

Interestingly, our study presented a notable twist in the narrative of NO-GC stimulators. The therapeutic landscape of cardiovascular diseases has significantly improved with the advent of the NO-GC stimulator vericiguat, which is now clinically used to treat heart failure with reduced ejection fraction. However, we demonstrated that pharmacological modulation of the cGMP signaling pathway with vericiguat drastically increased breast cancer tumor growth, at least in a preclinical mouse model. This discovery has significant implications for patient management, emphasizing the need for more extensive longitudinal surveillance and clinical research. Furthermore, our experiments aimed to evaluate the effect of vericiguat on host stromal cells, which are part of the TME. Thus, this suggests that the pro-tumor effect could potentially be replicable across diverse tumor types.

Our findings could introduce a new element of risk into the decision-making process for clinicians treating patients with cardiovascular diseases who have a history or elevated risk of breast cancer. However, understanding the mechanisms underlying its pro-tumor effect could categorize vericiguat as a vessel normalizing agent, which may lead to drug repurposing. For example, vericiguat could be used in combination with chemotherapy or immunotherapy, potentially enhancing anti-cancer drug delivery and reducing drug-induced hypertension.

In conclusion, by understanding the specific distribution and activity of the cGMP pathway within the TME, we can potentially exploit its modulation to target and manipulate the cellular processes involved in cancer development and progression. This newfound knowledge

provides a foundation for the design and optimization of therapeutic interventions that can selectively target cancer or stromal cells in the TME, thereby improving treatment outcomes and patient survival rates. Notably, the identification of NO-GC in the breast cancer TME presents promising opportunities for the development of novel therapeutics. The potential use of NO-GC stimulators as therapeutic agents holds potential in improving standard cancer therapies, acting as vessel normalizing agent. However, as already mentioned, further analysis is required for the validation of our hypothesis. Nevertheless, with these exciting advancements, we moved closer to realizing the potential of harnessing the cGMP signaling pathway as a valuable target in the fight against breast cancer.

7. References

Ager, E. I., Kozin, S. V., Kirkpatrick, N. D., Seano, G., Kodack, D. P., Askoxylakis, V., Huang, Y., Goel, S., Snuderl, M., Muzikansky, A., Finkelstein, D. M., Dransfield, D. T., Devy, L., Boucher, Y., Fukumura, D., & Jain, R. K. (2015). Blockade of MMP14 activity in murine breast carcinomas: implications for macrophages, vessels, and radiotherapy. *J Natl Cancer Inst*, *107*(4), djv017. https://doi.org/10.1093/jnci/djv017

Agilent. (2023). Real-time cell analysis (xCelligence). Retrieved 14.03.2023 from https://www.agilent.com/en/technology/cellular-impedance

Almutlaq, M., Alamro, A. A., Alamri, H. S., Alghamdi, A. A., & Barhoumi, T. (2021). The effect of local renin angiotensin system in the common types of cancer [Review]. *Front Endocrinol*, *12*. https://doi.org/https://doi.org/10.3389/fendo.2021.736361

Anand-Srivastava, M. B. (2005). Natriuretic peptide receptor-C signaling and regulation. *Peptides*, *26*(6), 1044-1059. https://doi.org/https://doi.org/10.1016/j.peptides.2004.09.023

Bagegni, N. A., Davis, A. A., Clifton, K. K., & Ademuyiwa, F. O. (2022). Targeted treatment for high-risk early-stage triple-negative breast cancer: spotlight on pembrolizumab. *Breast Cancer (Dove Med Press)*, *14*, 113-123. https://doi.org/10.2147/bctt.S293597

Basudhar, D., Glynn, S. A., Greer, M., Somasundaram, V., No, J. H., Scheiblin, D. A., Garrido, P., Heinz, W. F., Ryan, A. E., Weiss, J. M., Cheng, R. Y. S., Ridnour, L. A., Lockett, S. J., McVicar, D. W., Ambs, S., & Wink, D. A. (2017). Coexpression of NOS2 and COX2 accelerates tumor growth and reduces survival in estrogen receptor-negative breast cancer. *Proc Natl Acad Sci U S A*, *114*(49), 13030-13035. https://doi.org/10.1073/pnas.1709119114

Ben-David, U., Siranosian, B., Ha, G., Tang, H., Oren, Y., Hinohara, K., Strathdee, C. A., Dempster, J., Lyons, N. J., Burns, R., Nag, A., Kugener, G., Cimini, B., Tsvetkov, P., Maruvka, Y. E., O'Rourke, R., Garrity, A., Tubelli, A. A., Bandopadhayay, P., . . . Golub, T. R. (2018). Genetic and transcriptional evolution alters cancer cell line drug response. *Nature*, *560*(7718), 325-330. https://doi.org/10.1038/s41586-018-0409-3

Bender, A. T., & Beavo, J. A. (2006). Cyclic nucleotide phosphodiesterases: molecular regulation to clinical use. *Pharmacol Rev*, *58*(3), 488-520. https://doi.org/10.1124/pr.58.3.5

Biel, M., & Michalakis, S. (2009). Cyclic nucleotide-gated channels. *Handb Exp Pharmacol*(191), 111-136. https://doi.org/10.1007/978-3-540-68964-5_7

BioRender.com. (2023). Create professional science figures in minutes. https://www.biorender.com/

Bork, N. I., & Nikolaev, V. O. (2018). cGMP signaling in the cardiovascular system—the role of compartmentation and its live cell imaging. *Int J Mol Sci*, *19*(3). https://doi.org/10.3390/ijms19030801

Boucher, Y., Kumar, A. S., Posada, J. M., Gjini, E., Pfaff, K., Lipschitz, M., Lako, A., Duda, D. G., Rodig, S. J., Hodi, F. S., & Jain, R. K. (2021). Bevacizumab improves tumor infiltration of mature dendritic cells and effector T-cells in triple-negative breast cancer patients. *NPJ Precis Oncol*, *5*(1), 62. https://doi.org/10.1038/s41698-021-00197-w

Burstein, H. J. (2020). Systemic therapy for estrogen receptor-positive, HER2-negative breast cancer. *N Engl J Med*, *383*(26), 2557-2570. https://doi.org/10.1056/NEJMra1307118

Caporali, A., Martello, A., Miscianinov, V., Maselli, D., Vono, R., & Spinetti, G. (2017). Contribution of pericyte paracrine regulation of the endothelium to angiogenesis. *Pharmacol Ther*, *171*, 56-64. https://doi.org/10.1016/j.pharmthera.2016.10.001

Carmeliet, P., & Jain, R. K. (2000). Angiogenesis in cancer and other diseases. *Nature*, *407*(6801), 249-257. https://doi.org/10.1038/35025220

Catalano, S., Campana, A., Giordano, C., Gyorffy, B., Tarallo, R., Rinaldi, A., Bruno, G., Ferraro, A., Romeo, F., Lanzino, M., Naro, F., Bonofiglio, D., Ando, S., & Barone, I. (2016). Expression and function of phosphodiesterase type 5 in human breast cancer cell lines and tissues: implications for targeted therapy. *Clin Cancer Res*, *22*(9), 2271-2282. https://doi.org/10.1158/1078-0432.CCR-15-1900

Catalano, S., Panza, S., Augimeri, G., Giordano, C., Malivindi, R., Gelsomino, L., Marsico, S., Giordano, F., Győrffy, B., Bonofiglio, D., Andò, S., & Barone, I. (2019). Phosphodiesterase 5 (PDE5) is highly expressed in cancer-associated fibroblasts and enhances breast tumor progression. *Cancers (Basel)*, *11*(11). https://doi.org/10.3390/cancers11111740

Chung, A. W., Anand, K., Anselme, A. C., Chan, A. A., Gupta, N., Venta, L. A., Schwartz, M. R., Qian, W., Xu, Y., Zhang, L., Kuhn, J., Patel, T., Rodriguez, A. A., Belcheva, A., Darcourt, J., Ensor, J., Bernicker, E., Pan, P. Y., Chen, S. H., . . . Chang, J. C. (2021). A phase 1/2 clinical trial of the nitric oxide synthase inhibitor L-NMMA and taxane for treating chemoresistant triple-negative breast cancer. *Sci Transl Med*, *13*(624), eabj5070. https://doi.org/10.1126/scitranslmed.abj5070

Cohen, J. B., Brown, N. J., Brown, S.-A., Dent, S., van Dorst, D. C. H., Herrmann, S. M., Lang, N. N., Oudit, G. Y., Touyz, R. M., & null, n. (2023). Cancer therapy–related hypertension: a scientific statement from the american heart association. *Hypertension*, *80*(3), e46-e57. https://doi.org/10.1161/HYP.0000000000000224

Conole, D., & Scott, L. J. (2013). Riociguat: first global approval. *Drugs*, *73*(17), 1967-1975. https://doi.org/10.1007/s40265-013-0149-5

Correa, D., Somoza, R. A., Lin, P., Schiemann, W. P., & Caplan, A. I. (2016). Mesenchymal stem cells regulate melanoma cancer cells extravasation to bone and liver at their perivascular niche. *Int J Cancer*, *138*(2), 417-427. https://doi.org/https://doi.org/10.1002/ijc.29709

Dhayade, S., Kaesler, S., Sinnberg, T., Dobrowinski, H., Peters, S., Naumann, U., Liu, H., Hunger, R. E., Thunemann, M., Biedermann, T., Schittek, B., Simon, H. U., Feil, S., & Feil, R. (2016). Sildenafil potentiates a cGMP-dependent pathway to promote melanoma growth. *Cell Rep*, *14*(11), 2599-2610. https://doi.org/10.1016/j.celrep.2016.02.028

Di Iorio, P., Ronci, M., Giuliani, P., Caciagli, F., Ciccarelli, R., Caruso, V., Beggiato, S., & Zuccarini, M. (2021). Pros and cons of pharmacological manipulation of cGMP-PDEs in the prevention and treatment of breast cancer. *Int J Mol Sci*, *23*(1), 262. https://doi.org/10.3390/ijms23010262

Di, X., Gennings, C., Bear, H. D., Graham, L. J., Sheth, C. M., White, K. L., Jr., & Gewirtz, D. A. (2010). Influence of the phosphodiesterase-5 inhibitor, sildenafil, on sensitivity to chemotherapy in breast tumor cells. *Breast Cancer Res Treat*, *124*(2), 349-360. https://doi.org/10.1007/s10549-010-0765-7

Dobrowinski, H. G. (2019). Influence of cGMP signaling on VSMC growth and its dependence on fibronectin in cultured VSMCs and development of atherosclerosis [Doctoral thesis, University of Tubingen]. http://hdl.handle.net/10900/91054

Duggan, S. (2021). Vosoritide: first approval. *Drugs*, *81*(17), 2057-2062. https://doi.org/10.1007/s40265-021-01623-w

Ebctcg, McGale, P., Taylor, C., Correa, C., Cutter, D., Duane, F., Ewertz, M., Gray, R., Mannu, G., Peto, R., Whelan, T., Wang, Y., Wang, Z., & Darby, S. (2014). Effect of radiotherapy after mastectomy and axillary surgery on 10-year recurrence and 20-year breast cancer mortality: meta-analysis of individual patient data for 8135 women in 22 randomised trials. *Lancet*, *383*(9935), 2127-2135. https://doi.org/10.1016/S0140-6736(14)60488-8

Egbert, J. R., Uliasz, T. F., Shuhaibar, L. C., Geerts, A., Wunder, F., Kleiman, R. J., Humphrey, J. M., Lampe, P. D., Artemyev, N. O., Rybalkin, S. D., Beavo, J. A., Movsesian, M. A., & Jaffe, L. A. (2016). Luteinizing hormone causes phosphorylation and activation of the cGMP phosphodiesterase PDE5 in rat ovarian follicles, contributing, together with PDE1 activity, to the resumption of meiosis. *Biol Reprod*, *94*(5), 110. https://doi.org/10.1095/biolreprod.115.135897

El-Naa, M. M., Othman, M., & Younes, S. (2016). Sildenafil potentiates the antitumor activity of cisplatin by induction of apoptosis and inhibition of proliferation and angiogenesis. *Drug Des Devel Ther*, *10*, 3661-3672. https://doi.org/10.2147/DDDT.S107490

Elstrodt, F., Hollestelle, A., Nagel, J. H. A., Gorin, M., Wasielewski, M., van den Ouweland, A., Merajver, S. D., Ethier, S. P., & Schutte, M. (2006). BRCA1 mutation analysis of 41 human breast cancer cell lines reveals three new deleterious mutants. *Cancer Res*, *66*(1), 41-45. https://doi.org/10.1158/0008-5472.CAN-05-2853

Farah, C., Michel, L. Y. M., & Balligand, J.-L. (2018). Nitric oxide signalling in cardiovascular health and disease. *Nat Rev Cardiol*, *15*(5), 292-316. https://doi.org/10.1038/nrcardio.2017.224

Fares, J., Fares, M. Y., Khachfe, H. H., Salhab, H. A., & Fares, Y. (2020). Molecular principles of metastasis: a hallmark of cancer revisited. *Signal Transduct Target Ther*, *5*(1), 28. https://doi.org/10.1038/s41392-020-0134-x

Feil, R., Lohmann, S. M., de Jonge, H., Walter, U., & Hofmann, F. (2003). Cyclic GMP-dependent protein kinases and the cardiovascular system: insights from genetically modified mice. *Circ Res*, *93*(10), 907-916. https://doi.org/10.1161/01.RES.0000100390.68771.CC

Feil, R., Feil, S., & Hofmann, F. (2005). A heretical view on the role of NO and cGMP in vascular proliferative diseases. *Trends Mol Med*, *11*(2), 71-75. https://doi.org/10.1016/j.molmed.2004.12.001

Feil, R. (2007). Conditional somatic mutagenesis in the mouse using site-specific recombinases. In R. Feil & D. Metzger (Eds.), *Conditional mutagenesis: An approach to disease models* (pp. 3-28). Springer Berlin Heidelberg. https://doi.org/10.1007/978-3-540-35109-2_1

Feil, R. (2017). Viagra releases the brakes on melanoma growth. *Mol Cell Oncol*, *4*(5), e1188874. https://doi.org/10.1080/23723556.2016.1188874

Feil, R., Lehners, M., Stehle, D., & Feil, S. (2022). Visualising and understanding cGMP signals in the cardiovascular system. *Br J Pharmacol*, *179*(11), 2394-2412. https://doi.org/10.1111/bph.15500

Feil, S., Valtcheva, N., & Feil, R. (2009). Inducible Cre mice. *Methods Mol Biol*, *530*, 343-363. https://doi.org/10.1007/978-1-59745-471-1_18

Feil, S., Krauss, J., Thunemann, M., & Feil, R. (2014). Genetic inducible fate mapping in adult mice using tamoxifen-dependent Cre recombinases. *Methods Mol Biol*, *1194*, 113-139. https://doi.org/10.1007/978-1-4939-1215-5_6

Feng, M., Whitesall, S., Zhang, Y., Beibel, M., D'Alecy, L., & DiPetrillo, K. (2008). Validation of volume-pressure recording tail-cuff blood pressure measurements. *Am J Hypertens*, *21*(12), 1288-1291. https://doi.org/10.1038/ajh.2008.301

Ferland-McCollough, D., Slater, S., Richard, J., Reni, C., & Mangialardi, G. (2017). Pericytes, an overlooked player in vascular pathobiology. *Pharmacol Ther*, *171*, 30-42. https://doi.org/10.1016/j.pharmthera.2016.11.008

Fernando, V., Zheng, X., Walia, Y., Sharma, V., Letson, J., & Furuta, S. (2019). S-nitrosylation: an emerging paradigm of redox signaling. *Antioxidants (Basel)*, *8*(9). https://doi.org/10.3390/antiox8090404

Fleming, I., & Busse, R. (2003). Molecular mechanisms involved in the regulation of the endothelial nitric oxide synthase. *Am J Physiol Regul Integr Comp Physiol*, *284*(1), R1-12. https://doi.org/10.1152/ajpregu.00323.2002

Folkman, J. (2002). Role of angiogenesis in tumor growth and metastasis. *Semin Oncol*, *29*(6 Suppl 16), 15-18. https://doi.org/10.1053/sonc.2002.37263

Förstermann, U., & Sessa, W. C. (2012). Nitric oxide synthases: regulation and function. *Eur Heart J*, *33*(7), 829-837, 837a-837d. https://doi.org/10.1093/eurheartj/ehr304

Francis, S. H., Blount, M. A., & Corbin, J. D. (2011). Mammalian cyclic nucleotide phosphodiesterases: molecular mechanisms and physiological functions. *Physiol Rev*, *91*(2), 651-690. https://doi.org/10.1152/physrev.00030.2010

Friebe, A., Mergia, E., Dangel, O., Lange, A., & Koesling, D. (2007). Fatal gastrointestinal obstruction and hypertension in mice lacking nitric oxide-sensitive guanylyl cyclase. *Proc Natl Acad Sci U S A*, *104*(18), 7699-7704. https://doi.org/10.1073/pnas.0609778104

Friebe, A., Voußen, B., & Groneberg, D. (2018). NO-GC in cells 'off the beaten track'. *Nitric Oxide*, *77*, 12-18. https://doi.org/10.1016/j.niox.2018.03.020

Friedman, D. L. (1976). Role of cyclic nucleotides in cell growth and differentiation. *Physiol Rev*, *56*(4), 652-708. https://doi.org/10.1152/physrev.1976.56.4.652

Fukumura, D., Kloepper, J., Amoozgar, Z., Duda, D. G., & Jain, R. K. (2018). Enhancing cancer immunotherapy using antiangiogenics: opportunities and challenges. *Nat Rev Clin Oncol*, *15*(5), 325-340. https://doi.org/10.1038/nrclinonc.2018.29

Furuhashi, M., Sjöblom, T., Abramsson, A., Ellingsen, J., Micke, P., Li, H., Bergsten-Folestad, E., Eriksson, U., Heuchel, R., Betsholtz, C., Heldin, C. H., & Ostman, A. (2004). Platelet-derived growth factor production by B16 melanoma cells leads to increased pericyte abundance in tumors and an associated increase in tumor growth rate. *Cancer Res*, *64*(8), 2725-2733. https://doi.org/10.1158/0008-5472.can-03-1489

Garcia, J., Hurwitz, H. I., Sandler, A. B., Miles, D., Coleman, R. L., Deurloo, R., & Chinot, O. L. (2020). Bevacizumab (Avastin®) in cancer treatment: a review of 15 years of clinical experience and future outlook. *Cancer Treat Rev*, *86*, 102017. https://doi.org/10.1016/j.ctrv.2020.102017

Ghofrani, H. A., Osterloh, I. H., & Grimminger, F. (2006). Sildenafil: from angina to erectile dysfunction to pulmonary hypertension and beyond. *Nat Rev Drug Discov*, *5*(8), 689-702. https://doi.org/10.1038/nrd2030

Glynn, S. A., Boersma, B. J., Dorsey, T. H., Yi, M., Yfantis, H. G., Ridnour, L. A., Martin, D. N., Switzer, C. H., Hudson, R. S., Wink, D. A., Lee, D. H., Stephens, R. M., & Ambs, S. (2010). Increased NOS2 predicts poor survival in estrogen receptor–negative breast cancer patients. *J Clin Investig*, *120*(11), 3843-3854. https://doi.org/10.1172/JCI42059

Goel, S., Duda, D. G., Xu, L., Munn, L. L., Boucher, Y., Fukumura, D., & Jain, R. K. (2011). Normalization of the vasculature for treatment of cancer and other diseases. *Physiol Rev*, *91*(3), 1071-1121. https://doi.org/10.1152/physrev.00038.2010

Goetze, J. P., Bruneau, B. G., Ramos, H. R., Ogawa, T., de Bold, M. K., & de Bold, A. J. (2020). Cardiac natriuretic peptides. *Nat Rev Cardiol*, *17*(11), 698-717. https://doi.org/10.1038/s41569-020-0381-0

Gomes-Santos, I. L., Amoozgar, Z., Kumar, A. S., Ho, W. W., Roh, K., Talele, N. P., Curtis, H., Kawaguchi, K., Jain, R. K., & Fukumura, D. (2021). Exercise training improves tumor control by increasing CD8(+) T-cell infiltration via CXCR3 signaling and sensitizes breast cancer to immune checkpoint blockade. *Cancer Immunol Res*, *9*(7), 765-778. https://doi.org/10.1158/2326-6066.Cir-20-0499

Granados-Principal, S., Liu, Y., Guevara, M. L., Blanco, E., Choi, D. S., Qian, W., Patel, T., Rodriguez, A. A., Cusimano, J., Weiss, H. L., Zhao, H., Landis, M. D., Dave, B., Gross, S. S., & Chang, J. C. (2015). Inhibition of iNOS as a novel effective targeted therapy against triple-negative breast cancer. *Breast Cancer Res*, *17*(1), 1-16. https://doi.org/10.1186/s13058-015-0527-x

Greish, K., Fateel, M., Abdelghany, S., Rachel, N., Alimoradi, H., Bakhiet, M., & Alsaie, A. (2018). Sildenafil citrate improves the delivery and anticancer activity of doxorubicin formulations in a mouse model of breast cancer. *J Drug Target*, *26*(7), 610-615. https://doi.org/10.1080/1061186X.2017.1405427

Hall, K. C., Bernier, S. G., Jacobson, S., Liu, G., Zhang, P. Y., Sarno, R., Catanzano, V., Currie, M. G., & Masferrer, J. L. (2019). sGC stimulator praliciguat suppresses stellate cell fibrotic transformation and inhibits fibrosis and inflammation in models of NASH. *Proc Natl Acad Sci U S A*, *116*(22), 11057-11062. https://doi.org/10.1073/pnas.1821045116

Harbeck, N., Penault-Llorca, F., Cortes, J., Gnant, M., Houssami, N., Poortmans, P., Ruddy, K., Tsang, J., & Cardoso, F. (2019). Breast cancer. *Nat Rev Dis Primers*, *5*(1), 66. https://doi.org/10.1038/s41572-019-0111-2

Hassanvand, F., Mohammadi, T., Ayoubzadeh, N., Tavakoli, A., Hassanzadeh, N., Sanikhani, N. S., Azimi, A. I., Mirzaei, H. R., Khodamoradi, M., Goudarzi, K. A., Pourghadamyari, H., & Zaimy, M. A. (2020). Sildenafil enhances cisplatin-induced apoptosis in human breast adenocarcinoma cells. *J Cancer Res Ther*, *16*(6), 1412-1418. https://doi.org/10.4103/jcrt.JCRT_675_19

Helleday, T. (2011). The underlying mechanism for the PARP and BRCA synthetic lethality: clearing up the misunderstandings. *Mol Oncol*, *5*(4), 387-393. https://doi.org/10.1016/j.molonc.2011.07.001

Hofmann, F., Feil, R., Kleppisch, T., & Schlossmann, J. (2006). Function of cGMP-dependent protein kinases as revealed by gene deletion. *Physiol Rev*, *86*(1), 1-23. https://doi.org/10.1152/physrev.00015.2005

Hofmann, F. (2020). The cGMP system: components and function. *Biol Chem*, *401*(4), 447-469. https://doi.org/doi:10.1515/hsz-2019-0386

Holliday, D. L., & Speirs, V. (2011). Choosing the right cell line for breast cancer research. *Breast Cancer Research*, *13*(4), 215. https://doi.org/10.1186/bcr2889

Holtwick, R., Gotthardt, M., Skryabin, B., Steinmetz, M., Potthast, R., Zetsche, B., Hammer, R. E., Herz, J., & Kuhn, M. (2002). Smooth muscle-selective deletion of guanylyl cyclase-A prevents the acute but not chronic effects of ANP on blood pressure. *Proc Natl Acad Sci U S A*, *99*(10), 7142-7147. https://doi.org/10.1073/pnas.102650499

Horst, B. G., Yokom, A. L., Rosenberg, D. J., Morris, K. L., Hammel, M., Hurley, J. H., & Marletta, M. A. (2019). Allosteric activation of the nitric oxide receptor soluble guanylate cyclase mapped by cryo-electron microscopy. *eLife*, *8*, e50634. https://doi.org/10.7554/eLife.50634

Ibidi. (2023). Culture-Insert 2 well in µ-Dish 35 mm. Retrieved 15.03.2023 from https://ibidi.com/culture-inserts/24-culture-insert-2-well.html

Jain, R., Tikoo, S., On, K., Martinez, B., Dervish, S., Cavanagh, L. L., & Weninger, W. (2021). Visualizing murine breast and melanoma tumor microenvironment using intravital multiphoton microscopy. *STAR Protoc*, *2*(3), 100722. https://doi.org/10.1016/j.xpro.2021.100722

Jain, R. K. (2001). Normalizing tumor vasculature with anti-angiogenic therapy: a new paradigm for combination therapy. *Nat Med*, *7*(9), 987-989. https://doi.org/10.1038/nm0901-987

Jain, R. K. (2005). Normalization of tumor vasculature: an emerging concept in antiangiogenic therapy. *Science*, *307*(5706), 58-62. https://doi.org/10.1126/science.1104819

Kang, Y., Liu, R., Wu, J. X., & Chen, L. (2019). Structural insights into the mechanism of human soluble guanylate cyclase. *Nature*, *574*(7777), 206-210. https://doi.org/10.1038/s41586-019-1584-6

Karami-Tehrani, F., Fallahian, F., & Atri, M. (2012). Expression of cGMP-dependent protein kinase, PKGIalpha, PKGIbeta, and PKGII in malignant and benign breast tumors. *Tumour Biol*, *33*(6), 1927-1932. https://doi.org/10.1007/s13277-012-0453-9

Kashiwagi, S., Izumi, Y., Gohongi, T., Demou, Z. N., Xu, L., Huang, P. L., Buerk, D. G., Munn, L. L., Jain, R. K., & Fukumura, D. (2005). NO mediates mural cell recruitment and vessel morphogenesis in murine melanomas and tissue-engineered blood vessels. *J Clin Investig*, *115*(7), 1816-1827. https://doi.org/10.1172/JCI24015

Kashiwagi, S., Tsukada, K., Xu, L., Miyazaki, J., Kozin, S. V., Tyrrell, J. A., Sessa, W. C., Gerweck, L. E., Jain, R. K., & Fukumura, D. (2008). Perivascular nitric oxide gradients normalize tumor vasculature. *Nat Med*, *14*(3), 255-257. https://doi.org/10.1038/nm1730

Kisanuki, Y. Y., Hammer, R. E., Miyazaki, J., Williams, S. C., Richardson, J. A., & Yanagisawa, M. (2001). Tie2-Cre transgenic mice: a new model for endothelial cell-lineage analysis in vivo. *Dev Biol*, *230*(2), 230-242. https://doi.org/10.1006/dbio.2000.0106

Kitaeva, K. V., Rutland, C. S., Rizvanov, A. A., & Solovyeva, V. V. (2020). Cell culture based in vitro test systems for anticancer drug screening [Mini Review]. *Front Bioeng Biotechnol*, *8*. https://doi.org/10.3389/fbioe.2020.00322

Kokkonen, K., & Kass, D. A. (2017). Nanodomain regulation of cardiac cyclic nucleotide signaling by phosphodiesterases. *Annu Rev Pharmacol Toxicol*, *57*(1), 455-479. https://doi.org/10.1146/annurev-pharmtox-010716-104756

Kramer, C., Vreeswijk, M., Thijssen, B., Bosse, T., & Wesseling, J. (2022). Beyond the snapshot: optimizing prognostication and prediction by moving from fixed to functional multidimensional cancer pathology. *J Pathol*, *257*(4), 403-412. https://doi.org/10.1002/path.5915

Kuhn, M. (2012). Endothelial actions of atrial and B-type natriuretic peptides. *Br J Pharmacol*, *166*(2), 522-531. https://doi.org/10.1111/j.1476-5381.2012.01827.x

Kuhn, M. (2016). Molecular physiology of membrane guanylyl cyclase receptors. *Physiol Rev*, *96*(2), 751-804. https://doi.org/10.1152/physrev.00022.2015

Kumazoe, M., Sugihara, K., Tsukamoto, S., Huang, Y., Tsurudome, Y., Suzuki, T., Suemasu, Y., Ueda, N., Yamashita, S., Kim, Y., Yamada, K., & Tachibana, H. (2013). 67-kDa laminin receptor increases cGMP to induce cancer-selective apoptosis. *J Clin Invest*, *123*(2), 787-799. https://doi.org/10.1172/jci64768

Laemmli, U. K. (1970). Cleavage of structural proteins during the assembly of the head of bacteriophage T4. *Nature*, *227*(5259), 680-685. https://doi.org/10.1038/227680a0

Le Naour, A., Rossary, A., & Vasson, M. P. (2020). EO771, is it a well-characterized cell line for mouse mammary cancer model? Limit and uncertainty. *Cancer Med*, *9*(21), 8074-8085. https://doi.org/10.1002/cam4.3295

Lee, K., Lindsey, A. S., Li, N., Gary, B., Andrews, J., Keeton, A. B., & Piazza, G. A. (2016). β-catenin nuclear translocation in colorectal cancer cells is suppressed by PDE10A inhibition, cGMP elevation, and activation of PKG. *Oncotarget*, *7*(5), 5353-5365. https://doi.org/10.18632/oncotarget.6705

Lehners, M., Dobrowinski, H., Feil, S., & Feil, R. (2018). cGMP signaling and vascular smooth muscle cell plasticity. *J Cardiovasc Dev Dis*, *5*(2), 20. https://doi.org/10.3390/jcdd5020020

Lehners, M. (2022). CNP-dependent cGMP signalling in vascular smooth muscle cells: from phenotypic plasticity to atherosclerosis [Doctoral Thesis, University of Tubingen]. http://hdl.handle.net/10900/128603

Leung, Y. K., Du, J., Huang, Y., & Yao, X. (2010). Cyclic nucleotide-gated channels contribute to thromboxane A2-induced contraction of rat small mesenteric arteries. *PLoS One*, *5*(6), e11098. https://doi.org/10.1371/journal.pone.0011098

Liang, W. L., & Liang, B. (2023). Soluble guanylate cyclase activators and stimulators in patients with heart failure. *Curr Cardiol Rep*, *25*(6), 607-613. https://doi.org/10.1007/s11886-023-01884-9

Limame, R., Wouters, A., Pauwels, B., Fransen, E., Peeters, M., Lardon, F., De Wever, O., & Pauwels, P. (2012). Comparative analysis of dynamic cell viability, migration and invasion assessments by novel real-time technology and classic endpoint assays. *PLoS One*, *7*(10), e46536. https://doi.org/10.1371/journal.pone.0046536

Linderholm, B. K., Hellborg, H., Johansson, U., Elmberger, G., Skoog, L., Lehtiö, J., & Lewensohn, R. (2009). Significantly higher levels of vascular endothelial growth factor (VEGF) and shorter survival times for patients with primary operable triple-negative breast cancer. *Ann Oncol*, *20*(10), 1639-1646. https://doi.org/10.1093/annonc/mdp062

Liu, C., Wu, P., Zhang, A., & Mao, X. (2021). Advances in rodent models for breast cancer formation, progression, and therapeutic testing. *Front Oncol*, *11*, 593337. https://doi.org/10.3389/fonc.2021.593337

Liu, R., Kang, Y., & Chen, L. (2021). Activation mechanism of human soluble guanylate cyclase by stimulators and activators. *Nat Commun*, *12*(1), 5492. https://doi.org/10.1038/s41467-021-25617-0

Lowry, O. H., Rosebrough, N. J., Farr, A. L., & Randall, R. J. (1951). Protein measurement with the Folin phenol reagent. *J Biol Chem*, *193*(1), 265-275.

Łukasiewicz, S., Czeczelewski, M., Forma, A., Baj, J., Sitarz, R., & Stanisławek, A. (2021). Breast cancer-epidemiology, risk factors, classification, prognostic markers, and current treatment strategies-an updated review. *Cancers (Basel)*, *13*(17). https://doi.org/10.3390/cancers13174287

Lv, Y., Wang, X., Li, X., Xu, G., Bai, Y., Wu, J., Piao, Y., Shi, Y., Xiang, R., & Wang, L. (2020). Nucleotide de novo synthesis increases breast cancer stemness and metastasis via cGMP-PKG-MAPK signaling pathway. *PLoS Biol 18*(11), e3000872. https://doi.org/10.1371/journal.pbio.3000872

Mantovani, A., Allavena, P., Sica, A., & Balkwill, F. (2008). Cancer-related inflammation. *Nature*, *454*(7203), 436-444. https://doi.org/10.1038/nature07205

Markham, A., & Duggan, S. (2021). Vericiguat: first approval. *Drugs*, *81*(6), 721-726. https://doi.org/10.1007/s40265-021-01496-z

Martin, J. D., Seano, G., & Jain, R. K. (2019). Normalizing function of tumor vessels: progress, opportunities, and challenges. *Annu Rev Physiol*, *81*, 505-534. https://doi.org/10.1146/annurev-physiol-020518-114700

Mashimo, M., Onishi, M., Uno, A., Tanimichi, A., Nobeyama, A., Mori, M., Yamada, S., Negi, S., Bu, X., Kato, J., Moss, J., Sanada, N., Kizu, R., & Fujii, T. (2021). The 89-kDa PARP1 cleavage fragment serves as a cytoplasmic PAR carrier to induce AIF-mediated apoptosis. *J Biol Chem*, *296*, 100046. https://doi.org/10.1074/jbc.RA120.014479

McGuire, A., Brown, J. A., Malone, C., McLaughlin, R., & Kerin, M. J. (2015). Effects of age on the detection and management of breast cancer. *Cancers (Basel)*, *7*(2), 908-929. https://doi.org/10.3390/cancers7020815

McMurray, J. J., Packer, M., Desai, A. S., Gong, J., Lefkowitz, M. P., Rizkala, A. R., Rouleau, J. L., Shi, V. C., Solomon, S. D., Swedberg, K., & Zile, M. R. (2014). Angiotensin-neprilysin inhibition versus

enalapril in heart failure. *N Engl J Med*, *371*(11), 993-1004. https://doi.org/10.1056/NEJMoa1409077

Meder, L., Schuldt, P., Thelen, M., Schmitt, A., Dietlein, F., Klein, S., Borchmann, S., Wennhold, K., Vlasic, I., Oberbeck, S., Riedel, R., Florin, A., Golfmann, K., Schlößer, H. A., Odenthal, M., Buettner, R., Wolf, J., Hallek, M., Herling, M., . . . Ullrich, R. T. (2018). Combined VEGF and PD-L1 blockade displays synergistic treatment effects in an autochthonous mouse model of small cell lung cancer. *Cancer Res*, *78*(15), 4270-4281. https://doi.org/10.1158/0008-5472.Can-17-2176

Meyer, C., Sevko, A., Ramacher, M., Bazhin, A. V., Falk, C. S., Osen, W., Borrello, I., Kato, M., Schadendorf, D., Baniyash, M., & Umansky, V. (2011). Chronic inflammation promotes myeloid-derived suppressor cell activation blocking antitumor immunity in transgenic mouse melanoma model. *Proc Natl Acad Sci U S A*, *108*(41), 17111-17116. https://doi.org/10.1073/pnas.1108121108

Mohan, S. C., Lee, T. Y., Giuliano, A. E., & Cui, X. (2021). Current status of breast organoid models. *Front Bioeng Biotechnol*, *9*, 745943. https://doi.org/10.3389/fbioe.2021.745943

Morsi, D. S., Barnawi, I. O., Ibrahim, H. M., El-Morsy, A. M., El Hassab, M. A., & Abd El Latif, H. M. (2023). Immunomodulatory, apoptotic and anti-proliferative potentials of sildenafil in Ehrlich ascites carcinoma murine model: In vivo and in silico insights. *Int Immunopharmacol*, *119*, 110135. https://doi.org/https://doi.org/10.1016/j.intimp.2023.110135

Moyes, A. J., & Hobbs, A. J. (2019). C-type natriuretic peptide: a multifaceted paracrine regulator in the heart and vasculature. *Int J Mol Sci*, *20*(9). https://doi.org/10.3390/ijms20092281

Muller, W. J., Sinn, E., Pattengale, P. K., Wallace, R., & Leder, P. (1988). Single-step induction of mammary adenocarcinoma in transgenic mice bearing the activated c-neu oncogene. *Cell*, *54*(1), 105-115. https://doi.org/10.1016/0092-8674(88)90184-5

Murrell, W. (1879). Nitro-glycerine as a remedy for angina pectoris. *The Lancet*, *113*(2890), 80-81. https://doi.org/10.1016/s0140-6736(02)46032-1

Nolan, E., Lindeman, G. J., & Visvader, J. E. (2023). Deciphering breast cancer: from biology to the clinic. *Cell*, *186*(8), 1708-1728. https://doi.org/10.1016/j.cell.2023.01.040

Osborne, C. K., & Schiff, R. (2011). Mechanisms of endocrine resistance in breast cancer. *Annu Rev Med*, *62*, 233-247. https://doi.org/10.1146/annurev-med-070909-182917

Pandey, K. N. (2014). Guanylyl cyclase/natriuretic peptide receptor-A signaling antagonizes phosphoinositide hydrolysis, Ca(2+) release, and activation of protein kinase C. *Front Mol Neurosci*, *7*, 75. https://doi.org/10.3389/fnmol.2014.00075

Patel, S. A., Nilsson, M. B., Le, X., Cascone, T., Jain, R. K., & Heymach, J. V. (2023). Molecular mechanisms and future implications of VEGF/VEGFR in cancer therapy. *Clin Cancer Res*, *29*(1), 30-39. https://doi.org/10.1158/1078-0432.CCR-22-1366

Peterson, G. L. (1977). A simplification of the protein assay method of Lowry et al. which is more generally applicable. *Anal Biochem*, *83*(2), 346-356. https://doi.org/10.1016/0003-2697(77)90043-4

Piazza, G. A., Ward, A., Chen, X., Maxuitenko, Y., Coley, A., Aboelella, N. S., Buchsbaum, D. J., Boyd, M. R., Keeton, A. B., & Zhou, G. (2020). PDE5 and PDE10 inhibition activates cGMP/PKG signaling to block Wnt/beta-catenin transcription, cancer cell growth, and tumor immunity. *Drug Discov Today*, *25*(8), 1521-1527. https://doi.org/10.1016/j.drudis.2020.06.008

Piccart-Gebhart, M. J., Procter, M., Leyland-Jones, B., Goldhirsch, A., Untch, M., Smith, I., Gianni, L., Baselga, J., Bell, R., Jackisch, C., Cameron, D., Dowsett, M., Barrios, C. H., Steger, G., Huang, C.-S., Andersson, M., Inbar, M., Lichinitser, M., Láng, I., . . . Gelber, R. D. (2005). Trastuzumab after adjuvant chemotherapy in HER2-positive breast cancer. *N Engl J Med*, *353*(16), 1659-1672. https://doi.org/10.1056/NEJMoa052306

Pohlmann, P. R., Mayer, I. A., & Mernaugh, R. (2009). Resistance to trastuzumab in breast cancer. *Clin Cancer Res*, *15*(24), 7479-7491. https://doi.org/10.1158/1078-0432.Ccr-09-0636

Porter, R. J., Murray, G. I., & McLean, M. H. (2020). Current concepts in tumour-derived organoids. *Br J Cancer*, *123*(8), 1209-1218. https://doi.org/10.1038/s41416-020-0993-5

Potter, L. R., Abbey-Hosch, S., & Dickey, D. M. (2006). Natriuretic peptides, their receptors, and cyclic guanosine monophosphate-dependent signaling functions. *Endocr Rev* *27*(1), 47-72. https://doi.org/10.1210/er.2005-0014

Potter, L. R. (2011a). Natriuretic peptide metabolism, clearance and degradation. *FEBS J*, *278*(11), 1808-1817. https://doi.org/10.1111/j.1742-4658.2011.08082.x

Potter, L. R. (2011b). Guanylyl cyclase structure, function and regulation. *Cell Signal*, *23*(12), 1921-1926. https://doi.org/10.1016/j.cellsig.2011.09.001

Roberts, O. L., & Dart, C. (2014). cAMP signalling in the vasculature: the role of Epac (exchange protein directly activated by cAMP). *Biochem Soc Trans*, *42*(1), 89-97. https://doi.org/10.1042/bst20130253

Romond, E. H., Perez, E. A., Bryant, J., Suman, V. J., Geyer, C. E., Davidson, N. E., Tan-Chiu, E., Martino, S., Paik, S., Kaufman, P. A., Swain, S. M., Pisansky, T. M., Fehrenbacher, L., Kutteh, L. A., Vogel, V. G., Visscher, D. W., Yothers, G., Jenkins, R. B., Brown, A. M., . . . Wolmark, N. (2005). Trastuzumab plus adjuvant chemotherapy for operable HER2-positive breast cancer. *N Engl J Med*, *353*(16), 1673-1684. https://doi.org/10.1056/NEJMoa052122

Rueden, C. T., Schindelin, J., Hiner, M. C., DeZonia, B. E., Walter, A. E., Arena, E. T., & Eliceiri, K. W. (2017). ImageJ2: ImageJ for the next generation of scientific image data. *BMC Bioinform*, *18*(1), 529. https://doi.org/10.1186/s12859-017-1934-z

Russwurm, M., Mullershausen, F., Friebe, A., Jager, R., Russwurm, C., & Koesling, D. (2007). Design of fluorescence resonance energy transfer (FRET)-based cGMP indicators: a systematic approach. *Biochem J*, *407*(1), 69-77. https://doi.org/10.1042/BJ20070348

Russwurm, M., Russwurm, C., Koesling, D., & Mergia, E. (2013). NO/cGMP: the past, the present, and the future. *Methods Mol Biol*, *1020*, 1-16. https://doi.org/10.1007/978-1-62703-459-3_1

Sandner, P., Zimmer, D. P., Milne, G. T., Follmann, M., Hobbs, A., & Stasch, J. P. (2021). Soluble guanylate cyclase stimulators and activators. *Handb Exp Pharmacol*, *264*, 355-394. https://doi.org/10.1007/164_2018_197

Sangiorgi, G., Cereda, A., Benedetto, D., Bonanni, M., Chiricolo, G., Cota, L., Martuscelli, E., & Greco, F. (2021). Anatomy, pathophysiology, molecular mechanisms, and clinical management of erectile dysfunction in patients affected by coronary artery disease: a review. *Biomedicines*, *9*(4), 432. https://doi.org/https://doi.org/10.3390/biomedicines9040432

Saravani, R., Karami-Tehrani, F., Hashemi, M., Aghaei, M., & Edalat, R. (2012). Inhibition of phosphodiestrase 9 induces cGMP accumulation and apoptosis in human breast cancer cell lines, MCF-7 and MDA-MB-468. *Cell Prolif*, *45*(3), 199-206. https://doi.org/10.1111/j.1365-2184.2012.00819.x

Sarkar, M., Nguyen, T., Gundre, E., Ogunlusi, O., El-Sobky, M., Giri, B., & Sarkar, T. R. (2023). Cancer-associated fibroblasts: the chief architect in the tumor microenvironment. *Front Cell Dev Biol*, *11*, 1089068. https://doi.org/10.3389/fcell.2023.1089068

Savarirayan, R., Tofts, L., Irving, M., Wilcox, W. R., Bacino, C. A., Hoover-Fong, J., Font, R. U., Harmatz, P., Rutsch, F., Bober, M. B., Polgreen, L. E., Ginebreda, I., Mohnike, K., Charrow, J., Hoernschemeyer, D., Ozono, K., Alanay, Y., Arundel, P., Kotani, Y., . . . Day, J. R. S. (2021). Safe and persistent growth-promoting effects of vosoritide in children with achondroplasia: 2-year results from an open-label, phase 3 extension study. *Genet Med* *23*(12), 2443-2447. https://doi.org/10.1038/s41436-021-01287-7

Schindelin, J., Arganda-Carreras, I., Frise, E., Kaynig, V., Longair, M., Pietzsch, T., Preibisch, S., Rueden, C., Saalfeld, S., Schmid, B., Tinevez, J. Y., White, D. J., Hartenstein, V., Eliceiri, K., Tomancak, P., & Cardona, A. (2012). Fiji: an open-source platform for biological-image analysis. *Nat Methods*, *9*(7), 676-682. https://doi.org/10.1038/nmeth.2019

Schinner, E., Wetzl, V., Schramm, A., Kees, F., Sandner, P., Stasch, J. P., Hofmann, F., & Schlossmann, J. (2017). Inhibition of the TGFβ signalling pathway by cGMP and cGMP-dependent kinase I in renal fibrosis. *FEBS Open Bio*, *7*(4), 550-561. https://doi.org/10.1002/2211-5463.12202

Schlossmann, J., & Schinner, E. (2012). cGMP becomes a drug target. *Naunyn Schmiedebergs Arch Pharmacol*, *385*(3), 243-252. https://doi.org/10.1007/s00210-012-0730-6

Schmid, P., Adams, S., Rugo, H. S., Schneeweiss, A., Barrios, C. H., Iwata, H., Diéras, V., Hegg, R., Im, S.-A., Shaw Wright, G., Henschel, V., Molinero, L., Chui, S. Y., Funke, R., Husain, A., Winer, E. P., Loi, S., & Emens, L. A. (2018). Atezolizumab and Nab-paclitaxel in advanced triple-negative breast cancer. *N Engl J Med*, *379*(22), 2108-2121. https://doi.org/10.1056/NEJMoa1809615

Schmid, P., Cortes, J., Dent, R., Pusztai, L., McArthur, H., Kümmel, S., Bergh, J., Denkert, C., Park, Y. H., Hui, R., Harbeck, N., Takahashi, M., Untch, M., Fasching, P. A., Cardoso, F., Andersen, J., Patt, D., Danso, M., Ferreira, M., . . . O'Shaughnessy, J. (2022). Event-free Survival with Pembrolizumab in Early Triple-Negative Breast Cancer. *N Engl J Med*, *386*(6), 556-567. https://doi.org/10.1056/NEJMoa2112651

Schwappacher, R., Rangaswami, H., Su-Yuo, J., Hassad, A., Spitler, R., & Casteel, D. E. (2013). cGMP-dependent protein kinase Ibeta regulates breast cancer cell migration and invasion via interaction with the actin/myosin-associated protein caldesmon. *J Cell Sci*, *126*(Pt 7), 1626-1636. https://doi.org/10.1242/jcs.118190

Serafini, P., Meckel, K., Kelso, M., Noonan, K., Califano, J., Koch, W., Dolcetti, L., Bronte, V., & Borrello, I. (2006). Phosphodiesterase-5 inhibition augments endogenous antitumor immunity by reducing myeloid-derived suppressor cell function. *J Exp Med*, *203*(12), 2691-2702. https://doi.org/10.1084/jem.20061104

Shiovitz, S., & Korde, L. A. (2015). Genetics of breast cancer: a topic in evolution. *Ann Oncol*, *26*(7), 1291-1299. https://doi.org/10.1093/annonc/mdv022

Siegel, R. L., Miller, K. D., Wagle, N. S., & Jemal, A. (2023). Cancer statistics, 2023. *CA Cancer J Clin*, *73*(1), 17-48. https://doi.org/10.3322/caac.21763

Soare, G. R., & Soare, C. A. (2019). Immunotherapy for breast cancer: first FDA approved regimen. *Discoveries (Craiova)*, *7*(1), e91. https://doi.org/10.15190/d.2019.4

Solomon, S. D., Vaduganathan, M., B, L. C., Packer, M., Zile, M., Swedberg, K., Rouleau, J., M, A. P., Desai, A., Lund, L. H., Kober, L., Anand, I., Sweitzer, N., Linssen, G., Merkely, B., Luis Arango, J., Vinereanu, D., Chen, C. H., Senni, M., . . . McMurray, J. J. V. (2020). Sacubitril/valsartan across the spectrum of ejection fraction in heart failure. *Circulation*, *141*(5), 352-361. https://doi.org/10.1161/CIRCULATIONAHA.119.044586

Sörensen, I., Adams, R. H., & Gossler, A. (2009). DLL1-mediated Notch activation regulates endothelial identity in mouse fetal arteries. *Blood*, *113*(22), 5680-5688. https://doi.org/10.1182/blood-2008-08-174508

Sprenger, J. U., & Nikolaev, V. O. (2013). Biophysical techniques for detection of cAMP and cGMP in living cells. *Int J Mol Sci*, *14*(4), 8025-8046. https://doi.org/doi:10.3390/ijms14048025

Stehle, D. (2022). cGMP imaging uncovers new roles and therapeutic implications of NO/cGMP signaling in the kidney and in melanoma [Doctoral Thesis, University Tubingen]. http://hdl.handle.net/10900/128604

Stehle, D., Barresi, M., Schulz, J., & Feil, R. (2023). Heterogeneity of cGMP signalling in tumour cells and the tumour microenvironment: challenges and chances for cancer pharmacology and therapeutics. *Pharmacol Ther*, 108337. https://doi.org/10.1016/j.pharmthera.2023.108337

Stewart, T. A., Pattengale, P. K., & Leder, P. (1984). Spontaneous mammary adenocarcinomas in transgenic mice that carry and express MTV/myc fusion genes. *Cell*, *38*(3), 627-637. https://doi.org/10.1016/0092-8674(84)90257-5

Sugiura, K., & Stock, C. C. (1952). Studies in a tumor spectrum. I. Comparison of the action of methylbis (2-chloroethyl)amine and 3-bis(2-chloroethyl)aminomethyl-4-methoxymethyl -5-hydroxy-6-methylpyridine on the growth of a variety of mouse and rat tumors. *Cancer*, *5*(2), 382-402. https://doi.org/10.1002/1097-0142(195203)5:2<382::aid-cncr2820050229>3.0.co;2-3

Sung, Y. C., Jin, P. R., Chu, L. A., Hsu, F. F., Wang, M. R., Chang, C. C., Chiou, S. J., Qiu, J. T., Gao, D. Y., Lin, C. C., Chen, Y. S., Hsu, Y. C., Wang, J., Wang, F. N., Yu, P. L., Chiang, A. S., Wu, A. Y., Ko, J. J., Lai, C. P., . . . Chen, Y. (2019). Delivery of nitric oxide with a nanocarrier promotes tumour vessel normalization and potentiates anti-cancer therapies. *Nat Nanotechnol*, *14*(12), 1160-1169. https://doi.org/10.1038/s41565-019-0570-3

Takei, Y. (2022). Evolution of the membrane/particulate guanylyl cyclase: From physicochemical sensors to hormone receptors. *Gen Comp Endocrinol*, *315*, 113797. https://doi.org/10.1016/j.ygcen.2021.113797

Ter-Avetisyan, G., Rathjen, F. G., & Schmidt, H. (2014). Bifurcation of axons from cranial sensory neurons is disabled in the absence of Npr2-induced cGMP signaling. *J Neurosci*, *34*(3), 737-747. https://doi.org/10.1523/JNEUROSCI.4183-13.2014

Thrailkill, K. M., Kalaitzoglou, E., & Fowlkes, J. L. (2022). Emerging therapies for the treatment of rare pediatric bone disorders. *Front Pediatr*, *10*, 1012816. https://doi.org/10.3389/fped.2022.1012816

Thunemann, M. W., L., Hillenbrand, M., Vachaviolos, A., Feil, S., Ott, T., Han, X., Fukumura, D., Jain, R. K., Russwurm, M., de Wit, C., & Feil, R. (2013). Transgenic mice for cGMP imaging. *Circ Res*, *113*(4), 365-371. https://doi.org/10.1161/circresaha.113.301063

Tinsley, H. N., Gary, B. D., Keeton, A. B., Zhang, W., Abadi, A. H., Reynolds, R. C., & Piazza, G. A. (2009). Sulindac sulfide selectively inhibits growth and induces apoptosis of human breast tumor cells by phosphodiesterase 5 inhibition, elevation of cyclic GMP, and activation of protein kinase G. *Mol Cancer Ther*, *8*(12), 3331-3340. https://doi.org/10.1158/1535-7163.MCT-09-0758

Tinsley, H. N., Mathew, B., Chen, X., Maxuitenko, Y. Y., Li, N., Lowe, W. M., Whitt, J. D., Zhang, W., Gary, B. D., Keeton, A. B., Grizzle, W. E., Grubbs, C. J., Reynolds, R. C., & Piazza, G. A. (2023). Novel non-cyclooxygenase inhibitory derivative of sulindac inhibits breast cancer cell growth in vitro and reduces mammary tumorigenesis in rats. *Cancers (Basel)*, *15*(3). https://doi.org/10.3390/cancers15030646

Towbin, H., Staehelin, T., & Gordon, J. (1979). Electrophoretic transfer of proteins from polyacrylamide gels to nitrocellulose sheets: procedure and some applications. *Proc Natl Acad Sci U S A*, *76*(9), 4350-4354. https://doi.org/10.1073/pnas.76.9.4350

Turashvili, G., & Brogi, E. (2017). Tumor heterogeneity in breast cancer. *Front Med (Lausanne)*, *4*, 227. https://doi.org/10.3389/fmed.2017.00227

Tzoumas, N., Farrah, T. E., Dhaun, N., & Webb, D. J. (2020). Established and emerging therapeutic uses of PDE type 5 inhibitors in cardiovascular disease. *Br J Pharmacol*, *177*(24), 5467-5488. https://doi.org/10.1111/bph.14920

Valtcheva, N., Nestorov, P., Beck, A., Russwurm, M., Hillenbrand, M., Weinmeister, P., & Feil, R. (2009). The commonly used cGMP-dependent protein kinase type I (cGKI) inhibitor Rp-8-Br-PET-cGMPS can activate cGKI in vitro and in intact cells. *J Biol Chem*, *284*(1), 556-562. https://doi.org/10.1074/jbc.M806161200

Versmissen, J., Mirabito Colafella, K. M., Koolen, S. L. W., & Danser, A. H. J. (2019). Vascular cardio-oncology: vascular endothelial growth factor inhibitors and hypertension. *Cardiovasc Res*, *115*(5), 904-914. https://doi.org/10.1093/cvr/cvz022

Waks, A. G., & Winer, E. P. (2019). Breast cancer treatment: a review. *JAMA*, *321*(3), 288-300. https://doi.org/10.1001/jama.2018.19323

Wang, L., Wang, N., Zhang, W., Cheng, X., Yan, Z., Shao, G., Wang, X., Wang, R., & Fu, C. (2022). Therapeutic peptides: current applications and future directions. *Sig Transduct Target Ther*, *7*(1), 48. https://doi.org/10.1038/s41392-022-00904-4

Wendling, O., Bornert, J. M., Chambon, P., & Metzger, D. (2009). Efficient temporally-controlled targeted mutagenesis in smooth muscle cells of the adult mouse. *Genesis*, *47*(1), 14-18. https://doi.org/10.1002/dvg.20448

Windham, P. F., & Tinsley, H. N. (2015). cGMP signaling as a target for the prevention and treatment of breast cancer. *Semin Cancer Biol*, *31*, 106-110. https://doi.org/10.1016/j.semcancer.2014.06.006

Xu, X., Wagner, K.-U., Larson, D., Weaver, Z., Li, C., Ried, T., Hennighausen, L., Wynshaw-Boris, A., & Deng, C.-X. (1999). Conditional mutation of Brca1 in mammary epithelial cells results in blunted ductal morphogenesis and tumour formation. *Nat Genet*, *22*(1), 37-43. https://doi.org/10.1038/8743

Yamahara, K., Itoh, H., Chun, T. H., Ogawa, Y., Yamashita, J., Sawada, N., Fukunaga, Y., Sone, M., Yurugi-Kobayashi, T., Miyashita, K., Tsujimoto, H., Kook, H., Feil, R., Garbers, D. L., Hofmann, F., & Nakao, K. (2003). Significance and therapeutic potential of the natriuretic peptides/cGMP/cGMP-dependent protein kinase pathway in vascular regeneration. *Proc Natl Acad Sci U S A*, *100*(6), 3404-3409. https://doi.org/10.1073/pnas.0538059100

Yao, X., Leung, P. S., Kwan, H. Y., Wong, T. P., & Fong, M. W. (1999). Rod-type cyclic nucleotide-gated cation channel is expressed in vascular endothelium and vascular smooth muscle cells. *Cardiovasc Res*, *41*(1), 282-290. https://doi.org/10.1016/s0008-6363(98)00158-8

Yonenaga, Y., Mori, A., Onodera, H., Yasuda, S., Oe, H., Fujimoto, A., Tachibana, T., & Imamura, M. (2005). Absence of smooth muscle actin-positive pericyte coverage of tumor vessels correlates with hematogenous metastasis and prognosis of colorectal cancer patients. *Oncology*, *69*(2), 159-166. https://doi.org/10.1159/000087840

Zeng, L., Li, W., & Chen, C. S. (2020). Breast cancer animal models and applications. *Zool Res*, *41*(5), 477-494. https://doi.org/10.24272/j.issn.2095-8137.2020.095

Zhou, Y., Liu, L., Tao, S., Yao, Y., Wang, Y., Wei, Q., Shao, A., & Deng, Y. (2021). Parthanatos and its associated components: promising therapeutic targets for cancer. *Pharmacol Res*, *163*, 105299. https://doi.org/10.1016/j.phrs.2020.105299

8. Declaration of contributions

This work was written entirely by the author. The use of artificial intelligence (e.g., ChatGPT) was limited to proofreading some paragraphs of the thesis.

The *in vitro* and *in vivo* studies were planned, executed, and analyzed by the author, with the following exceptions:

- Culture and stimulation of patient-derived TNBC organoids were carried out by C. Öder, MSc, in the working group of Dr. A. Koch and Prof. S. Brucker at the Gynecological Hospital in Tübingen.
- Preparation and sectioning of paraffin-embedded human biopsies were conducted by Ingrid Teufel in the working group of Dr. A. Koch and Prof. S. Brucker at the Gynecological Hospital in Tübingen.
- Analysis of vericiguat concentration in the plasma of experimental animals was performed by Dr. Ute Hofmann at the Dr. Margarete Fischer-Bosch Institute of Clinical Pharmacology in Stuttgart.
- Imaging of immunostained tumor sections was conducted under the supervision of Oliver Hihn, MSc, and Prof. Dr. Bettina Weigelin at the Werner Siemens Imaging Center, Eberhard Karls Universität in Tübingen.

9. Publications by the author

The presented work has contributed to the following publications:

Stehle, D.*, **Barresi, M.***, Schulz, J., …, Feil, S., Feil, R. NO/cGMP signaling in pericytes regulates tumor growth. *In preparation*. *Authors contributed equally.

Stehle, D., **Barresi, M.**, Schulz, J., & Feil, R. (2023). Heterogeneity of cGMP signalling in tumour cells and the tumour microenvironment: challenges and chances for cancer pharmacology and therapeutics. *Pharmacol Ther*, 108337. https://doi.org/10.1016/j.pharmthera.2023.108337

In addition, the author has contributed to the following unrelated publications:

Tikoo, S., …, **Barresi, M.**, …, Feil, S., Feil, R., …, Weninger, W. A distinct CD115-erythro-myeloid precursor present at the maternal-embryonic interface and in the bone marrow of adult mice. *In revision*.

The author has also presented her work on the following conferences:

Barresi, M., Roessing, M., Menges, R., Stehle, D., Feil, R. (2022). The cGMP signaling pathway in breast cancer cell lines. Meeting abstracts from the 10th International Conference on cGMP: Generators, Effectors and Therapeutic Implications. *J Transl Med*, 21(1):P3. https://doi.org/10.1186/s12967-022-03800-1. Augsburg, Germany

Barresi, M., Roessing, M., Schmidt, H., Fukumura, D., Feil, R. (2021). The cGMP signaling pathway in breast cancer cells. *The 1st PhD Student Conference of the GRK 2381 on Cancer, Cardiovascular diseases & Neurological disorders*. Tübingen, Germany.

10. Supplementary

Table S1. The different diets used in the present study.

Animal Cohort	Group	Diet
1st	ND*	Standard rodent chow
1st	HFD#	EF TD88137 mod. +1.25% Cholesterol Western Diet - 10 mm
1st	HFD + V#	EF TD99137 mod. +150 mg/kg Vericiguat Western Diet +1.25% Cholesterol - 10 mm Verquvo 10 mg Tablette
2nd	ND#	1534-04 SM RM-H, V1534 | Kontrolle /Placebo 10 mm ROT
2nd	ND + V#	S4088-P012 PS RM-H, V1534 | +150 mg/kg Vericiguat Verquvo 10 mg Tabl. - 10 mm BLAU

Footnotes: *purchased from Altromin; #purchased from Ssniff. ND; normal diet; HFD, high-fat diet, HFD + V, vericiguat-supplemented HFD; ND + V, vericiguat-supplemented ND.

Table S2. Blood pressure values of mice fed with normal diet or vericiguat-supplemented diet.

Group	Day	Mean BP	Systolic BP	Diastolic PB
Female mice				
ND (n=4)	-2	97.7 ± 5.7	108.6 ± 3.3	85.8 ± 4.4
	0	94.8 ± 6.3	119.5 ± 5.5	83.4 ± 2.6
	18	104.5 ± 7.7	107.6 ± 3.5	93.8 ± 7.5
ND + V (n=4)	-2	92.7 ± 3.3	104.4 ± 7.5	84.4 ± 5.7
	0	81.1 ± 6.6	105.3 ± 3.1	70.9 ± 6.5
	18	81.5 ± 9.9	114.9 ± 12.7	72.8 ± 9.1
Male mice				
ND (n=4)	-2	88.5 ± 5.5	108.7 ± 4.9	78.9 ± 5.8
	0	87.6 ± 5.0	106.7 ± 6.8	78.5 ± 4.2
	18	94.4 ± 3.5	117.7 ± 6.7	83.2 ± 2.2
ND + V (n=4)	-2	91.5 ± 0.7	111.9 ± 1.0	81.9 ± 0.9
	0	83.7 ± 4.1	108.0 ± 8.9	71.2 ± 5.8
	18	85.6 ± 9.2	103.2 ± 10.5	77.4 ± 8.6

Footnotes: ND, normal diet; ND + V, vericiguat-supplemented normal diet. Day -2, before diet exchange; Day 0, supposed tumor cells injection day; Day 18 before animal sacrifice. All data represent mean ± SEM. Note that these mice did not receive tumor cells.

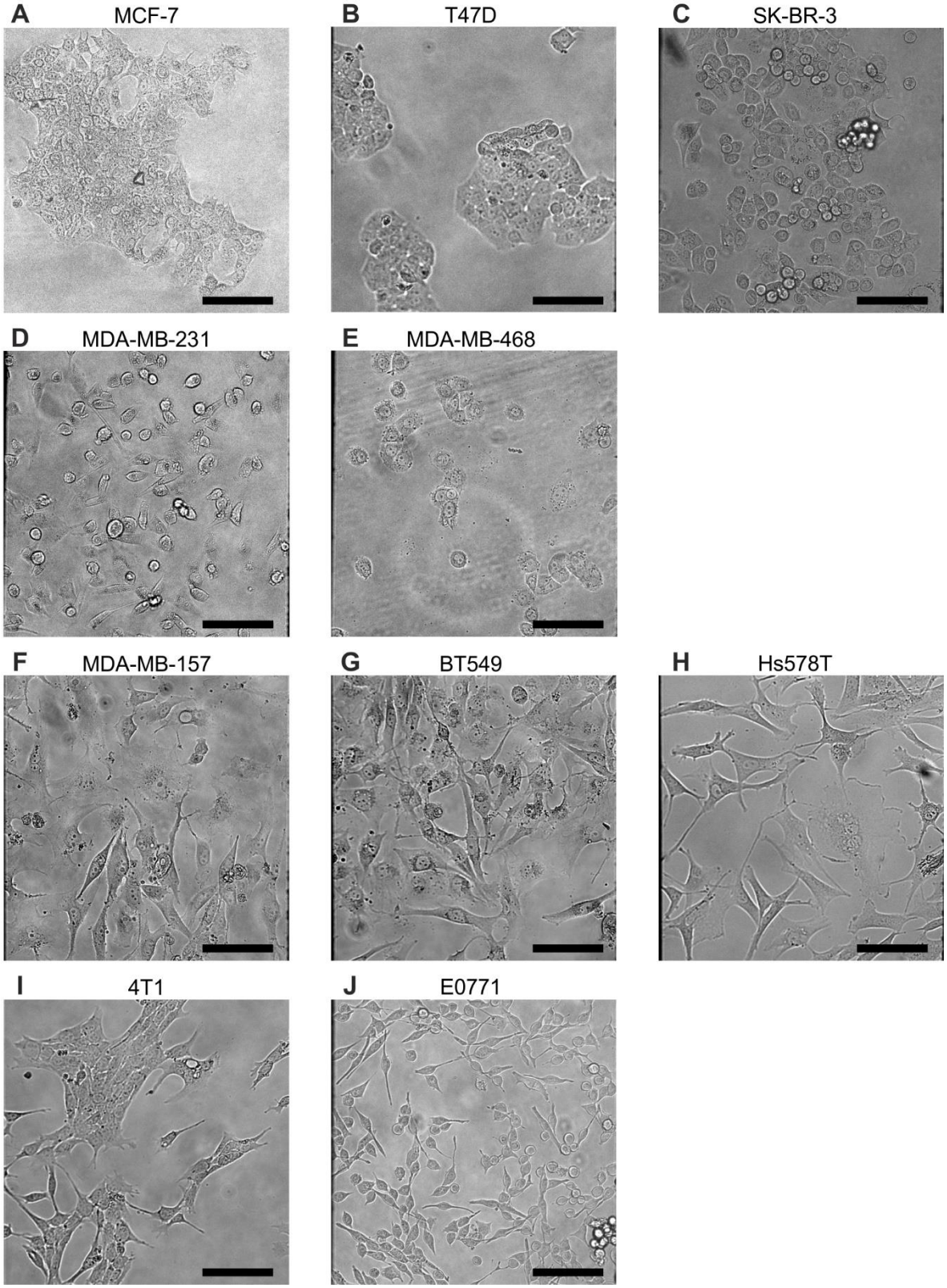

Figure S1. Phase contrast pictures of the breast cancer cell lines used in this study. Breast cancer cells were thawed and cultured as described in **3.2**. Every two days, cells either received fresh medium (≤ 60 % confluence) or were passaged in the following splitting ratios: (**A**) MCF-7, 1/10 to 1/15; (**B**) T47D, 1/7 to 1/10; (**C**) SK-BR-3, 1/5 to 1/10; (**D**) MDA-MB-231, 1/10 to 1/15; (**E**) MDA-MB-468, 1/5 to 1/8; (**F**) MDA-MB-157, 1/2 to 1/3; (**G**) BT549, 1/3; (**H**) Hs578T, 1/3 to 1/5; (**I**) 4T1, 1/5 to 1/8; (**J**) E0771, 1/5 to 1/10. Panels show phase contrast pictures of the different cell lines taken before performing FRE/cGMP imaging. Scale bars, 100 µm.

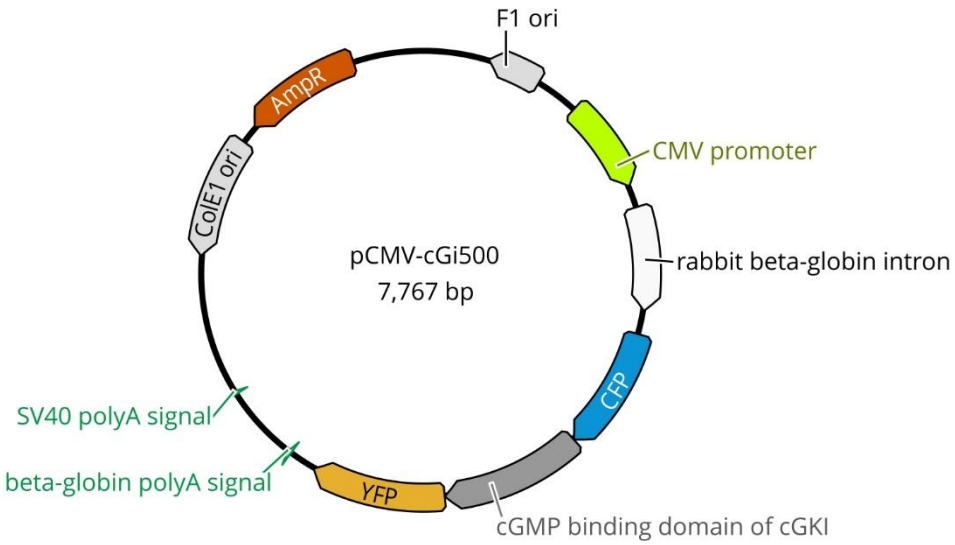

Figure S2. Map of the pCMV-cGi500 plasmid. The pCMV-cGi500 expression vector encodes the cGMP sensor cGi500, consisting of CFP (cyan) and YFP (yellow) linked by the tandem cGMP-binding domain of the bovine cGKI (dark gray). The cGi500 gene expression is under the control of the strong ubiquitous cytomegalovirus (CMV) promoter (lime), a rabbit β-globin intron (white) and polyadenylation (polyA) signals from SV40 and β-globin (green). The plasmid has the two origins of replication (ori, light gray): ColE1, allowing the amplification in bacteria, and F1 ori, facilitating the single strand DNA replication and phage packaging. The ampicillin resistance gene (AmpR; orange) allows selection in bacteria.

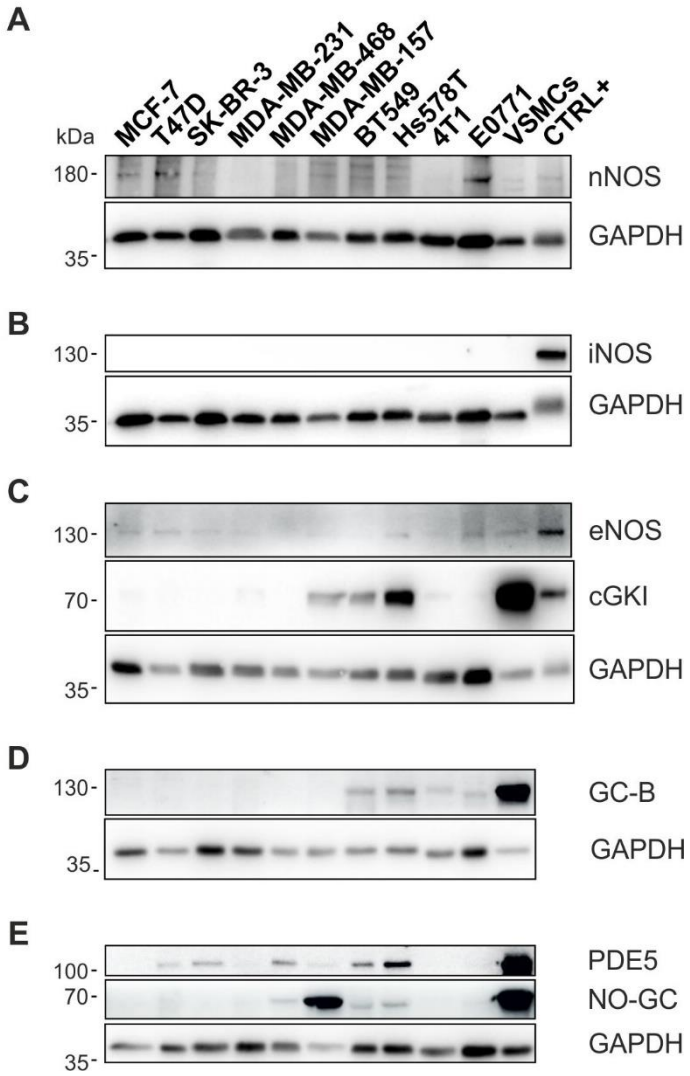

Figure S3. Expression of the cGMP signaling pathway components in different breast cancer cell lines. Western blot was used to detect cGMP pathway components in the protein lysates from various breast cancer cell lines. Brain, dendritic cells, and kidney lysates were used as positive controls (CTRL+) for the detection of nNOS, iNOS, and eNOS, respectively, while VSMC lysate was used as a positive control for other proteins. Expression of **A**, nNOS; **B**, iNOS; **C**, eNOS and cGKI, **D**, GC-B; **E**, PDE5 and NO-GC among breast cancer cell lines is shown together with the expression of their respective GAPDH, as housekeeping gene.

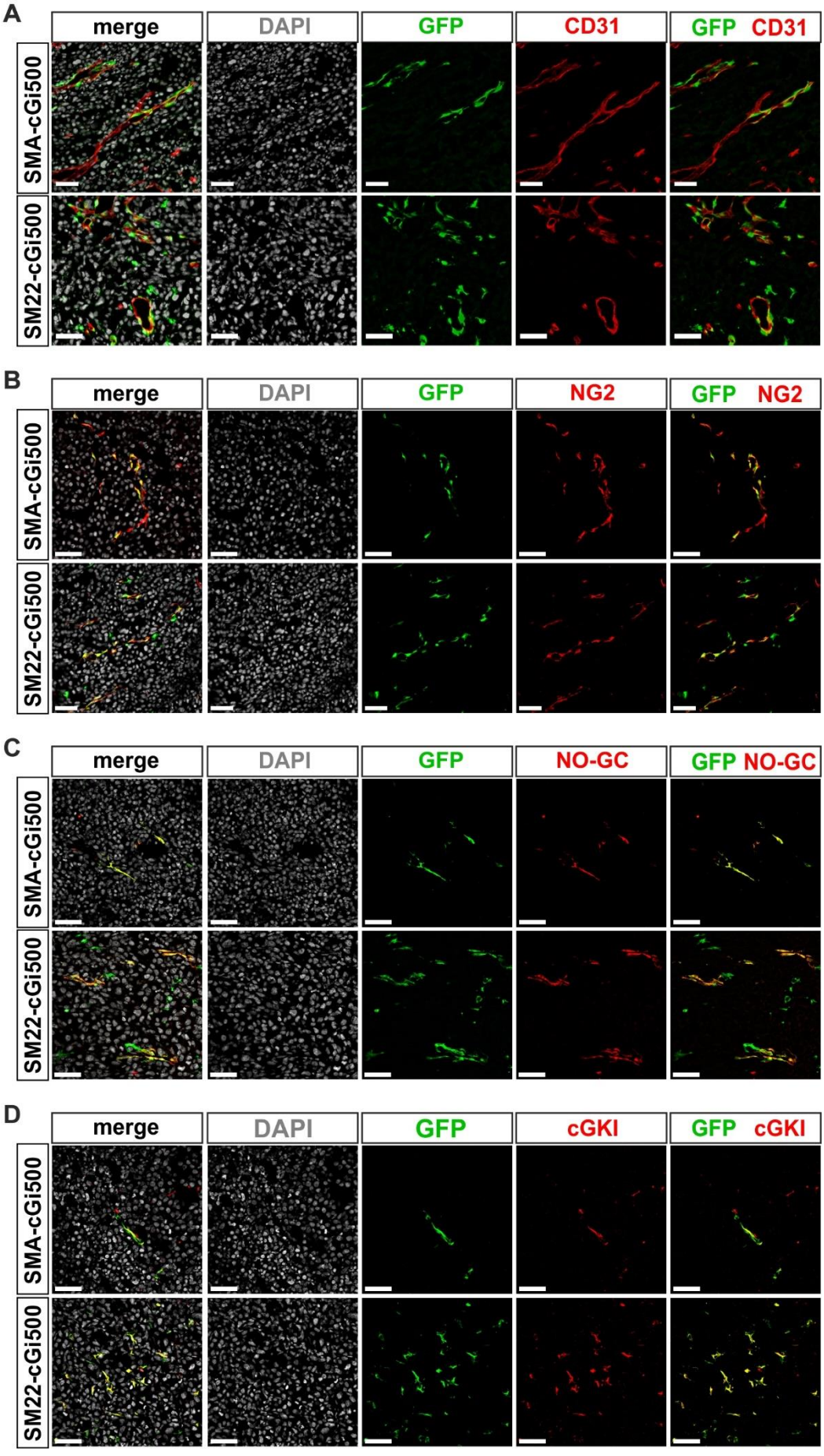
A
merge
DAPI
GFP
CD31
GFP CD31
SMA-cGi500
SM22-cGi500
B
merge
DAPI
GFP
NG2
GFP NG2
SMA-cGi500
SM22-cGi500
C
merge
DAPI
GFP
NO-GC
GFP NO-GC
SMA-cGi500
SM22-cGi500
D
merge
DAPI
GFP
cGKI
GFP cGKI
SMA-cGi500
SM22-cGi500

Figure S4. Identification of recombinant cells in cell-specific cGi500 sensor mice. E0771 cells were implanted into the 3rd left mammary fat pad of female SMA-cGi500 or SM22-cGi500 mice. Genotypes: SMA-CreERT2$^{tg/+}$ mT/cGi500(L2)$^{+/L2}$ and SM22CreER$^{tg/+}$ mT/cGi500(L2)$^{+/L2}$. SMA-cGi500 mice were tamoxifen injected starting 6 weeks before tumor cell injection, as for the protocol described in section **3.7.4**. Following resection, tumors were fixed and sectioned into 10 µm slices. Frozen sections underwent IF staining using (**A**) CD31 as an endothelial marker, (**B**) NG2 as a smooth muscle cell/pericyte marker, (**C**) NO-GC, and (**D**) cGKI, together with DAPI as a nuclear marker and GFP to detect the cGi500 sensor in the recombinant cells. Note that the anti-cGKI antibody might also stain the cGi500 sensor in these sections. The panels display (from left to right) merge overview, DAPI (gray); GFP (green), protein of interest (red) and combined view of GFP and protein of interest. Colocalization can be observed as region in Yellow (Green + Red) in the last combined view. Scale bars, 50 µm.

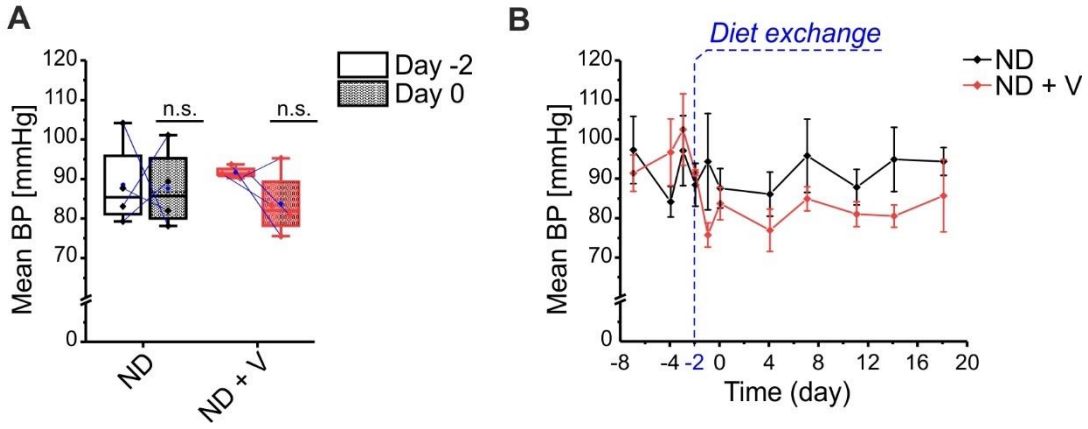

Figure S5. Effect of vericiguat-supplemented diet (150 mg/kg) on blood pressure in male mice. **A**, Mean blood pressure (BP) recorded at day -2 (before diet exchange) and at day 0 (formal tumor cell injection day) for control (ND) and vericiguat-treated (ND + V) groups. Boxes indicate 25%–75% interquartile range; horizontal lines in boxes, median; blue dots in boxes, mean; whiskers, 5%–95% range; dots, n = 4 male animals per conditions; blue lines, data points connectors. **B**, Mean BP over time for both control (ND) and vericiguat-treated (ND + V) groups. Data represent mean ± SEM of n = 4 animals. Time on X axis considered as 0 corresponds formally to the tumor cell injection day. Note that these mice did not receive tumor cells.

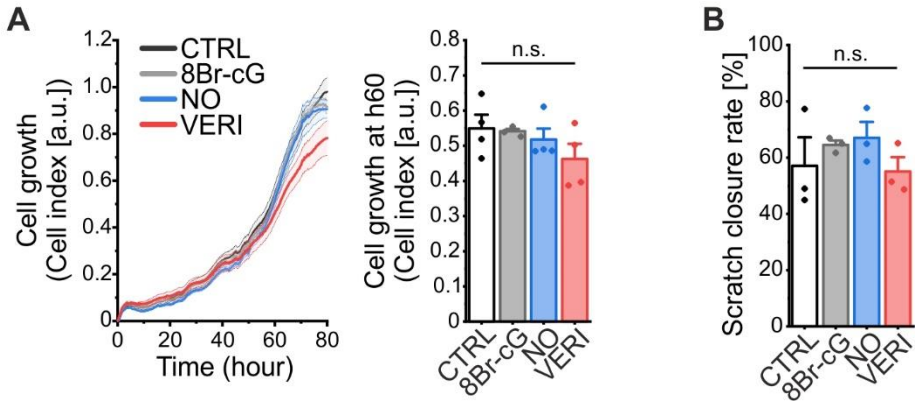

Figure S6. Effect of cGMP pathway stimulation on E0771 cell growth and migration. E0771 cells were stimulated with 8-Br-cGMP (8Br-cG, 1 mM), DETA/NO (NO, 10 µM) or vericiguat (VERI, 10 µM). **A**, E0771 cell growth is illustrated as an xCELLigence growth curve (left) and as cell index at 60 hours of n = 4 wells per condition of a representative experiment out of 3. **B**, Quantification of cell migration based on measuring the scratch closure rate at 24 hours after scratch formation of n = 3 experiments. Data represent mean ± SEM.

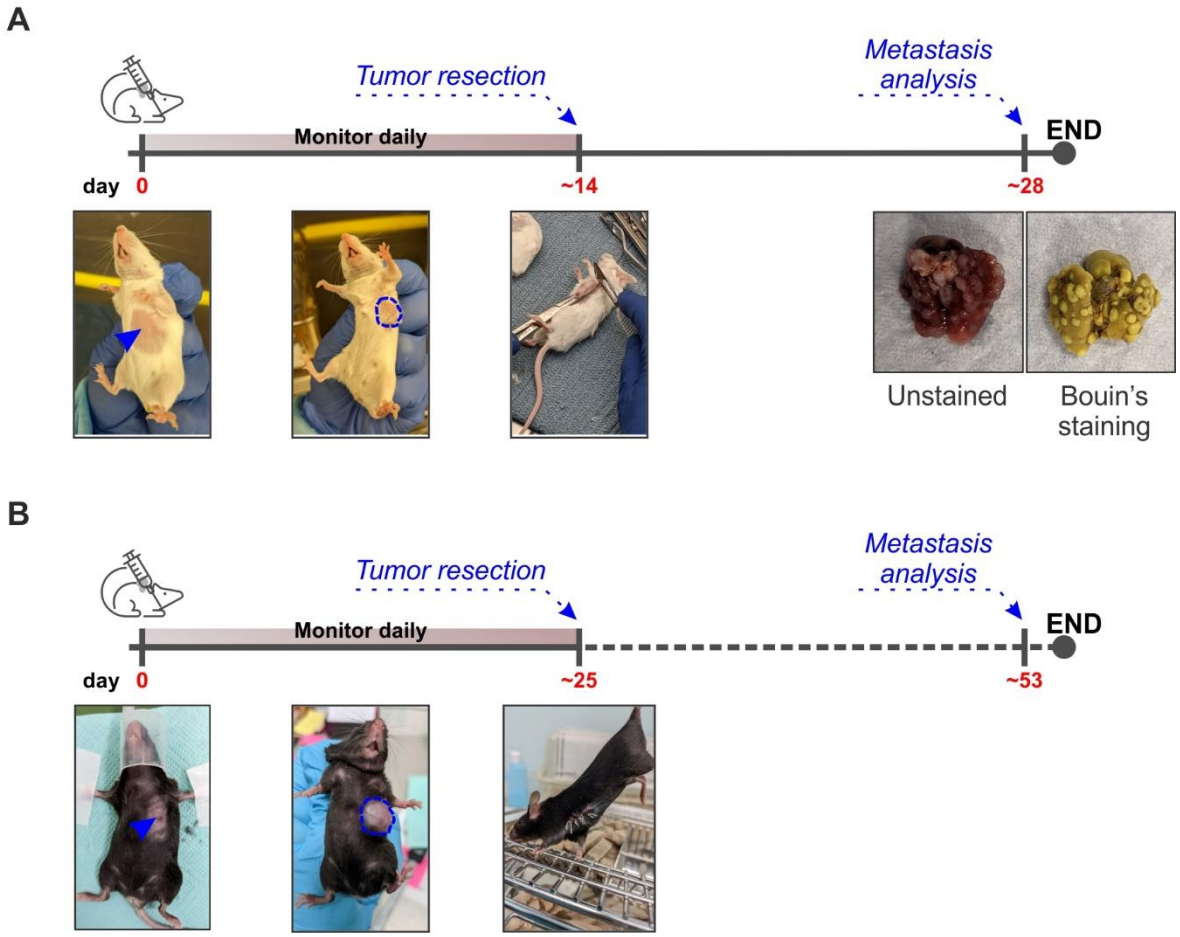

Figure S7. Breast cancer metastasis models. A, Timeline and representative steps of the highly metastatic 4T1 breast cancer model. The panels show (from left to right) 4T1 cell injection into the 3rd mammary fat pad (blue arrowhead indicates the injection site), monitoring of tumor growth (blue dashed circles indicates the tumors borders), tumor resection, and analysis of metastasis in unstained or Bouin's stained lungs (Pictures acquired during the visit in the laboratory of Prof. Dai Fukumura, MD, PhD at the Edwin L. Steele Laboratory, Radiation Oncology, Massachusetts General Hospital in Boston). **B**, Timeline and representative steps of the E0771 breast cancer model for metastasis established in our working group. The panels show (from left to right) E0771 cell injection into the 3rd mammary fat pad (blue arrowhead indicates the injection site), monitoring of tumor growth (blue dashed circles indicates the tumors borders), and a mouse after tumor resection.

Acknowledgment

I stand in gratitude at the end of this challenging and enlightening journey, acknowledging the contributions of all those who have made my doctoral research possible.

At the outset, I would like to express my deepest gratitude to my mentor and advisor, Prof. Dr. Robert Feil. Firstly, for the opportunity to join his working team, and then for his mentorship, which has been essential in guiding my research and improving my critical thinking. I am also profoundly thankful to my co-supervisors: PD Dr. Hannes Schmidt for the daily scientific confrontations and discussions in the laboratory, and Prof. Dai Fukumura, MD, PhD, for his insightful comments and the opportunity to join his laboratory in Boston to learn essential techniques for this project.

I want to extend my acknowledgement to Prof. Dr. Peter Ruth for the great discussion within our GRK meeting and for reviewing my thesis.

Thanks also to Dr. Susanne Feil for her help with all the *in vivo* experiments, from animal ethics writing to mouse handling, and to Dr. Ursula Kohlhofer for sharing her experience in animal surgery.

I am very grateful for all the contributions to this project, including those from my students: Alicia Geier, Rahel Menges and especially to Ezgi Atay. Additionally, I want to thank our collaborators Cansu Öder, Dr. Andrè Koch, and Prof. Dr. med. Sara Brucker (Gynecological Hospital Tübingen) for the various breast cancer cell lines and organoid samples. Furthermore my gratitude goes also to Oliver Hihn and Prof. Dr. Bettina Weigelin (Werner Siemens Imaging Center, Eberhard Karls Universität Tübingen) for the help in imaging tumor sections. Thanks to Dr. Ute Hofmann (Dr. Margarete Fischer-Bosch Institute of Clinical Pharmacology Stuttgart) to analyze the content of vericiguat in murine plasma. Many thanks to Prof. Dr. Andreas Friebe (Julius-Maximilians-Universität Würzburg), Prof. Laurinda Jaffe. Jaffe PhD (University of Connecticut Health Center), PD Dr. Hannes Schmidt (Eberhard Karls Universität Tübingen), as well as Prof. Dr. Hiltrud Brauch (Institute of Clinical Pharmacology and Head of Breast Cancer Susceptibility and Pharmacogenomics Stuttgart), for providing us with essential antibodies and cell lines.

My sincere appreciation extends to my research training group, GRK 2381. Being part of it not only facilitated my research and skill improvement but most importantly, it led me to meet amazing people who significantly touched my life. In particular, my deepest gratitude goes to Malte Roessing, Alexandra Böttcher, and Jennifer Schulz for their daily support, help with experiments, and above all friendship. Many thanks also to all past and present members of the Feil group. Special thanks to Barbara Birk for her kindness and help, and to Maria Teresa

Kristina Zaldivia PhD for her great advice during these years and for proofreading the first draft of this thesis.

My deepest love and gratitude go to my family for their unconditional love and tireless support and my friends for their constant cheerleading. I am incredibly thankful for my partner, Alberto, for his patience and for being my calm place during this stressful time.

Lastly, I am grateful to everyone who directly or indirectly contributed to this journey.